National Technical University of Athens

School of Mechanical Engineering

Machine Design Laboratory

Diploma Thesis

Charalampos Lazaridis

Design and FEA Study of a Novel Modular Multi-functional Tribological Laboratory Test Rig

Supervisor: Dr. V. Spitas

Associate Professor NTU Athens

Athens

September 2021

Περίληψη

Σε αυτή τη διπλωματική διατριβή, σχεδιάζεται ένα αρθρωτό, πολυλειτουργικό, Τριβόμετρο εργαστηριακών δοκιμών. Οι λειτουργίες της διάταξης περιλαμβάνουν έλεγχο της φθοράς σε ζέυγη δειγμάτων, σύμφωνα με τυποποιημένες διεθνείς διαδικασίες, όπως και τον έλεγχο φαινομένων λίπανσης που σχετίζονται με τη ροή του λαδιού σε μονούς δίσκους συμπλέκτη υγρής τριβής. Αρχικά, παρουσιάζονται οι κατηγορίες δειγμάτων που μπορούν να δοκιμαστούν. Αυτά περιλαμβάνουν υλικά τριβής, επιστρώσεις και επιφανειακά μοτίβα. Μια άλλη παράμετρος που μπορεί να δοκιμαστεί είναι οι τύποι των μοντέλων φθοράς που περιγράφουν την διεπαφή των δειγμάτων. Επίσης, αναλύονται τα φαινόμενα που θα εξετασθούν στην πειραματική διάταξη μονού δίσκου συμπλέκτη. Η πρώτη κατηγορία δοκιμών πραγματοποιείται στο τμήμα της κατασκευής που παρέχει περιστροφική και γραμμική κίνηση στα πειραματικά τεμάχια, τα οποία τοποθετούνται σε στεγανό περιβάλλον, ελεγχόμενης θερμοκρασίας και υγρασίας. Οι δοκιμές μπορούν να διεξαχθούν σε ξηρές συνθήκες ή συνθήκες λίπανσης. Δίπλα στη διάταξη ελέγχου φθοράς τοποθετείται η διάταξη μονού δίσκο υγρού συμπλέκτη, η οποία περιλαμβάνει ένα τμήμα που είναι υπέυθυνο για την περιστροφική κίνηση του δίσκου και ένα τμήμα που παλινδρομεί γραμμικά. Η διαδικασία σχεδιασμού περιγράφεται διεξοδικά, συμπεριλαμβανομένων των απορριπτόμενων σχεδίων και των εναλλακτικών λύσεων. Η αντοχή του τελικού κατασκευάσματος ελέγχεται χρησιμοποιώντας ένα συνδυασμό αναλυτικών εξισώσεων και υπολογιστικών μεθόδων πεπερασμένων στοιχείων, χρησιμοποιώντας το λογισμικό ANSYS. Τέλος, κατασκευάζονται τα διδιάστατα μηχανολογικά σχέδιατα των εξαρτημάτων της μηχανής (πλαίσιο στήριξης, εξαρτήματα δοκιμής φθοράς, εξαρτήματα δοκιμής μονού δίσκου συμπλέκτη, σύστημα κυκλοφορίας και λίπανσης λαδιού κ.λπ.).

Abstract

In this thesis, a modular, multi-functional, Tribological laboratory test rig it is designed. The functions of the rig include the testing of material wear on sets of specimens, according to standardized procedures and the testing of oil flow related phenomena on single wet clutch disks. Initially, the specimen categories that can be tested in the rig are presented. These include frictional materials, surface coatings and surface textures. Another parameter that can be tested is the wear model formulas that describe the wear contact types. The phenomena that will be investigated on the single disk tester are also analyzed. The first category of tests take place on a configuration of the assembly that provides rotational and linear motion profiles for the specimens, which are placed in a sealed environment, with controlled temperature and humidity. The tests can be carried out in dry or lubricated conditions. Alongside the wear multi-tester is the wet clutch tester, which includes a subassembly that provides rotational motion to the clutch disk and a subassembly that simulates a reciprocating linear motion. The design process is thoroughly described including discarded designs and alternative solutions. The durability of the final assembly is tested using a combination of analytical and computer-aided FEA methods using ANSYS software. Finally, the machine components (support frame, wear test rig parts, single disk tester parts, oil circulation and heating system etc.) dimensioned and 2D mechanical drawings are produced.

Thank you note

First and foremost, I would like to express my deep gratitude to my family, for their continuous support all these years and for the fact that they are always present when I need them. Their contribution to all stages of my life, during my school and student years, has been decisive. I thank them for all kind of sacrifices they made for me, for the ethical values they gave me, that were the foundation of the effort that led to this diploma thesis.

I would also like to thank my professor Dr. V. Spitas for the time he devoted in making suggestions and helping with various presented issues, but above all for trusting me and giving me the opportunity to work on a diploma thesis about industrial machine design.

I should also like to thank PhD candidate Nikos Rogkas for his valuable help during the work I did in the previous semesters, throughout all the designing process and research, and for his continuous support till its completion, despite his heavy workload.

Αναφορά

Η παρούσα διπλωματική εργασία καταπιάνεται με τον σχεδιασμό μιας εργαστηριακής μηχανής δοκιμών. Η διάταξη είναι πολυλειτουργική και περιλαμβάνει δύο βασικά μέρη. Το πρώτο μέρος είναι ένα τριβόμετρο με δυνατότητα εκτέλεσης (τυποποιημένων και μη) τριβολογικών δοκιμών, ενώ το δεύτερο μέρος εκτελεί δοκιμές λίπανσης σε ανοικτούς συμπλέκτες μονού δίσκου.

Η διάταξη του τριβόμετρου εκτελεί τριβολογικές μελέτες πάνω σε υλικά τριβής, υλικά και μεθόδους επιστρωμάτων, επιφανειακών μοτίβων αλλά και μοντέλων φθοράς. Όσων αφορά στα υλικά τριβής, τα υλικά που μπορούν να μελετηθούν είναι συμβατικά υλικά μεταλλικής μήτρας χαλκού, σιδήρου, μπρούτζου ή ατσαλιού, συμβατικά υλικά ημι-μεταλλικής μήτρας, δηλαδή συνδιασμοί των παραπάνω μετάλλων με σταθεροποιητές όπως η ζιρκονία και το οξείδιο του πυριτίου, αλλά και υλικά μη μεταλλικής μήτρας. Η τελευταία κατηγορία υλικών περιλαμβάνει σύνθετες δομές από συνδετικό υλικό όπως φαινολική ρητίνη που ενισχύονται με ίνες υλικών μεγαλύτερης μηχανικής αντοχής, όπως μεταλλικές και κεραμικές ίνες. Στην κατηγορία αυτή πραγματοποιείται συνεχώς έρευνα για την εύρεση σύνθετων υλικών με πολύ συγκεκριμένα τριβολογικά χαρακτηριστικά, κατάλληλα για ειδικές εφαρμογές όπως σε συμπλέκτες και δισκόφρενα. Στην περίπτωση των επιστρώσεων, η πειραματική μελέτη επιτρέπει την αξιολόγηση τόσο των υλικών της επίστρωσης όσο και της μεθόδου που χρησιμοποιήθηκε για την δημιουργία της. Συγκεκριμένα, λόγω του μικρού πάχους μιας επίστρωσης (συγκριτικά με το πάχος του υποστρώματος), η μέθοδος παρασκευής επηρεάζει έντονα τις τριβολογικές ιδιότητες, όπως και την μηχανική αντοχή του τελικού προιόντος. Τα επιφανειακά μοτίβα μεταβάλλουν χαρακτηριστικές ιδιότητες δοκιμίων όπως ο συντελεστής τριβής, αλλά και η αντοχή στη φθορά. Τα μοντέλα φθοράς που μπορούν να διερευνηθούν και να μελετηθεί η εγκυρότητά τους για νέα υλικά, μέσω της διάταξης, είναι η φθορά λόγω συγκόλλησης, απόξεσης, κόπωσης, όπως και η φθορά διάβρωσης. Η διαφοροποίηση μεταξύ των μοντέλων βασίζεται στις διαφορετικές κινηματικές και περιβαλλοντικές συνθήκες κάτω από τις οποίες συμβαίνει η φθορά, όπως και στις ιδιότητες των υλικών των δοκιμίων που συμμετέχουν. Επομένως, η πολυμορφικότητα της διάταξης θα επιτρέψει και την μελέτη συνδιαστικών περιπτώσεων φθοράς.

Οι παραπάνω κατηγορίες εξετάζονται στο τριβόμετρο μέσω τεσσάρων τυποποιημένων και μη διατάξεων. Τα τυποποιημένα δοκιμαστήρια που περιλαμβάνονται είναι τα Pin-on-Disc, Ball-on-Flat και Block-on-Ring, ενώ το μη τυποποιημένο δοκιμαστήριο είναι το Disc-on-Disc. Τα τρία πρώτα δοκιμαστήρια τυποποιούνται κατά ASTM G99–17, G133 – 05 και G77 – 17 αντίστοιχα και διαφοροποιούνται κυρίως ως προς τον προσανατολισμό και το είδος κίνησης των δοκιμίων που αλληλεπιδρούν. Το δοκιμαστήριο Disc-on-Disc είναι ειδικά προσαρμοσμένο για την μελέτη της τριβολογικής συμπεριφοράς των επιφανειών δύο δίσκων συμπλέκτη που έρχονται σε επαφή. Όλα τα αναφερόμενα δοκιμαστήρια μπορούν να λειτουργήσουν τόσο σε ξηρές συνθήκες όσο και σε συνθήκες λίπανσης.

Στο τμήμα της μηχανής που είναι υπεύθυνο για τις μελέτες λίπανσης σε ανοικτούς συμπλέκτες μονού δίσκου, λαμβάνονται μετρήσεις της στρεπτικής ροπής και της πίεσης πάνω στην επιφάνεια του δίσκου και συνολικά μελετώνται φαινόμενα όπως η διφασική ροή λαδιού/αέρα και η ταλάντωση του δίσκου. Στην προσομοίωση διφασικής ροής, εισέρχεται αέρας στο υγρό περιβάλλον του διακένου μεταξύ του κινούμενου δίσκου και του απέναντι σταθερού τοιχώματος, λόγω υποπίεσης. Το φαινόμενο αυτό μπορεί να παρατηρηθεί εξωτερικά της διάταξης, και η εισαγωγή του αέρα μεταφράζεται σε πτώση της στρεπτικής ροπής που αναπτύσεται στις επιφάνειες, η οποία και καταγράφεται. Στην περίπτωση όπου μελετάται η ταλάντωση του δίσκου σε διάφορες συχνότητες, ο δίσκος υπόκειται σε ταλαντωτική κίνηση κατά τον άξονά του, κατά την διάρκεια της περιστροφής του. Αυτή η ταλαντωτική κίνηση προκαλεί κρούσεις μεταξύ του δίσκου και του απέναντι τοιχώματος, οι οποίες εντοπίζονται με κατάλληλους αισθητήρες απόστασης.

Οι διατάξεις τοποθετούνται πάνω σε κοινή προυπάρχουσα βάση με σκοπό να εκμεταλλευτούν υπάρχοντες πόροι. Η βάση αυτή προήλθε από μια παλιότερη εργαστηριακή μηχανή και φέρει πατήματα στο εσωτερικό της στα οποία τοποθετήθηκε το σύστημα λίπανσης και το κοινό μοτέρ των διατάξεων.

Το αρθρωτό τριβόμετρο αποτελείται από δύο υποδιατάξεις: μια διάταξη η οποία είναι υπεύθυνη για την περιστροφική κίνηση και συγκράτηση των δοκιμίων με τις μεγαλύτερες διαστάσεις (για παράδειγμα το δοκίμιο του δίσκου στο δοκιμαστήριο Pin-on-Disc) και μια διάταξη η οποία είναι υπεύθυνη για την τοποθέτηση, γραμμική κίνηση και συγκράτηση των συμπληρωματικών δοκιμίων, αλλά και για την άσκηση της κάθετης δύναμης. Τα δύο δοκίμια σε κάθε περίπτωση έρχονται σε επαφή μέσα σε ένα κλειστό, στεγανό δοχείο, το οποίο γεμίζει με λάδι θερμοκρασίας εως 150^{o}C για την εκτέλεση δοκιμών σε συνθήκες λίπανσης. Η διάταξη της

περιστροφικής κίνησης παίρνει κίνηση από το κοινό μοτέρ της κατασκευής, που βρίσκεται στο εσωτερικό της βάσης, μέσω ιμάντα. Η διάταξη που είναι υπεύθυνη για τις γραμμικές κινήσεις αποτελείται από ενα χωροδικτύωμα από δοκούς ακριβείας, στους οποίους στερεόνονται γραμμικοί οδηγοί. Οι οδηγοί του δικτυώματος επιτρέπουν την μονοαξονική κίνηση μιας πλάκας, πάνω στην οποία τοποθετείται το σύστημα έδρασης του δοκιμίου. Το σύστημα έδρασης, μέσω ενός νέου συστήματος οδηγών, κινείται κατά μια διεύθυνση κάθετη στην διεύθυνση κίνησης της πλάκας και ανεξάρτητα από αυτήν. Με τον τρόπο αυτό επιτυγχάνεται κίνηση του δοκιμίου σε δύο άξονες. Το σύστημα έδρασης του δοκιμίου περιλαμβάνει έναν άξονα στο ένα άκρο του οποίου στερεώνεται το δοκίμιο και στο άλλο εδράζονται διάφορα εναλλάξιμα ελατήρια ίδιου μήκος αλλά διαφορετικής σταθεράς k, ανάλογα με τις απαιτήσεις της δοκιμής που εκτελείται. Τα ελατήρια εδράζονται σε δυναμόμετρο το οποίο τα ενώνει με το υπόλοιπο σύστημα. Οι γραμμικές κινήσεις πραγματοποιούνται με την βοήθεια ενός γραμμικού επενεργητή και ενός συστήματος σερβομοτέρ, μειωτήρα και κοχλία κίνησης. Μέσα στο δοχείο που εκτελούνται τα πειράματα τοποθετούνται αισθητήρες θερμοκρασίας και αισθητήρες απόστασης για την σωστή τοποθέτηση των δοκιμίων.

Το δοκιμαστήριο λίπανσης μονού δίσκου συμπλέκτη περιλαμβάνει μία βάση στην οποία στηρίζεται ο άξονας που παρέχει την περιστροφική κίνηση του δίσκου του συμπλέκτη. Ο άξονας παίρνει κίνηση από το κοινό μοτέρ της κατασκευής. Το δοχείο που περικλείει τον συμπλέκτη δεν πακτώνεται στην βάση αλλά συνδέεται με αυτήν μέσω γραμμικών αγωγών. Με τον τρόπο αυτό είναι ελεύθερο να κινηθεί παράλληλα με τον άξονα του δίσκου. Μέσω ενός συστήματος σερβομοτέρ, μειωτήρα και κοχλία κίνησης το δοχείο μπορεί να ακολουθήσει μια παλινδρομική γραμμική κίνηση, συχνότητας εως 50Hz, για την προσομοίωση του φαινομένου της ταλάντωσης του δίσκου. Στο δοχείο τοποθετούνται αντεπίστροφες βαλβίδες οι οποίες επιτρέπουν την εισροή αέρα στο σύστημα. Επίσης, πάνω στο δοχείο και απέναντι από τον δίσκο του συμπλέκτη είναι τοποθετημένο ένα καπάκι το οποίο αλλάζει ανάλογα με τη δοκιμή που εκτελείται. Για την παρατήρηση της διφασικής ροής τοποθετείται ένα πλαστικό καπάκι, ενώ για την δοκιμή ταλάντωσης τοποθετείται ένα ανθεκτικότερο μεταλλικό καπάκι. Το καπάκι αυτό είναι στερεωμένο σε ένα έδρανο κύλισης που του επιτρέπει να περιστραφεί. Επομένως η στρεπτική ροπή που τείνει να περιστρέψει το καπάκι μετράται από ένα δυναμόμετρο που ενώνεται σε συγκεκριμένη ακτίνα πάνω στο καπάκι, ενώ στερεώνεται στη βάση της κατασκευής. Παράλληλα μετράται και η στρεπτική ροπή που αναπτύσσεται στον κινούμενο δίσκο, μέσω ενός μετρητή ροπής που παρεμβάλλεται στον άξονα κίνησης. Πάνω στο καπάκι, προς το εσωτερικό του δοχείου, τοποθετούνται επίσης αισθητήρες πίεσης και αισθητήρες απόστασης για την μέτρηση του διακένου μεταξύ του κινούμενου δίσκου του συμπλέκτη και του καλύμματος, αλλά και για την ανίχνευση των κρούσεων κατά τη διάρκεια της ταλάντωσης. Τέλος χρησιμοποιείται και ένας αισθητήρας θερμοκρασίας για την μέτρηση της θερμοκρασίας του λαδιού.

Το σύστημα λίπανσης και θέρμανσης του λαδιού τοποθετείται στο εσωτερικό της βάσης, παροχεύοντας λάδι στις δύο διατάξεις ανεξάρτητα. Περιλαμβάνει ένα τροφοδοτικό δοχείο από το οποίο το λάδι διοχετεύεται στο φίλτρο για την απομάκρυνση στερεών σωματιδίων και στη συνέχεια οδηγείται σε μια γραναζωτή αντλία. Από την αντλία το λάδι προωθείται στην κατάλληλη διάταξη μέσω του κλεισίματος της αντίστοιχης βαλβίδας. Μέσα στο τροφοδοτικό δοχείο τοποθετείται ένα θερμοστοιχείο που είναι υπέυθυνο για την αύξηση της θερμοκρασίας του λαδιού και ένα θερμόμετρο για την μέτρησή της.

Για τον έλεγχο της αντοχής της κατασκευής χρησιμοποιήθηκε το πρόγραμμα ανάλυσης πεπερασμένων στοιχείων ANSYS. Συγκεκριμένα πραγματοποιήθηκαν μελέτες ιδιοσυχνοτήτων, όπως και μελέτες στατικών και δυναμικών καταπονήσεων. Για την εύρεση των ιδιοσυχνοτήτων της κατασκευής πραγματοποιήθηκε modal and rotordynamic analysis, από το οποίο προέκυψε πως όλες οι ιδιοσυχνότητες της κατασκευής είναι επαρκώς μεγαλύτερες από τις μέγιστες συχνότητες λειτουργίας. Ακολούθως, μοντελοποιόντας μεμονομένες περιπτώσεις καταπόνησης για τα διάφορα τριβολογικά τεστ σε static structural analysis, εντοπίστηκαν οι περιοχές στις οποίες αναπτύσσονται οι μέγιστες ισοδύναμες τάσεις στην διάταξη. Στην περίπτωση του δοκιμαστηρίου λίπανσης ανοικτού δίσκου συμπλέκτη, πραγματοποιήθηκε transient structural study, καθώς κατά την παλινδρόμιση του δίσκου αναπτύσσεται κάθετη δύναμη μεταβλητού μέτρου στις επιφάνειες του δίσκου και του καλλύμματος. Από την προσομοίωση αυτή εντοπίστηκαν οι περιοχές μέγιστης καταπόνησης και για την διάταξη του συμπλέκτη. Από τις παραπάνω αναλύσεις οδηγήθηκε μια διαδικασία βελτιστοποίησης με κατάλληλες τροποποιήσεις τόσο στη γεωμετρία όσο και στα υλικά των επιμέρους τμημάτων της διάταξης.

Από τις σχεδιαστικές απαιτήσεις της κατασκευής αυτής της διατριβής, φαίνεται ότι υπάρχουν αρκετά αυστηρά χαρακτηριστικά που πρέπει να ακολουθηθούν. Παρόλο που συμβατικά ανταλλακτικά, υλικά και μέθοδοι παρασκευής έχουν χρησιμοποιηθεί όπου είναι δυνατόν, οι απαιτήσεις σε ορισμένες περιοχές της διάταξης

καθιστούν την κατασκευή αρκετά περίπλοκη, με περισσότερες από μία μεθόδους κατασκευής και επεξεργασίας. Ωστόσο, κάτι τέτοιο είναι αναμενόμενο κατά το σχεδιασμό ενός δοκιμαστηρίου ακριβείας που ακολουθεί πολλά διεθνή πρότυπα. Επιπλέον, το γεγονός ότι η διάταξη συνδυάζει πολλά διαφορετικά δοκιμαστήρια σε μία ενιαία κατασκευή σημαίνει ότι, σε σύγκριση με τα αυτόνομα τριβόμετρα του εμπορίου, η προσφερόμενη αξία στην κατασκευαστική διαδικασία και το κόστος είναι πολύ μεγαλύτερη. Τέλος, η επαναχρησιμοποίηση παλαιών εργαστηριακών ανταλλακτικών στην περίπτωση του σκελετού της μηχανής υπογραμμίζει την αποτελεσματικότητα της ανακύκλωσης στην κατασκευή εργαστηριακών μηχανημάτων, χωρίς θυσίες στις παραμέτρους λειτουργίας.

Contents

1 Introduction

From brakes and clutches to high friction surfaces for slippage control, frictional devices are widely used in the automotive and industrial landscape. The concept of these devices in the form we know them today had been around at least as early as 1900 with the example of the first modern automobile drum brake used in a car, made by Maybach. Since then, the progress in manufacturing technology and material science have allowed for leaps in the performance and the usability of such parts.

The common ground for all these devices, is that they need to have a predictable wear and frictional behavior, suitable for their designated use. And yet, whereas the scientific study of friction dates back some 300 years, and that of lubrication more than a century, wear has received similar attention for only the latest 40 years. The areas to focus on and investigate, in order to appreciate their properties are the materials and the surface textures. A first step is the creation of mathematical formulas that appropriately describe the physical phenomenon of wear and provide a common classification method for the materials. These formulas are called wear models and the calculation of coefficient parameters, specific for each processed material is required for their use. These coefficients can be obtained by standardized experimental testing between sets of material samples. For this purpose, several different types of wear test rigs or tribometers have been created, each offering a setup that is better suitable for a specific type of wear. Despite the relatively recent naming of the field of tribology, quantitative studies of friction can be traced as far back as 1493, when Leonardo da Vinci first noted the two fundamental 'laws' of friction. Similarly, the first tribometer was invented by the 18th century Dutch scientist Musschenbroek. Apart from providing experimental data for the values of the wear coefficients, tribotesters are used to evaluate the wear formulas, and its variations depending on the operational parameters. The whole process of creating a novel material, coating or surface texture pattern is nowadays a standardized procedure of testing, using the type of tribometer best suited to the application. Also, the rate at which wear particles are created can be evaluated with these machines, which can lead to various environmental and health discoveries. In the last decades tribology expanded to qualitatively new fields of applications, in particular micro- and nanotechnology as well as biology and medicine. An attempt has been made to qualify the impact of friction and wear particles on an international level which concluded that, in total, ~23% of the world's energy consumption originates from tribological contacts. Of that, 20% is to overcome friction and 3% to remanufacture worn parts and spare equipment due to wear and wear-related (1). By taking advantage of the new technologies for friction reduction and wear protection, energy losses due to friction and wear in vehicles, machinery and other equipment worldwide could be reduced by 40% in the long term (15 years) and 18% in the short term (8 years). On a global scale, these savings would amount to 1.4% of GDP annually and 8.7% of total energy consumption in the long term.

It is very practical to be able to combine multiple wear test rigs in the same configuration, the creation of which, is the scope of this thesis. More precisely, the subject of this diploma thesis is the creation of a wear multi-tester and a novel open clutch single disc lubrication testing assembly, both designed to share the same platform.

During the design process the basic guidelines of design for manufacturability and assembly (DFM and DFA) were followed, in the scope of creating a machine in such a way that it is easy to manufacture and put together, while considering the manufacturing costs. DFM will allow potential problems to be fixed in the design phase which is the least expensive place to address them. Other factors may affect the manufacturability such as the type and the form of raw material, dimensional tolerances, and secondary processing such as finishing.

The requirements when creating a multi-functioning testing machine are many, since there are standards that should be followed but also limitations regarding the available space, hardware and materials to use. For this reason, the initial concept design was changed several times, to introduce better solutions, to solve possible complications or just to simplify the design. The goal was to create a testing machine that is modular, easy to use and that the parameters of one of its testing configurations do not compromise the others. The designed machine has two compartments. On the first one several types of wear tests can take place, both on dry or lubricated conditions. The specimens can be easily inserted into the tester without any need to interfere with the assembled parts. On the second test rig, several design features and operation phenomena of a wet clutch disk can be evaluated. For this test, a single clutch disk is inserted in the assembly.

2 Novel Materials for Industrial and Automotive Frictional Applications

2.1 About Friction Materials

Friction materials are widely used in applications that include braking and power transfer, most commonly in the form of brakes, clutches, limited slip differentials, tires and belt drives. Given the nature of these applications, it is required that the materials have a sufficiently high friction coefficient that remains stable during their gradual deterioration and the operating temperatures. Also, they need to have an adequate mechanical strength and rigidity in order to endure impact and centrifugal forces. Apart from the material composition, the shape and texture of the surface is investigated in order to enhance the friction properties. The operating conditions for the materials can be dry or wet, since it is noticed that the flow of the liquid increases the heat dissipation. All these aspects of the materials are tested exclusively on wear test rigs. Particularly, the most common test rig for a material specimen is Pin-on-Disk tester, but when the tribological properties of a specimen under a very specific type of wear need to be evaluated, other test configurations can be used, to better simulate the nature of the contact. The wear test rig of this thesis will be able to verify properties of existing materials under various testing conditions and also examine novel materials that are created in the scope of introducing enhanced tribological properties in specific applications.

2.2 Materials

There is a variety of composite friction materials that can meet the requirements of different applications. The most common constituent components of composites used on clutches or brake pads through the years are the following (2), (3): Steel, Iron, Copper, Bronze, Carbon, Natural / Artificial Rubber, Silicon dioxide, Aramid, Glass, Cellulosic fiber, Thermoplastic fiber (PTFE, PEEK, PPS, Nylon, Acetal, Polyester), Organic fiber, Asbestos etc

As mentioned, not every constituent component is suitable for every case. Some components even produce environmental and health hazards and have since been banned. Some of the problems of the fiber materials are shown below (2):

Aramid	expensive, extra care against pulp on mixing, alone not adequate, needs other ingredients
Glass	week heat resistance causes fade, loses fiber form in high shear mixing, molding, springs back, unsteady coefficient of friction, low wear characteristic
Carbon	expensive, loses fiber form in mixing
Steel	heavy, corrodes, abrades disc, rotors, noise
Cellulosic fiber	low strength and modulus, low char temperature
Thermoplastic fiber	melts causing fade
Asbestos	health hazard

Table 1 Problems on common fiber materials, (2)

2.3 General material categories

Depending on their consistency, friction composite materials can be divided on three general categories:

2.3.1 Metallic matrix friction materials

The materials of this category are manufactured either by molding or by sintering / powder metallurgy. The main frictional constituents are steel, iron, bronze and copper. For a high temperature strength, hardness, and thermal stability the iron-based friction materials are superior to the copper-based friction materials. Still, the latter presents more stable friction coefficient, greater thermal conductivity and wear resistance. To combine characteristics of both types combined copper and iron materials are created with excellent mechanical properties and good wear resistance (4). Gyimah et al. investigated the effect of sintering temperature on the tribological properties of copper-based materials, finding that higher sinter temperatures not only allow for a lower wear rate to the materials, but they also increase the wear and friction coefficients (5).

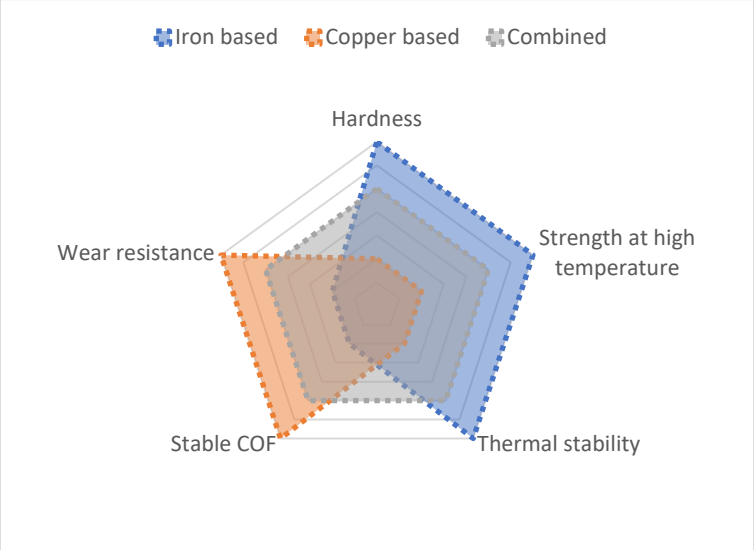

Figure 1 Schematic radar chart comparison between Iron, Copper based and Combined materials

2.3.2 Semi metallic matrix friction materials

This material type consists of both fibers and metal powders. The most common powders are made of steel, iron, copper or brass and they are combined with ceramic, metallic, carbon or aramid fibers. The great wear resistance and the superlative coefficient of friction especially under high temperatures render these materials ideal for the automotive industry. For further increase and stabilization of the friction coefficient on high temperatures abrasive additives are used. The most common are zircon ($ZrSiO_4$), corundum (Al_2O_3), silicon oxide (SiO_2), silicon carbide (SiC) and zirconia (ZrO_2) (6). Some downsides of these materials are operational noise, easy corrosion and destruction on the mating brake discs because of the abrasive additives. The production methods for these materials are similar to the methods of metallic matrix friction materials. Here, studies suggest that elevated molding temperatures don't affect the friction performance, but they affect the wear rate of the material, depending on the energy level of the wear operation. Specifically molding at high temperature creates the best wear resistance for a low energy wear test, when for the medium and high energy wear tests the results are the opposite (7).

2.3.3 Nonmetallic matrix friction materials

Nonmetallic matrix friction materials are composed of the binder material, the reinforcing fibers, frictional additives and fillers. Analytically (8), (9):

- Binder: The binder is the matrix of the friction material that connects all of the other components together and it defines the tribological properties and the heat resistance of the material. The most common binder materials are phenolic resin, condensed polynuclear aromatic (COPNA) resin, silicone-modified resin, cyanate ester resin, epoxy-modified resin and thermoplastic polyimide resin.
- Fibers: The reinforcing fibers are used to improve the mechanical properties of the composite, with the most typical material examples being ceramic, metallic, carbon, glass, Kevlar, sepiolite, potassium titanate, cellulose and aramid.

- Additives: Frictional additives are a combination of abrasives and lubricants. Similarly, to the case of the semi metallic composites, abrasives are used to increase the coefficient of friction and lubricants are used to reduce the wear rate of the material.
- Fillers: The purpose of fillers is the improvement of cost and manufacturability of the material with no crucial effect on the friction parameters of it. Mainly there are two types of fillers, the organic and the inorganic.

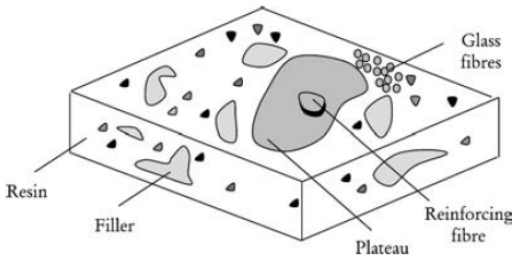

Figure 2 Example of isometric view of brake pad material, (8)

Two distinctive subcategories of the nonmetallic matrix friction materials based on their manufacturing process are the paper based and the woven composites.

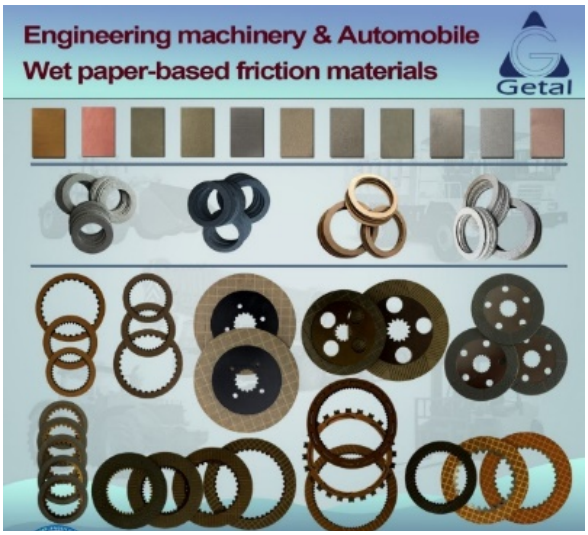

Figure 3 Wet paper-based friction materials for Clutches and Brakes. Source: Zhejiang Gaocheng Autoparts Co., Ltd.

Paper based materials are mostly used in wet applications and they are manufactured with a process that resembles the production of normal paper. They show very little deviation between their static and dynamic friction coefficients, which prevents abrupt changes, vibrations and low frequency noise during their use (8). This is an ideal trait to have on clutches of automatic transmissions. One drawback present on most paper-based materials is their high wear rate at elevated temperatures (9). A study of the wear characteristics of this type of materials under dry working conditions using a pin on disc testing apparatus offers some insight on the variations of the friction coefficient in relevance with operating parameters like loading and moving speed. The study indicates that the coefficient of friction shows steady and then decreasing behaviour as the loading increases and that it decreases with the increase of rotating speed (10).

Woven materials are made out of bundles of fibers interwoven into a single ply. This characteristic fabric-like form provides mechanical strength in both longitudinal and transverse directions. Given the nature of this manufacturing method the resulting material has a high porosity (8). Thus, when a woven material for wet applications is constructed the binder material (for example resin) is used in low quantities, in order to maintain some gaps inside the final product. According to Gibson, Mack and Pepper, these gaps allow the fluid to be absorbed from the external surface, which results in an increased flow rate and permeability during the use of a wet clutch. A common manufacturing method is a compression molding technique called thermostamping or thermoforming. Improper values of the parameters of thermostamping like stamping rate and stamp force greatly affect the mechanical properties of the final product as they can result in incorrect yarn tensile stress and manufacturing defects (11).

Figure 4 Organic Woven friction material. Source: Fricwel Automotive Limited

2.4 Novel trends in friction materials

Nowadays the efforts to create friction materials with better tribological characteristics, better mechanical properties and lower cost continue, but these efforts are heavily influenced by environmental and health concerns. It is intended to create materials that are made by eco-friendly or natural components or even recycled waste that do not pollute the environment or cause health hazards during their operation and are biodegradable. Some of the latest examples are the following.

Considering the health hazards caused by the aspiration of toxic brake wear particles, J. Wahlstrom et al. investigated the wear particle size emitted by the operation of conventional brake pads and compared it to the equivalent particle size of nanoporous composite-based brake pad materials (12). The results suggest that two of the tested nanoporous composites released 3 to 7 times less airborne particles. That is to say their particle size was much smaller than the size of the particle of conventional materials, hence it is less likely to reach and be absorbed by the human lungs.

Under the scope of creating a material from natural materials using a low-cost manufacturing technique, A. Alavudeen et al. created a hybrid banana/kenaf woven fabric composite reinforced with polyester by hand lay-up technique, for use on clutch plates (13). The material was found to have more than sufficient mechanical strength and rigidity.

Figure 5 Banana and kenaf woven hybrid composite, (13)

Figure 6 Friction composite by waste tyre rubber particles. (14)

Efforts have been made to utilise recycled components as ingredients friction materials. For instance, waste tyre rubber particles were used as a property modifying additive for brakes. These tyres are not biodegradable, so their utilisation as a brake pad additive offers a solution to their uncontrollable disposal. Tej Singh et al. investigated the effect of the percentage of the added rubber on the performance of the brakes, finding that a lower concentration of rubber offers a high and stable coefficient of friction and low fade during operation, when a higher rubber content has better recovery, wears out less and contributes to a lower rise in the temperature of the brake (14).

Koya and Fono developed a brake pad composite from palm kernel shell as an alternative to asbestos and investigated its fade and recovery properties depending on the particle size used (15). According to the results, palm kernel shells with a 0.3 mm particle size are a possible asbestos alternative but in the need of further analysis, since they show poor fade behaviour but also a high recovery rate.

Figure 7 Fibres of palm kernel. (15)

Figure 8 Coconut based composite specimen. (16)

According to R. J. Talib et al. using natural bamboo fiber on a semi metallic brake pad implementation is a viable possibility (17). When compared to commercial brake samples, a specimen with a composition of 10 wt. % bamboo fiber and 10 wt. % copper showed a greater coefficient of friction and fade resistance.

Another material that has been tested for both clutch and brake applications is coconut fiber due to its adequate mechanical properties, its low cost and density and its biodegradability. For the case of the clutch, it is proved that even though the material doesn't meet the required standards, there is much room for optimisation by the use of additives (18). As a brake material coconut fiber has more positive results. It is deduced that it presents a proper reinforcing fiber for automotive brakes given its tribological properties and its slow wear rate (19). Another study investigated further on the coconut-based composites, testing composites made from a mixture of wood powder, coconut fibre and green mussel shell. A specific combination of percentages of these materials creates a specimen with a hardness similar to the respective value on commercial motorcycle brakes, with an even higher thermal resistance than the required (16). Thus, this material is very appropriate for motorcycle pads.

Although not particularly new, the ceramic matrix composites have been found to be lighter and to have more stable mechanical properties at elevated temperatures than the conventional grey cast iron disc brakes (20). Also, they are less prone to wear and their coefficient of friction doesn't get affected by temperature or humidity changes as it does on the carbon/carbon composites which are the lighter and less heat dependent alternative to the grey cast iron disc brakes. For these reasons the ceramic matrix composites gradually became the go to for high performance and heavy loading brake discs. Particularly, a combination of ceramic and carbon/carbon composites called C/C–SiC is now widely used in the automotive industry (21). In order to take full advantage of the power performance of this disc material, ceramic pad counterparts were created to replace the organic, steel or iron brake pads previously used in the industry (21). Recent studies on full carbon ceramic braking pairs showed that the ceramic pads created an unsuitably high coefficient of friction that cannot be used in the automotive industry and they suffered by a very high wear rate (22). Both these drawbacks can be addressed by adding a ductile phase like FeSi2 into the pads as it will reduce the coefficient of friction and it will contribute to a better wear resistant behavior.

Figure 9 C/SiC ceramic brake pad. (21)

2.5 Coatings

Coatings are used on both brake and clutch applications. On brakes, coatings are applied on the disc plate material as a protective film that helps reduce the corrosion and the wear rate of the disc. The former is particularly important since during service of the brake the amount of the released particulate matter is concerning for the health (23). The reason coatings are used on clutches is to improve the tribological characteristics of the surfaces in order to prevent unwanted behaviors like the stick-slip effect that leads to an unsteady contact between the clutch surfaces and vibrations during operation (24). The ability of a coating to stay in contact with the covered surface and its resistance to degradation are characteristics that are constantly under research and in need of improvement. They can be tested on tribometers, most commonly on Pin-on-Disk testers.

The coatings for brakes (but also applicable to coatings for clutches) can be distinguished in two general categories, depending on the process of their application, the coatings that are used with non-thermal spray processes and coatings that are used with thermal spray processes. Non-thermal spray processes are generally electrochemical surface treatment methods. On the other hand, during a thermal spray process the molten powder particles are sprayed to the surface at high speed and at high temperature to form splats that will eventually create the coating. The choice of manufacturing method for a coating is quite critical, since it greatly affects the tribological properties of the final product.

2.5.1 Non-thermal spray processes

A quite old and widely spread non-thermal technique is Hard Chrome Plating. The produced coating has high hardness and corrosion resistance as well as a low coefficient of friction. On the other hand, it is prone to

microcracking which at a later stage worsens and can make the material brittle (25) and it is known to produce carcinogenic fumes as it wears out.

Plasma electrolytic oxidation (PEO) is a process comparable to anodising but at greater voltage and current, which results in an oxidised metal film up to 100μm thick (26). Suitable metals that can be used for this process are aluminum, magnesium, titanium and their alloys. Although this oxidised coating has many advantages including thermal, corrosion and wear protection properties (27), (28), (29), a deterrent is its porous nature which should be kept at a minimum (30).

Coating Process	Source	Possible Coatings	Microstructural Features	Drawbacks
Hard chrome plating	Electrolyte	CrO_3	Metallurgical bonding, highly dense and thin coating	Hexavalent Chromium—carcinogenic
PEO	Electrolyte	Oxides of Al, Mg, Ti	Protective oxide scale, metallurgical bonding and uniform coating thickness	Suited only for few metals like Al, Mg, Ti, and their alloys capable of forming protective oxides by chemical conversion
Laser Cladding	Wire or powder	Wide range of Metals alloys, cermets and ceramics	Metallurgical bonding, dense and thick coatings	Different laser beam absorptivity at GCI surface can result in non-homogeneous thermal fields; excessive heating can lead to thermal damage to feedstock (e.g., decarburization of WC to W_2C)
PTA	Wire or powder	Wide range of Metals, alloys, cermets and ceramics	Metallurgical bonding, dense and thick coatings	Possibility of dilution from cast iron, to change coating composition and influence mechanical properties

Figure 10 Non-thermal spray processes for brake coatings, (23)

2.5.2 Thermal spray processes

Atmospheric Plasma Spray (APS) provides coatings of metallic, cermet or ceramic materials with strong anti-corrosion characteristics. The mentioned material variety is possible due to the high temperature of the plasma jet. A drawback of this technique is possible porosity, cracks and oxides on the substrate of the coating. Also the adhesion of the coating film suffers greatly for coatings with more than 0.5 mm of thickness (23).

The high temperatures of High Velocity Oxy-Fuel (HVOF) process are sufficient to melt the metallic powders and partly melt the cermet powders creating a quality coating of high strength, hardness and wear resistance with low porosity (31).

In order to overcome brittleness related problems observed in HVOF coatings, High Velocity Air Fuel (HVAF) uses a lower temperature and higher feed rate speed (32). This cost-effective technique creates thick and strong coatings that are very promising for low wear brake discs.

2.5.3 Brake coatings materials

Brake coating materials with a vast use in the industry are the oxides of aluminum, titanium, chromium and ceramics. The later present desirable mechanical properties as well as wear and corrosion resistance. Since the mentioned materials have a high melting point, APS is the preferable method to use for the coatings (33).

For applications with high requirements on wear and corrosion resistance cermets of metal carbides like tungsten carbide (WC) and chromium carbide (Cr3C2) combined with metals like cobalt (Co), nickel (Ni), chromium (Cr) and iron (Fe) are regularly used (34). The most suitable spray methods for these carbides need to have high particle velocities like on HVOF and HVAF (35).

Recent developments like the identification of Ni, Co and WC-Co based powders as carcinogens (36) have led the industry to seek other more environmentally friendly materials like stellite, Ni-Cr-B-Si, Fe-V-Cr-C or WC-FeCrAl alloys.

2.5.4 Clutch coatings materials

As mentioned, the coatings for clutches are created with similar techniques to the ones mentioned for brake coatings. A popular wet clutch material ingredient is phosphorus. Specifically, polar phosphoric acids combined with a lipophilic group are known to heavily affect the static to to dynamic friction coefficient ratio (37). Zinc and iron phosphates have been tested and their stick-slip, stability and friction coefficient characteristics were found to be superior to those of an uncoated surface (24). Another study proposes a coating made of basalt minerals on Al alloy surfaces for increased friction coefficient and improved wear resistance, as an alternative to resin composite materials on steel surfaces (38). A suitable spray method for this coating is PEO, as it produces a thick, homogeneous material with high hardness, stable friction behaviour and low wear coefficient. Importantly, the latter is smaller than the respective coefficient of resin-based materials by two to three orders of magnitude.

2.6 Surface textures

2.6.1 Brake surface textures

Depending on the finish process on the surface of the friction materials of brakes, the tribological properties of the brakes can change. These alterations are especially noticeable during the running-in stage of the brake and they can also affect the adhesion behavior of the transfer film (a film created by particles that don't belong to the disc material, i.e., pad debris) (39). The importance to further investigate the parameters of the surface textures that cause these variations is underlined by the increased diameters of the disc brakes for high performance applications and by the lighter loading behavior on regenerative brakes on hybrid and electric vehicles. In both of these cases the running-in periods are getting larger so it is important to suitably select the disc textures in order to achieve a uniform contact surface between the pad and the disc. The most common processes for surface finishing are grinding, turning, milling, and roller burnishing.

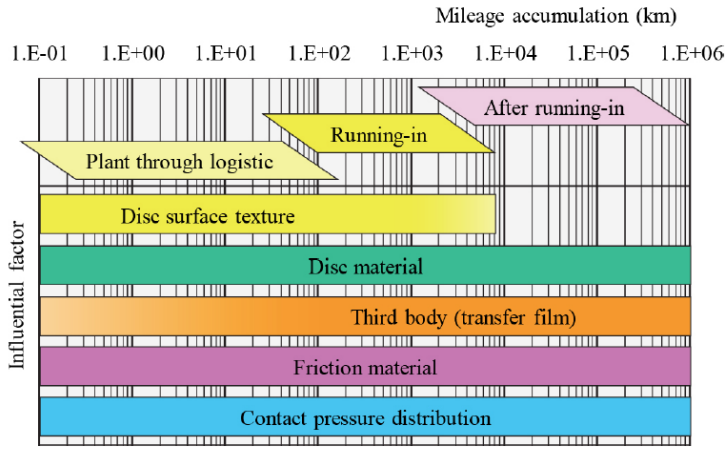

Figure 11 Factors affecting friction of disc brake during vehicle life. (40)

The direction of the surfacing process is confirmed to have an impact on the friction properties and the wear of the disc (39).

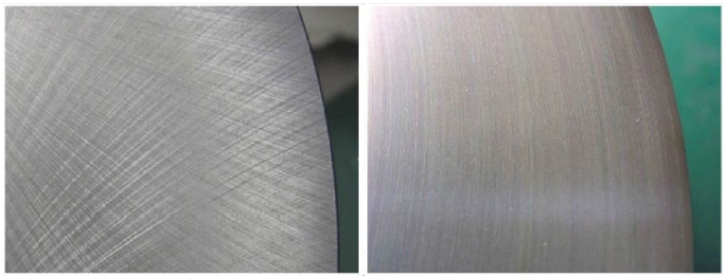

A numerical study has verified that early in the running-in process, the abrasive wear is larger on a grinding finished disc than that on a disc finished with roller-burnishing because of its larger tangential roughness of the first (40).

Figure 12 Friction surface texture of grinding-finished and roller-burnished discs. (39)

Also, roller-burnishing finished discs need a longer running-in period than grinding finished discs because the later are smoother during the final running-in stages and they have a greater adhesive wear behaviour.

Another interesting find suggests that creating groove patterns on the surface of a brake can improve both the tribological and the noise performance of a railway brake system (41). The wear of the brake is improved since

the debris from the pad gets trapped inside the grooves, leaving a clean contact surface for the disc and pad assembly.

2.6.2 Clutch surface textures

In the case of a clutch, the investigation around the surface textures is much more complicated, especially for wet clutch systems. The reason for this is that the engagement of a wet clutch combines hydrodynamic, elastohydrodynamic, mixed and boundary lubrication modes (42). Both the peak temperatures and the wear of the clutch material during the engagement stage can be affected by grooves on the friction surface of variable possible shapes, profiles and groove area ratios.

The most common profile shapes on linear grooves are round, trapezoidal and triangular (43). Studies verify that the triangular shape allows for a faster engagement time than the round and trapezoidal ones, since it has the smallest cross-section area which allows for a very low hydrodynamic load and resistance to squeeze (42).

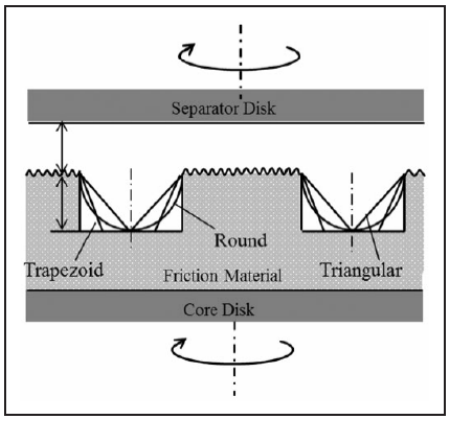

Figure 13 Trapezoid, triangle and round groove profiles. (43)

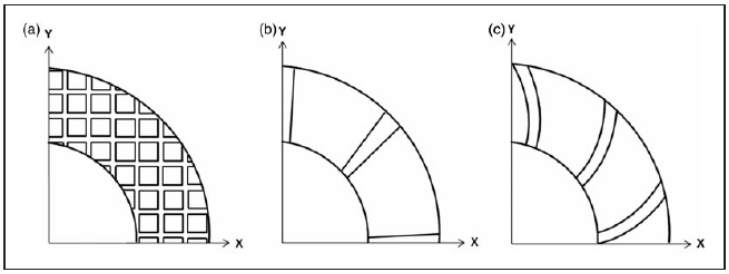

Figure 14 Waffle, radial and spiral surface groove patterns. (43)

The most common groove shapes are radial, spiral and waffle. The waffle groove design offers successful results regarding the surface lubrication but suffers in terms of heat dissipation as only the grooves that have a radial direction contribute to cooling (43). For this reason, the radial groove shape design is much more efficient having a higher heat dissipation rate. Finally, with the spiral groove design a pumping effect is created, so this shape helps to increase the drag loss associated with hydrodynamic lubrication. A smaller spiral angle creates a greater pumping effect and it creates better cooling (42).

Interestingly, plain clutch discs with no grooves show less wear for very small engagement times, but for larger engagement times the opposite is true. For instance, the waffle shaped type offers a longer operation life by 30% (43).

Regarding the number and the area ratio for the case of radial grooves, it is generalized that more grooves and grooves with a bigger width result in increased engagement times.

2.7 Material, Coating and Texture testing on the Tribometer

The mentioned materials, coatings and textures can be tested for their tribological properties in the designed wear test rig. For the testing, specimens with specific dimensions will be created and placed inside the rig. In these configurations the contacting specimens can be of the same or different material and they can be examined under lubricated or dry conditions, on a controlled environment regarding temperature and humidity. The specimens on which the surface texture or coating are tested undergo the same procedure, and are later examined under an optical microscope for deformations and material separation. This way, the effectiveness of their manufacturing method is also be tested. Specifically, in the case of clutch disk textures, the specimens can be tested on a customized Disk-on-Disk rig, which corelates much better to the operation of a clutch than the traditional Pin-on-Disk apparatus.

3 Wear models

3.1 Wear models and Tribometry testing

The mathematical formulas describing the rate of the material removal between two interacting interfaces are called wear models. These models vary depending on the characteristics of each wear contact. During the latest decades, formulas have been created about most types of wear, but the parameters used in these formulas are dependent on the examined materials. This means that in order to verify a wear type formula, several tests are required with all the possible materials of this category, in order to pinpoint possible deviations. This, combined with the fact that the creation of new materials and material combinations is an ongoing process, underlines the need for a wear testing apparatus that is able to simulate the conditions of as many wear types as possible. In the rig of this thesis, such a thing is made possible by providing different combinations of motions for the examined specimens, as well as dry or lubricated environmental conditions.

3.2 Model of Archard

The material wear between moving mating surfaces is generally described by Archard's formula. This model was originally created to describe the wear on metal parts but it is indicative for other materials as well. It is based on asperity contact theory which means the following assumptions are made:

1. There is contact between two surfaces when there is contact between the asperities of the surfaces
2. The area of the contact surface is equal to the sum of the various contact surface areas of the asperity contacts

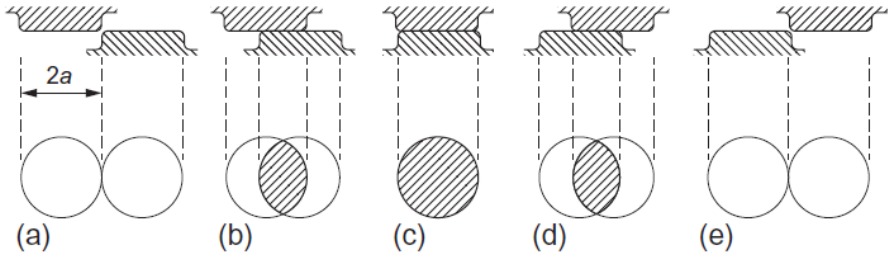

Figure 15 Schematic diagram showing the evolution of a single contact patch as two asperities move over each other, (44)

Considering a disc contact profile of the asperities in a case of maximum surface contact the nominal force is (44):

$$\delta W = P\pi\alpha^2$$

where:

W = nominal force, P = yield pressure, α = radius of the circular contact

The detached volume of the asperities can be taken to be that of a hemisphere, giving:

$$\delta V = \frac{2}{3}\pi\alpha^3$$

By defining κ as the proportion of the asperities that produce wear particles, the average volume of the worn material for a 2α sliding distance is:

$$\delta V = \frac{\kappa\delta V}{2a} = \frac{\kappa\pi\alpha^2}{3}$$

Thus, the overall wear rate Q and total normal load W are respectively:

$$V = \sum \delta V = \frac{\kappa}{3}\sum \pi\alpha^2$$

and

$$W = \sum \delta W = P \sum \pi \alpha^2$$

Thus:

$$V = \frac{\kappa W}{3P}$$

It is convenient to combine the factor of 1/3 into the constant of proportionality, by putting K =κ/3, and to assume that P=H, the indentation hardness which converts the equation to:

$$V = \frac{KW}{H}$$

or alternatively

$$V = \frac{KWL}{H}$$

where V is defined as the volume of the removed material and L the total sliding distance.

Apart from the possibility of asperity material detachment, the wear coefficient K can be correlated with:

- The size of the detached particle of the asperity
- The lifecycle of the asperity until the detachment

A parameter that is useful for the comparison of materials from different categories is the specific wear rate $k = \frac{K}{H}$, since, for example, on elastomer materials the hardness H cannot be defined.

Being fairly simple, Archard's formula is easy to use and applies to a wide range of wear cases, but it has some constraining issues:

1. If K is a constant for a given sliding system, the volume of the removed material should be proportional to the sliding distance L, according to the formula. Although this is experimentally verified for steady sliding conditions, a variation is noticed in the initial sliding phase. This variation depends on the nature of the wear case (pin on disk, ball on flat etc).
2. If the nominal load W changes, the ratio of removed material volume per sliding distance (V/L) should change proportionally (multiplied by K/H). This is not the case for some loading ranges. where it is noticed that the proportion factor is multiplied by x100.
3. In the same logic, a deviation is noticed for the suggested value of wear volume V for some ranges of the sliding velocity and the total contact surface (these factors do not contribute to the formula).
4. For materials with high hardness and/or brittleness the wear rate also depends on the fracture toughness K_c which is not present in the formula.

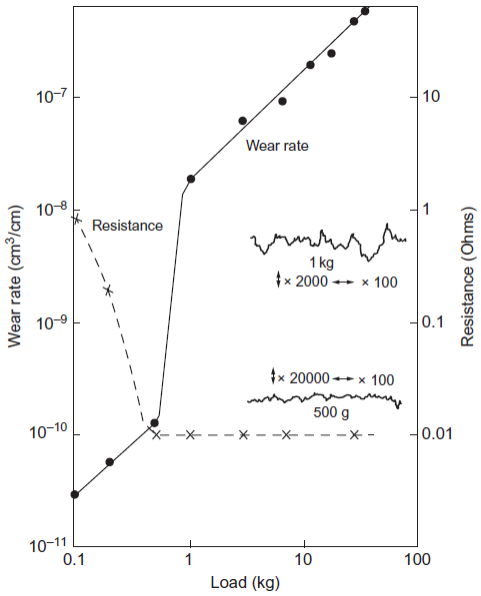

Figure 16 Deviation of the proportion factor K/H in Archard's law, (45)

For the mentioned reasons, it becomes clear that the original equation of Archard is not suitable for every wear model. In order to truthfully describe each of these models, Archard's model is modified respectively. The most prominent wear models are:

1. Adhesive wear
2. Abrasive wear
3. Fatigue wear
4. Chemical - Corrosive wear

3.3 Adhesive wear

Adhesive wear occurs when two nominally flat solid bodies are in sliding contact, whether lubricated or not (45). Adhesion (or bonding) occurs at the asperity contacts at the interface, and these contacts are sheared by sliding, which may result in the detachment of a fragment from one surface and attachment to the other surface.

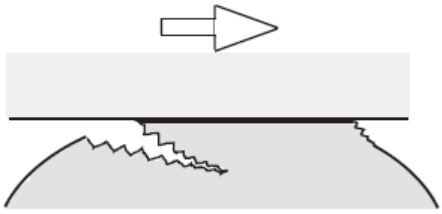

As the sliding continues, the transferred fragments may come off the surface on which they are transferred and be transferred back to the original surface, or else form loose wear particles.

Figure 17 Adhesive wear, (45)

The wear model is described by a variation of Archard's formula (46):

$$V = \frac{K_{ad} W L}{H}$$

Where the wear coefficient's K_{ad} values are in the range of 10^{-8} to 10^{-4} for mild wear and 10^{-4} to 10^{-2} for severe wear. However, this formula is valid for plastic asperity contacts. For elastic contacts the following can be used:

$$V = \frac{K_{ad} W}{E^*(\sigma p / Rp)^{1/2}} L$$

Or

$$V = \frac{K_{ad} W}{E^*(\sigma / \beta^*)} L$$

where E^* is the composite or effective modulus of elasticity, σ_p is the composite standard deviation of the summits of the mating surfaces, $1/R_p$ is the composite mean curvature of the summits of the mating surfaces, σ is the composite standard deviation of surface heights (RMS) and β^* is the correlation length or independence distance.

3.4 Abrasive wear

Abrasive wear occurs when asperities of a rough, hard surface or hard particles slide on a softer surface and damage the interface by plastic deformation or fracture (45).

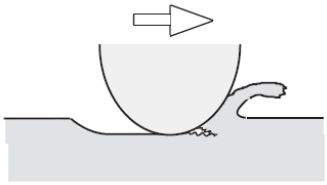

Figure 18 Abrasive wear, (45)

It can be distinguished in two separate cases:

1. Abrasive wear of brittle materials (the weaker material is brittle)
2. Abrasive wear of ductile materials (the weaker material is ductile)

3.4.1 Abrasive wear of brittle materials

In the case of a brittle material, which is indented and ploughed by the abrasive, a wear particle is generated due to mainly brittle fractures caused by initiation and propagation of cracks, such as the median and lateral cracks (46). Therefore, the wear rate of the brittle material is strongly dependent on fracture toughness.

There are two alternative formulas for this model:

$$V = a_3 \frac{W^{9/8}}{K_c^{1/2} H^{5/8}} \frac{E}{H} L$$

and

$$V = a_4 \frac{W^{5/4}}{K_c^{3/4} H^{1/2}} L$$

where K_c is the fracture toughness, E is Young modulus, and α_3 and α_4 are constants that depend on the material.

3.4.2 Abrasive wear of ductile materials

Even in the case of sliding contact between smooth surfaces of the same ductile material, parallel grooves are generally found on the wear surface after sliding. Hard abrasive asperities are formed on the mating surface because of, for example, work hardening, phase transitions, and third-body formation at the contact interface

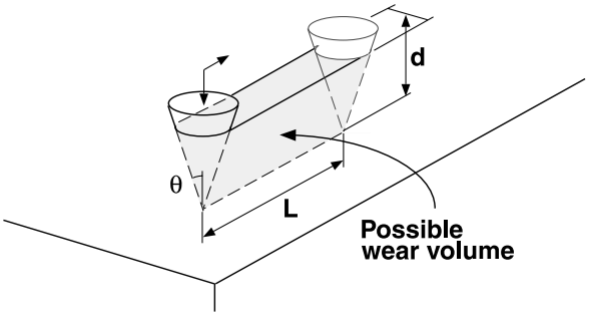

Figure 19, (46)

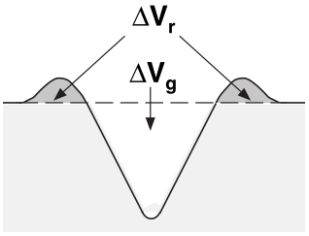

Figure 20 Schematic diagram of cross-sectional profile of groove formed after scratching, (46)

during repeated sliding contact. Therefore, abrasive wear is recognized as a more representative wear mode of ductile material in repeated sliding.

Considering a point contact of a conical asperity, the wear equation is:

$$V = \frac{2}{\pi \tan\theta}\frac{WL}{H}$$

It is important to point out that the equation suffers in some areas:

1. For high nominal loads there is not always a linear relation between the wear volume and the load
2. The wear rate is affected by the size of the abrasive particles, which is not considered in the equation.
3. The roughness of the surface of higher hardness affects the wear rate but it is not included in the formula
4. There are several cases where the sliding distance also affects the wear volume. Such an example is a case of multicyclic RCA abrasion test.

3.5 Fatigue wear

Fatigue wear can be divided in three subcategories:

1. Rolling contact fatigue wear
2. Sliding contact fatigue wear
3. Static fatigue wear

The first two cases include material separation in the form of big shrapnel which are created by cracks on the surfaces after a critical loading cycle number. These large particles create pits on the surfaces. Due to the nature of this wear model, it is more practical to use the loading cycles and the lifespan as calculation parameters, instead of the wear volume.

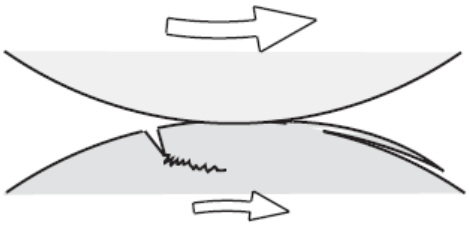

Figure 21 Fatigue wear, (45)

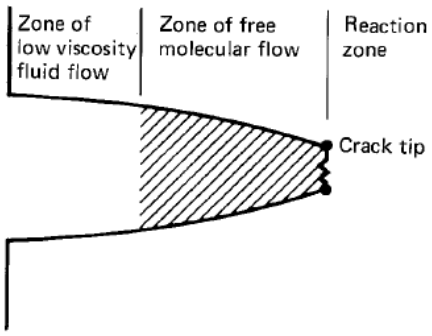

Figure 22 Gaseous flow along interface to tip of brittle crack. (45)

As an example, in the case of bearings, the lifespan in millions of revolutions is:

$$L_{10} = (C/W)^p$$

Where C is the dynamic load, W the equivalent radial or axial load and p is a coefficient (3 for ball and 10/3 for roller bearings)

The static fatigue wear model is not a separate model, but a combination of the previous. Specifically, it appears on the tips of cracks when humidity and tensile stresses are present, mostly on ceramic materials. It acts as a chemical acceleration on the crack propagation. The stress is greatest at the roots (or tips) of small cracks in the material, and consequently the reaction proceeds at its greatest rate from these roots (45).

3.6 Corrosive wear

When sliding takes place, especially in corrosive liquids or gases, reaction products are formed on the surface mainly by chemical or electrochemical interactions. If these reaction products adhere strongly to the surface and behave like the bulk material, the wear mechanism should be almost the same as that of the bulk material. In

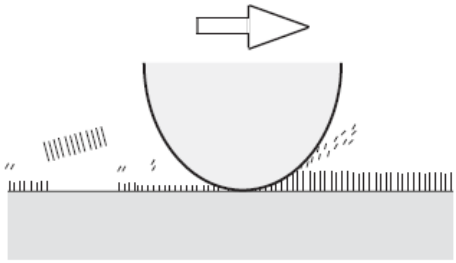

many cases, however, such reaction products behave very differently from the bulk material. Therefore, wear is quite different from that of the bulk material, and is dominated by the reaction products formed by the interaction of solid materials with the corrosive environment. This kind of tribochemical wear accelerated by corrosive media is called corrosive wear (45).

Figure 23 Corrosive wear, (45)

The corrosive wear coefficient is defined differently for metals and ceramics.

For metals:

$$K_{ox} = \frac{\mathrm{dA}}{\xi^2 \rho^2 v} \exp\left(-\frac{\mathrm{Q}}{R_{\mathrm{g}} T}\right)$$

where A is the Arrhenius constant, Q the activation energy, Rg the gas constant, T the absolute temperature, ρ the density of oxide, v the sliding velocity, and L the distance along which a wearing contact is made.

For ceramics:

$$K_{ox} = \frac{A_{\mathrm{c}}}{\rho v} \exp\left(-\frac{\mathrm{Q}}{R_{\mathrm{g}} T}\right)$$

where Q is the activation energy, Rg the gas constant, T the reaction temperature, ρ the density of oxide, and v the sliding velocity.

3.7 Simulation of wear models on the Tribometer

All of the mentioned wear types and their subcategories can be effectively simulated on the designed multi-tester. Abrasive and adhesive wear can be tested in standardized configurations like Pin-on-Disk or Ball-on-Flat, using brittle or ductile material specimens, in lubricated or dry conditions. Fatigue wear can also be replicated in high-cycling applications of the mentioned testers, and corrosive wear can be simulated by introducing certain mildly corrosive liquids to the machine.

4 Testing Apparatus Standards and Design Requirements

There are several testing devices in the industry that measure the tribological aspects of specimens, by implementing standardized simulations. There are many variations of these machines and the most commonly acquired testing data include: wear rate, wear volume, friction coefficient and hertzian contact pressure. Some machines provide some modularity and they can accommodate more than one testing configurations.

Some widely used tribometers include:

1. Pin-on-Disk Wear Testing Apparatus
2. Ball-on-Flat Sliding Wear Apparatus
3. Block-on-Ring Wear Test Apparatus

There are also some variations of the above, like:

1. Disk-on-Disk Wear Testing Apparatus
2. Pin-on-Vee Wear Testing Apparatus
4. Ball-on-Disk Wear Testing Apparatus
5. Twin Ring Tester

The tester of this assembly can successfully replicate Pin-on-Disk, Ball-on-Flat, Block-on-Ring, Disk-on-Disk and a custom Single clutch disk test rig. The wear test rigs measure wear characteristics on standardized specimens. Yet, there are testers that include whole machine elements, like automotive clutches or industrial brakes, instead of just the friction material which is used in a simple Disk-on-Disk tester. In this case, the testers are much larger and much more complex devices. Due to this complexity though, the most common wear testing method of a new clutch texture/material is still the Pin-on-Disk or Disk-on-Disk apparatus. A tribo-tester for an automotive wet clutch is standardized by the JASO M348-2012 or the SAE No.2 standards. Among others, the testing parameters that are measured in these machines are: sliding speed, contact surface, contact pressure, temperature, oil flow and static and breakaway friction coefficients. Values like the minimum surface contact size are also specified, to take into account the uneven clutch surface composition and the channeling effect of surface roughness and porosity. There are variations on these larger scale machines that allow for the measurement of other features than the tribological characteristics, like oil flow related phenomena on impact and multi-flow simulating clutch testers. The standalone clutch tester of this thesis, focuses on these phenomena. This means that, while the wear properties can be tested only on the Disk-on-Disk apparatus, the rest of the clutch operational parameters can be tested on the single clutch tester configuration, without the compromises in terms of complexity and available space that appear of the commercial SAE No.2 complying machines.

Figure 24 Model 3100 SAE No. 2 Test Stand by © 2020 LINK ENGINEERING COMPANY

4.1 Pin-on-Disk Wear Testing Apparatus

Wear testing with a Pin-on-Disk apparatus is standardized by ASTM G99 – 17. The specimens used have the form of a pin and a disc. The typical pin specimen is cylindrical or spherical in shape. Typical cylindrical or spherical pin specimen diameters range from 2 to 10 mm. The typical disk specimen diameters range from 30 to 100 mm and have a thickness in the range of 2 to 10mm. There is a variation (not standardized) of this test, called Ball-on-Disk or Four-Ball testing where multiple spherical specimens are applied on a disc, in order to simulate the wear behavior of surfaces on a ball bearing. The pin specimen is vertically applied on a specific radius on the surface of the disk, while the disc is rotating with a specific speed, typically in the range of 60 to 600rpm. The pin specimen is pressed against the disk at a specified load usually by means of an arm or lever and attached weights. Other loading methods have been used, such as hydraulic or pneumatic. The orientation of the pin and disk assembly can be either vertical or horizontal. Also, the test can take place in dry or lubricated environment.

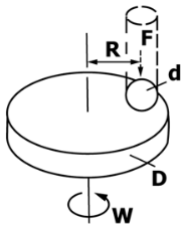

Figure 25 Schematic representation of a Pin-on-Disk Wear Testing Apparatus, (47)

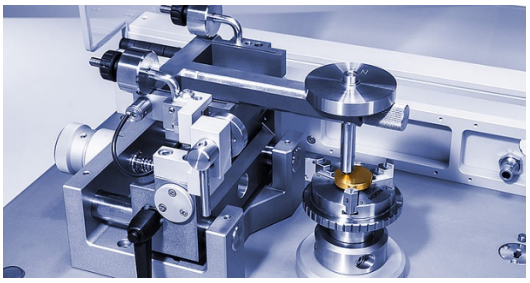

Figure 26 Vertical application of a Pin-on-disk tribometer by Anton Paar GmbH

If linear measures of wear are used, the length change or shape change of the pin, and the depth or shape change of the disk wear track are determined by any suitable metrological technique, such as electronic distance gaging or stylus profiling. It is not recommended that continuous wear depth data obtained from position-sensing gages be used because of the complicated effects of wear debris and transfer films present in the contact gap, and interferences from thermal expansion or contraction. Instruments to obtain linear measures of wear on this testing method should have a sensitivity of 2.5μm or better. The system may have a friction force measuring system, for example, a load cell, that allows the coefficient of friction to be determined.

A Pin-on-Disk machine is equipped with a revolution counter that records the number of disk revolutions. The temperature of one or both specimens at locations close to the wearing contact is recorded during the test. Also, the atmosphere (laboratory air, relative humidity, argon, lubricant, and so forth.) surrounding the wearing contact is recorded. The mass loss of the test specimen is measured by means of a balance which has a sensitivity of 0.1 mg or better (47).

The tester of the designed multi-tester will abide by the standard, having the following specifications:

Pin-on-Disk	
Spec	**Value**
Pin specimen diameters	2mm-10mm
Disc specimen diameters	30mm-100mm
Disc rotational speed	600rpm
Applied force	No recommendation by standard, up to 2600N
Oil Temperature T	No recommendation by standard, 150°C
Force control	within a maximum deviation of +/- 2.0 % of the test load, depending on the selected spring

4.2 Ball-on-Flat Sliding Wear Apparatus

Linearly reciprocating Ball-on-Flat sliding wear testing is standardized by ASTM G133 − 05 (Reapproved 2016). It consists of two specimens, a ball shaped pin acting against a flat static surface. The oscillating motion

of the pin differentiates the results of this type of test from the rest where the motion takes place only in one direction (i.e. on a Pin-on-Disk tester), even for comparable durations of contact.

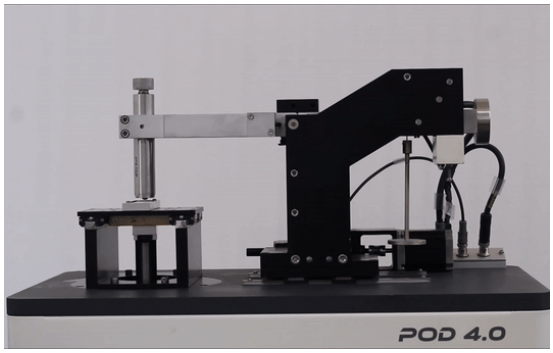

Figure 27 Ball-on-Flat application on a multi capability tribometer POD 4.0 of Ducom Instruments

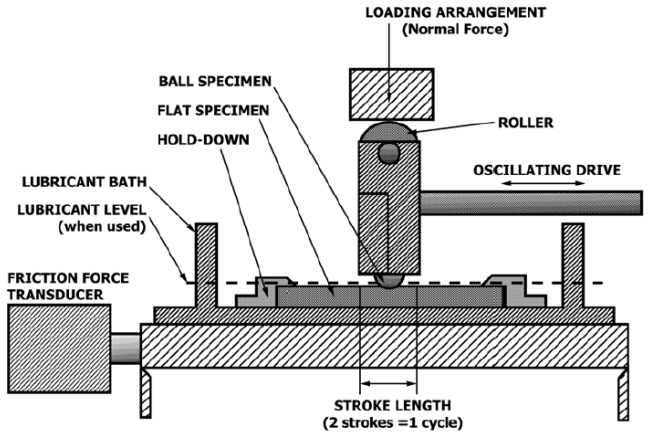

Figure 28 Schematic representation of a Ball-on-Flat Sliding Wear Testing Apparatus, (48)

A Scotch yoke drive mechanism can provide a smooth, sinusoidal velocity profile for the ball specimen relative to the flat specimen without the need for the motor to stop and reverse direction periodically. Stepper-type motors can also be used provided that the motion is smooth and uniform.

A tension-compression load cell or similar force-sensing device may be used to measure the friction forces generated during sliding. Calibration of the friction force in both forward and reverse sliding directions is required. The load applied to the specimen is checked periodically. In machines which apply the load by a spring/lever arrangement and indicate the load on a dial age, this can be done by substituting a previously calibrated compression load cell for the specimen and checking the applied load indicated on the loading dial against the calibrated load cell output. The ambient temperature is measured and reported during room temperature tests, while in full immersion, liquid-lubricated tests, the bath temperature is measured and reported. The temperature is also controlled to within a maximum deviation of +/- 2.0°C from the desired value. Afresh supply of lubricant is used for each test unless the objective is to evaluate the effects of used lubricants on friction and wear.

Pin scar measurements can be made by removing the ball specimen holder and placing the wear scar portion under a reflecting microscope. For lubricated tests in which the wear is minimal, it is possible to be misled in reading the apparent wear scar diameter of the ball tip optically because of elastic recovery. A small, shallow annulus surrounding the elastically deformed area may give the impression of wear, whereas little or no appreciable wear has actually occurred. Profilometry may be used to determine whether the wear scar is flat (48).

The wear test rig of this thesis will be able to simulate the two standardized procedures, according to the ASTM G133 − 05 standard. There are two different testing procedures, one for lubricated conditions and one for dry conditions:

Procedure A (dry conditions)

- Pin tip radius, 4.76 mm (3⁄16 in.),
- Normal force, 25.0 N,
- Stroke length, 10.0 mm,
- Oscillating frequency, 5.0 Hz,
- Test duration, 16 min 40 s (sliding distance 100 m),
- Ambient temperature, 22 +/- 3°C,
- Relative humidity, 40 to 60 %, and
- Lubrication, none applied

Procedure B (lubricated conditions)

- Pin tip radius, 4.76 mm (3⁄16 in.),
- Normal force, 200.0 N,
- Stroke length, 10.0 mm,
- Oscillating frequency, 10.0 Hz,
- Test duration, 33 min 20 s (sliding distance 400 m),
- Temperature, 150 +/- 2°C,
- Relative humidity, 40 to 60 %, and
- Lubrication, full immersion under the selected lubricant

4.3 Block-on-Ring Wear Test Apparatus

Block-on-Ring wear testing is standardized by the ASTM G77-17 standard. In this testing method the small block specimen is vertically applied on the outer surface of the ring specimen. This configuration is ideal for modeling applications that suffer from abrasive wear due to the presence of third body particles in the contact surface, for example in a train wheel and rail interaction. The test ring has an outer diameter of 34.99 +/- 0.025 mm and the block width is 6.35 + 0.000, −0.025 mm.

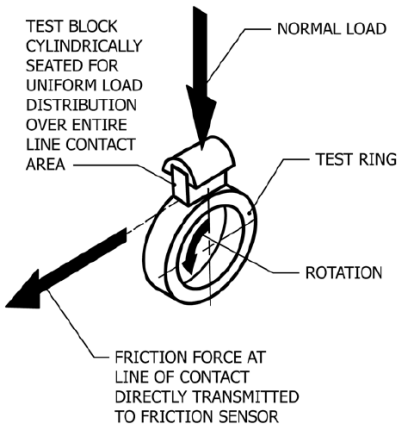

Figure 29 Schematic representation of a Block-on-Ring Wear Test Apparatus, (49)

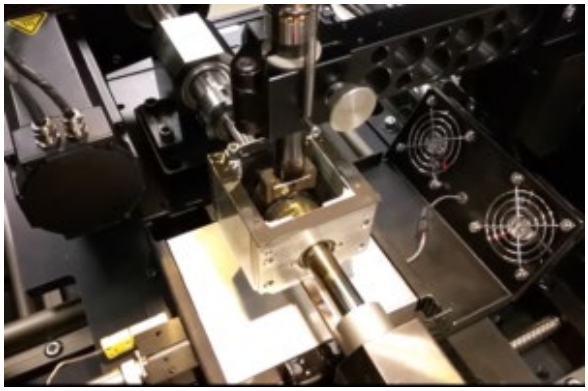

Figure 30 Block-on-Ring Wear test rig by ST Instruments B.V.

If the loading is applied step by step, the testing starts with no weights, then a 133-N (30-lbf) load is added every 200 revolutions until the required test load is reached. If the required load is less than 133 N, the load is applied in one step. During the test, the friction force, lubricant or block temperature, are recorded, and, if desired, the vertical displacement of the block. For the wear measurements, the scar width is calculated on the test block in the center and ~1 mm away from each edge, to the nearest 0.025 mm. The average of the three readings is recorded (49).

The designed tester will abide by the standard, having the following specifications:

Block-on-Ring	
Spec	**Value**
Block specimen width	6.35mm
Ring specimen diameter	34.99mm
Disc rotational speed	No recommendation by standard, up to 600rpm
Applied force	No recommendation by standard, up to 2800N
Oil Temperature T	No recommendation by standard, 150°C
Force control	No recommendation by standard

4.4 Disk-on-Disk Wear Testing Apparatus

Since this type of test doesn't follow some standard, the requirements are defined according to the maximum allowed loads and sizes of the existing configuration. Thus, the specifications are:

Disk-on-Disk	
Spec	**Value**
Disc specimens diameters (max)	192mm
Disc rotational speed	up to 600rpm
Applied force	up to 2800N
Oil Temperature T	150°C
Force control	within a maximum deviation of +/- 2.0 % of the test load, depending on the selected spring

4.5 Open Clutch Single Disc lubrication testing Apparatus

The differentiating factor on this type of test when compared to the other mentioned testers is that it doesn't measure the wear characteristics of a disk clutch. Instead, it can simulate wet clutch phenomena like Drag torque, Multi-phase flow and Wobbling. When the clutch is in disengaged condition, ideally no torque should be transmitted. However, in reality, the relative motion between the disks causes viscous shearing of fluids in the gap. This results in a drag torque which is considered as a loss. The operations of the tester are defined by the examined phenomenon to Multi-phase flow tester and Wobble effect tester. The designed clutch tester will have the ability to simulate both phenomena, by changing the attachment method of the clutch disk on the rig.

4.5.1 Multi-phase flow Configuration

Multi-phase flow is the behavior of the flow at a high rotational clutch speed. At a specific differential speed, the conveying capacity of the disc reaches the oil flow rate and a maximum drag torque is reached. Starting at this speed, air is sucked into the grooves due to the negative pressure on the outer radius area, which causes an immediate sharp drop of the drag torque in most cases.

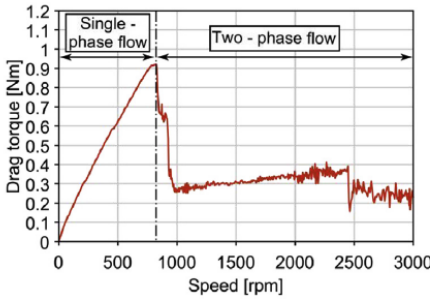

Figure 31 Drag torque curve progression and flow states for linear run (50)

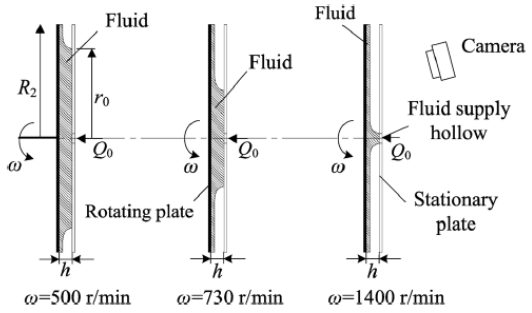

Figure 32 Flow pattern in the clearance at different rotating speeds of the clutch (51)

The introduction of air in the system is visible on testers where the disc opposite to the clutch is made of a transparent material and its progression along with the increase of the rotational velocity can be recorded by a high-speed camera.

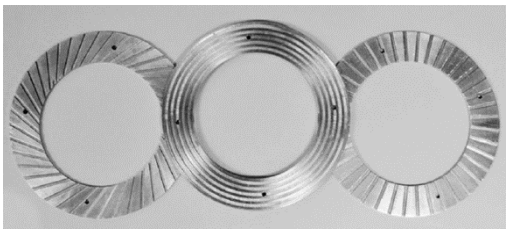

Figure 33 Three pattern groove plates (51)

Parameters that affect Multi-phase flow and generally need to be tested are the design features of the clutch disc surface. For example, the groove design and quantity of a clutch has a significant influence on this transition speed.

For this procedure, the tester will be able to operate under the following specifications:

Multi-phase flow Configuration	
Spec	**Value**
Clutch disc diameter range (Din-Dout)	95mm-192mm
Disc rotational speed	4770rpm
Clearance distance h	0.05mm
Oil supply Q	up to 2.5 l/min
Oil Temperature T	90°C

The experiment can be recorded by a high-speed camera, located opposite the transparent disk of the test rig.

4.5.2 Wobble effect Configuration

In applications of multi-plate wet clutches that rotate at high speeds a Wobble effect is noticed:

1. Local vacuum is formed due to negative pressure where the oil film ruptures
2. The local vacuum draws the discs close to each other resulting in high-frequency mechanical contacts
3. The drag torque rises at high values during the contact periods

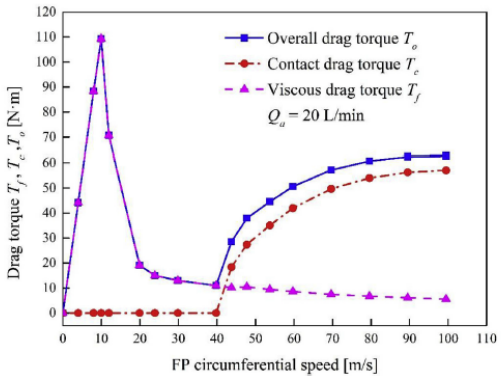

Figure 34 The effect of the disk collision on the drag torque of the plate (52)

There are different specifications for this configuration, depending on the needed clearance of the operating parameters. The reason there are separate optimal cases is that the parameters of this configuration are interlacing with each other and the durability of the machine should not be exceeded.

Wobble effect Configuration for minimum clearance distance h	
Spec	**Value**
Clutch disc diameter range (Din-Dout)	95mm-192mm
Disc rotational speed	800rpm
Clearance distance h (min)	0.2mm

Frequency (max)	50Hz
Oscillation width A (max)	0.1mm
Oil supply Q	up to 2.5 l/min
Oil Temperature T	90°C

Even smaller clearance can be achieved for lower frequency values. The smallest clearance is at 0,1mm, with 10Hz and 0,1mm oscillation width.

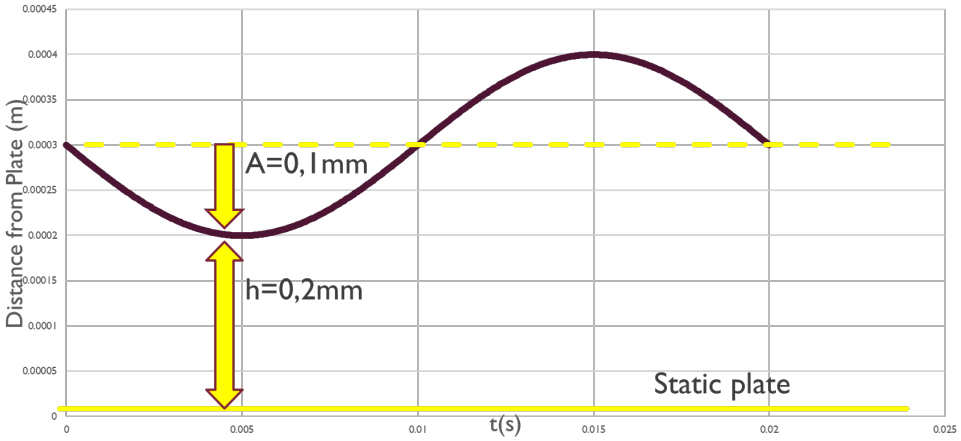

Figure 35 Considering a static disk opposite the clutch disk, this graph depicts the position of the clutch disc (purple line) for a full period of the oscillating linear motion

Wobble effect Configuration for maximum oscillation width A	
Spec	**Value**
Clutch disc diameter range (Din-Dout)	95mm-192mm
Disc rotational speed	800rpm
Clearance distance h (min)	0.3mm
Frequency (max)	50Hz
Oscillation width A (max)	0.6mm
Oil supply Q	up to 2.5 l/min
Oil Temperature T	90°C

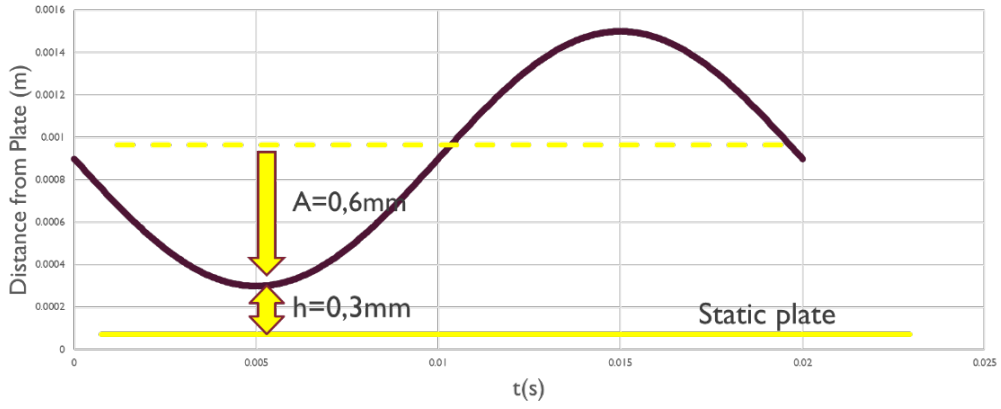

Figure 36 Considering a static disk opposite the clutch disk, this graph depicts the position of the clutch disc (purple line) for a full period of the oscillating linear motion

Compared to other clutch disk testers in the industry, this design offers the unique feature to be able to simulate a linear reciprocating motion with the use of a servo motor. This way the Wobble effect can be simulated even with a stationary shaft (no rotational velocity), and the eigenvalues of the disk can be further investigated.

Specifications	Prototype	Otto von Guerick University	State Key Laboratory	Beijing Institute of Technology	Technical University of Munich
Clutch disc diameter range (max)	95mm-192mm	220mm	120mm (in experiment)	N/A	250mm
Disc rotational speed	4770rpm (800rpm in config. 2)	3000rpm	240rpm (in experiment)	5,000rpm (and 3,000 rpm)	3,000rpm
Clearance distance h (min)	0.1/0.2/0.3mm	0.05mm	0.15mm (in experiment)	Fixed	Fixed
Frequency (max)	10/50/50Hz	-	-	-	-
Oscillation width A (max)	0.1/0.1/0.6mm	-	-	-	-
Oil supply Q	up to 2.5 l/min	0.05 l/min – 2.5 l/min	0.01 l/min – 1 l/min	N/A	N/A
Oil Temperature T	90°C	30°C – 90°C	Only controlled at +/- 2 °C	N/A	N/A
Features	Visual inspection, Drag torque measurement, Impact detection, Forced vibrations	Visual inspection, Drag torque measurement	Visual inspection, Drag torque measurement	Visual inspection, Drag torque measurement, Impact detection	Drag torque measurement,

5 Multi Tester Design

5.1 Description

This multi-tester was created under the environmentally friendly scope of taking advantage of used machinery equipment. For this reason, the two main testers, the wear test rig and the single clutch disc tester were designed to be installed on the same existing frame.

Figure 37 The internal structure of the old machine

The parts from the previous machine that were maintained in the design include the external panels, all the structural beams of the frame, a base plate for the motor that has adjustable height for belt tensioning, the base plates for the oil circulation and heating system and lastly the table plate.

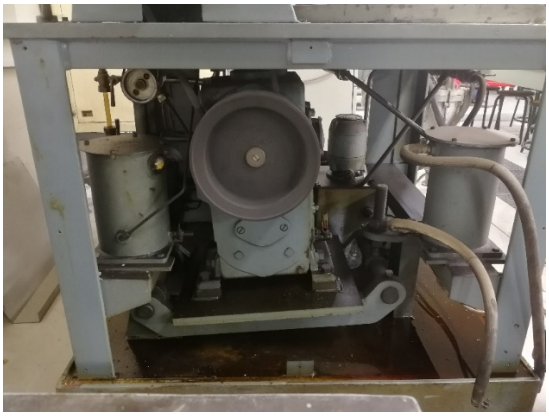

Figure 38 The internal structure. The leveling bed of the motor and the side bases are included in the new design

Figure 39 The side panels

Since the design process started, many parts of the assembly have changed in order to overcome manufacturing, operational of cost related difficulties.

The two test rigs are placed on top of the structural frame, when the oil circulation/heating system is placed inside the frame, with pipes leading to each tester.

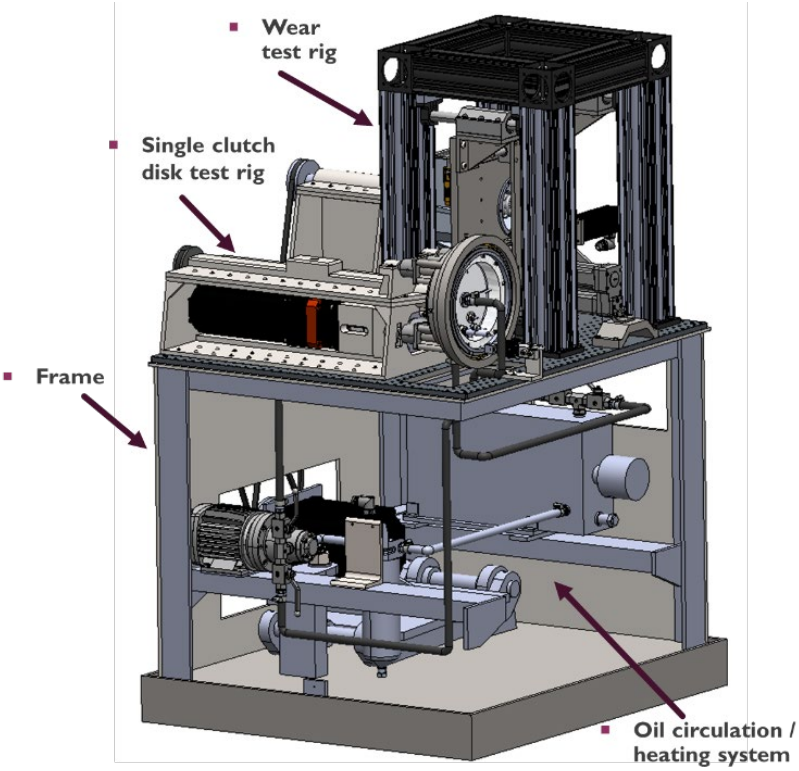

Figure 40 Main parts of the assembly

5.2 Design Steps of the Wear Testing Assembly

Initially, the wear testing apparatus and especially the assembly of the linear motion of the specimens was much more complicated. It was designed to provide to the specimen linear motion in three axes. This was accomplished by the use of eight rectangular profile rail guides and the combined use of seven stepper motors. The main drawbacks of this design were the difficulty to combine and synchronize the simultaneous operation of the stepper motors (the motors were used for the motion of each axis in pairs) and the added assembly complexity. More specifically, the pairs of the profile rail guides have a strict perpendicularity assembly tolerance, which makes the assembly more difficult, especially when each subassembly is affected by the positioning of its parent assembly.

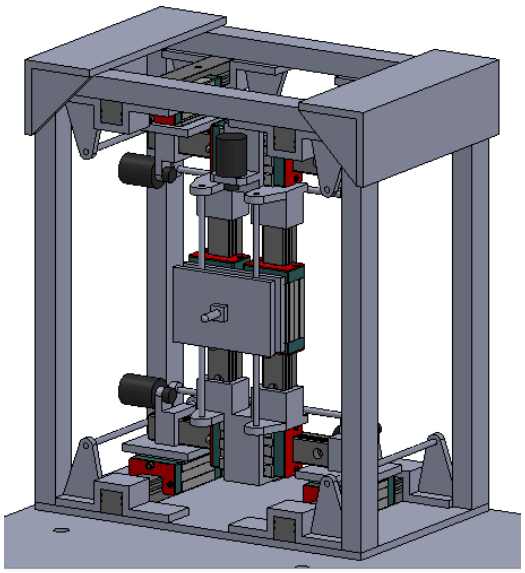

Figure 41 The initial design of the wear tester with multiple profile rail guides and stepper motors.

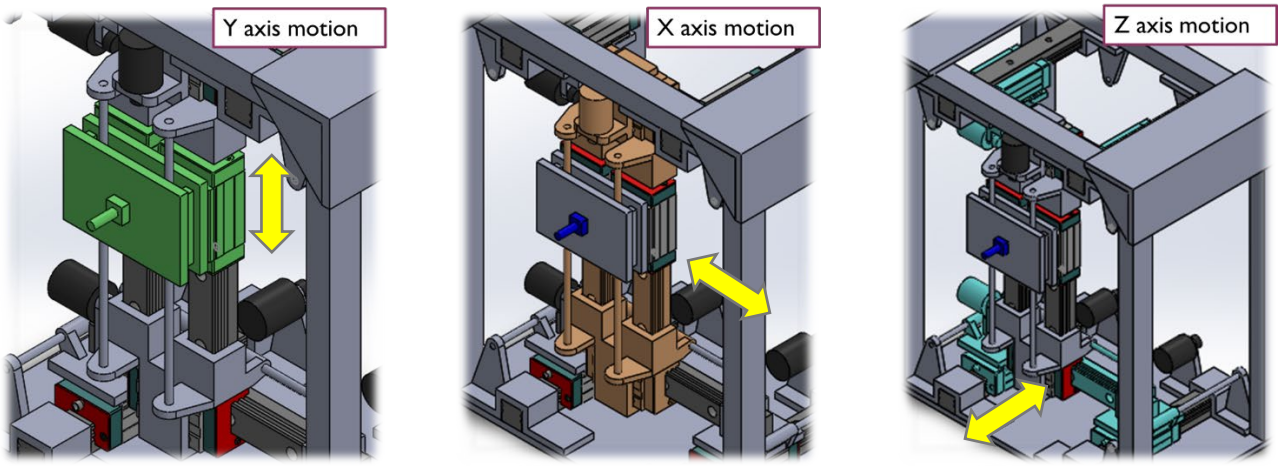

Figure 42 Parts participating in the linear motion of the specimen in X,Y and Z axes

To resolve these issues, the profile rail guides were replaced by round rail linear guides except for one single acting profile rail guide which was positioned inside the oil hub. Also, the total number of the guides was reduced, due to the application of a metal plate in the back of the oil hub, which provided greater stiffness and rigidity to the assembly. the number of the motors was reduced too, retaining one motor for each motion.

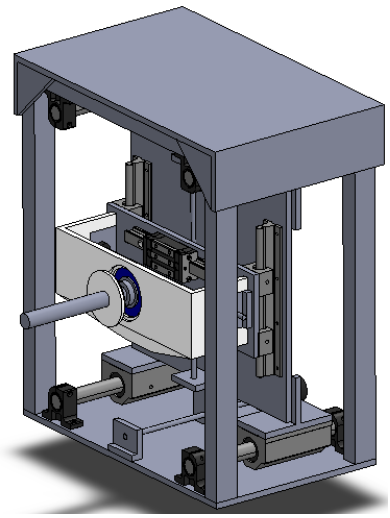

Figure 43 Reduction in the total number of motors and guides

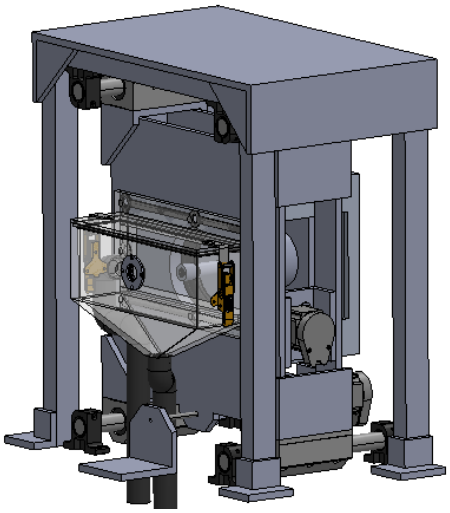

Figure 44 Addition of a collet chuck and merge of the back plate to the oil hub

The next set of changes included the addition of a collet chuck assembly that clamps the specimen, instead of the conventional attachment with bolts. This change was made for the better usability of the tester. For the same reason, a set of toggle latches were attached on the oil hub which release the top lid, in order to apply or remove the specimens inside the hub. The parts responsible for the vertical motion were removed, since they needlessly added to the complexity: the horizontal motion is sufficient for all the movements required for the tests. For example, in the Pin-on-Disk test, it makes no difference of the pin is radially located on the disk on the horizontal or vertical direction. Consequently, the total number of motors is reduced to just two. Also, in this configuration the supportive metal plate was merged with the back of the oil hub, to reduce the interfering parts. The guides and the motor for the linear radial motion were moved to the back of the plate. A rubber bellow was also applied on the back of the plate to seal the inside of the hub, when still allowing movement to the specimen.

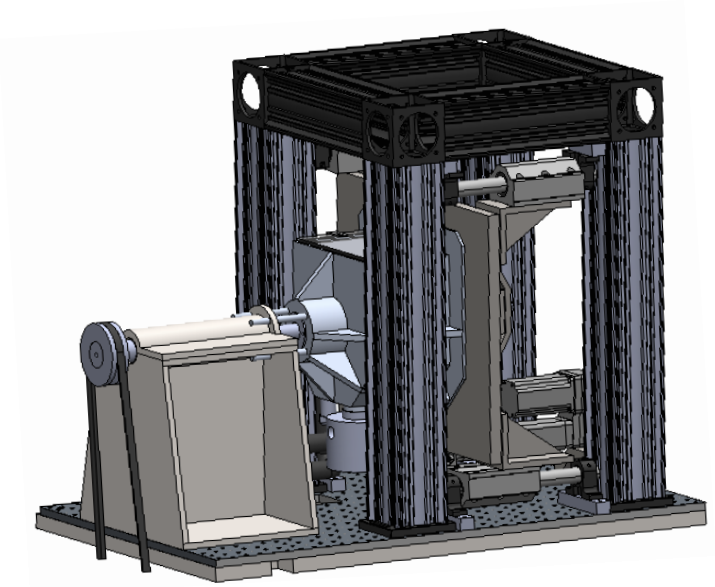

Figure 45 Final assembly with the addition of dowel pins and precision structural beams

This design was maintained in the final edition, with the difference that the structural beams were replaced with wide, precision construction rails, used in optomechanical applications, in order to increase the rigidity of the assembly. Finally, a pair of four dowel pins were attached on the oil hub. These pins are used for the more accurate centering between the assembly on the linear motion and the assembly of the rotational motion, as they enter four openings on the metal piece surrounding the shaft, while the linear motion assembly is moving forward.

5.3 Final Design of the Wear Testing Assembly

The compartment of the machine that will conduct the wear tests is a multi-tester by itself. It will be able to conduct the following standardized tests:

1. Pin-on-Disk (ASTM G99 − 17)
2. Ball-on-Flat (ASTM G133 − 05)
3. Block-on-Ring (ASTM G77 – 17)
4. Disk-on-Disk (non standardized clutch friction disc test)

All these tests will be conducted in the same space, under dry or lubricated conditions, with controlled environment. After testing, the specimen parts will be removed and placed on suitable measuring stations in order to retrieve the needed wear data. The various needed motion profiles for these tests are achieved by a system of linear guides and motors on one side and another system for the rotary motion on the other side.

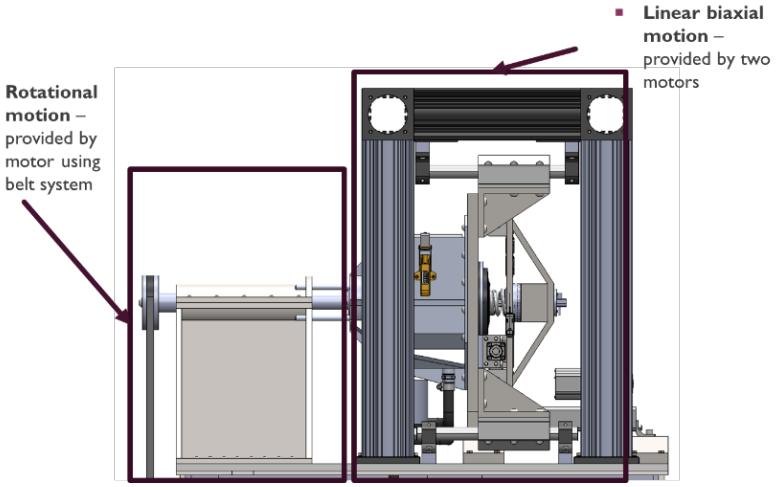

Figure 46 The assembly responsible for the rotational motion and the assembly responsible for the linear biaxial movements

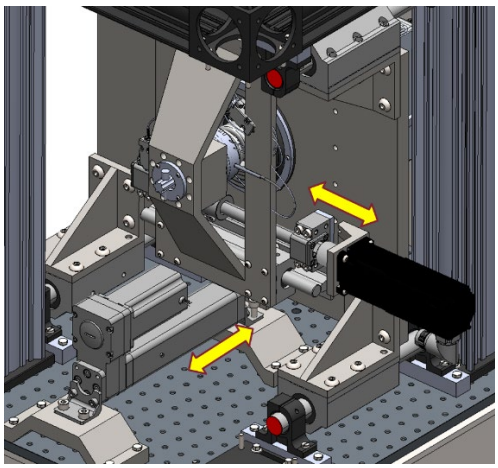

Figure 47 The central actuator moves the vertical rectangular plate, compressing and depressing the springs and the side mounted motor is used for the radial motion for example during the Ball on Flat test

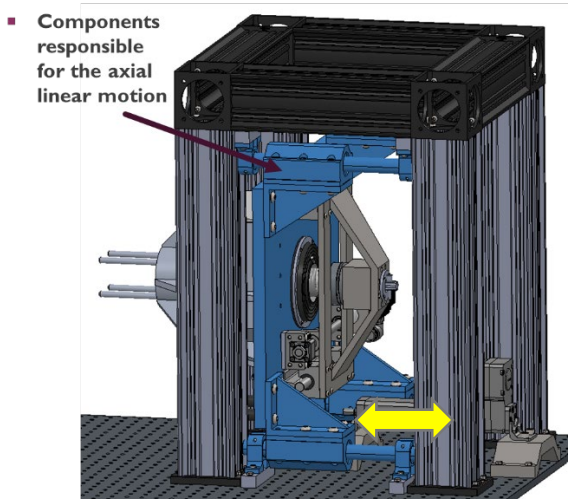

Figure 48 The parts of the subassembly that move along the axial linear motion

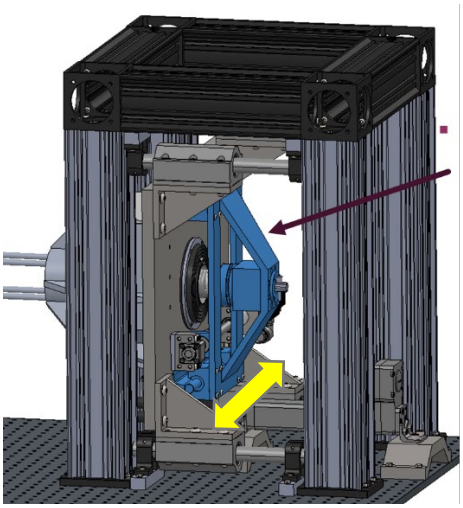

Figure 49 The parts of the subassembly that move along the radial linear motion

On the Rotary motion subassembly, the following specimens can be placed, depending on the testing apparatus (whether they are static or rotating during the test):

- Disc rotation (Pin-on-Disc)
- Flat surface attachment (Ball-on-Flat)
- Ring rotation (Block-on-Ring)
- Disc rotation (Disk-on-Disk)

On the Linear motion subassembly, the following specimens can be placed:

- Pin attachment (Pin-on-Disc)
- Ball reciprocating motion (Ball-on-Flat)
- Block attachment (Block-on-Ring)
- Disc attachment (Disk-on-Disk)

On each test a different motion/position combination is used for each specimen

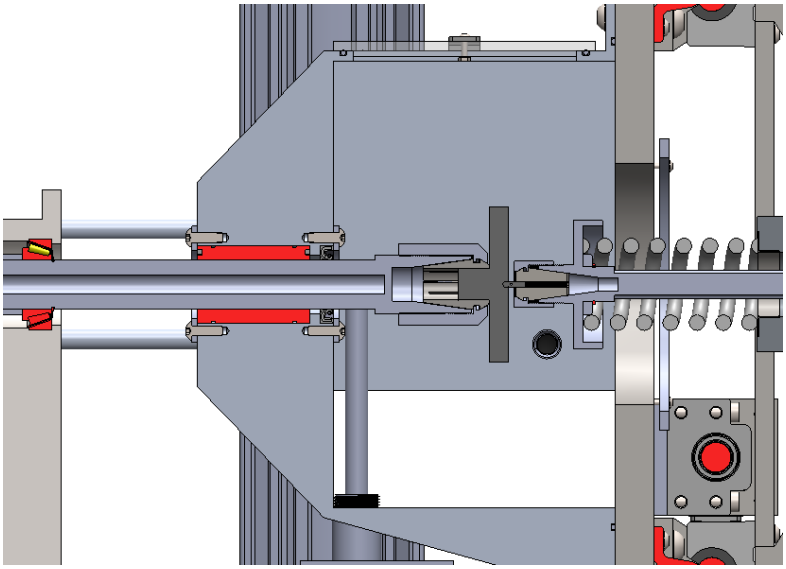

Figure 50 The configuration of the Pin-on-Disk wear test rig apparatus. The disk rotates and the pin is pressed by a spring mechanism on a specific radius of the disk

Table 2 Different configurations of the wear test rig for each test

	Specimen 1 (form/motion/position)	Specimen 2 (form/motion/position)
Pin-on-Disk	Disc/rotating/centrally located	Pin/stationary/on specified radius along the disc
Ball-on-Flat	Flat surface/stationary/centrally located	Ball/reciprocating linear motion/along a specified radius on the flat surface
Block-on-Ring	Ring/rotating/centrally located	Block/stationary/on specified position, vertically on the perimeter of the Ring
Disk-on-Disk	Disc 1/rotating/centrally located	Disc 2/stationary/centrally located

The specimens can be attached to the tester by means of collets which means that i.e. for the case of a disk specimen, there should be a cylindrical detail on its back to allow the connection.

The requirements for the force control for the tests are satisfied by using a system of springs acting along with the linear motion provided by the motors. The springs are interchangeable as there is a specific needed force value for each case. This way, the nominal applied force value is maintained unchanged during the material removal, as the motor pushes the spring/specimen assembly during the test, by calculated steps.

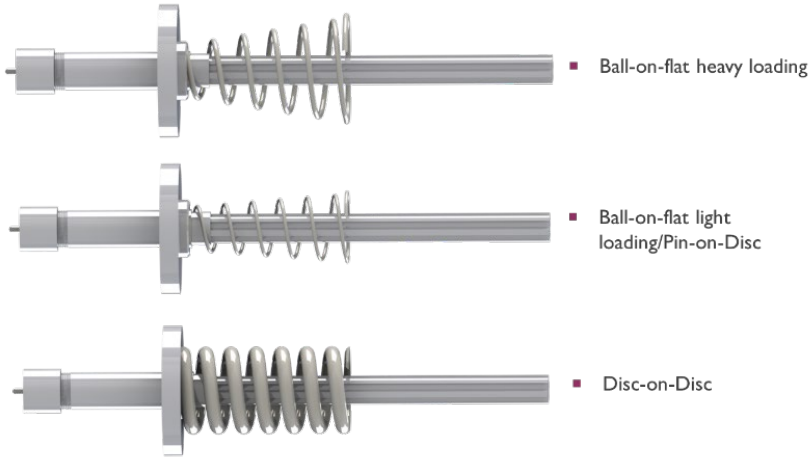

Figure 51 Different springs of the same length are used to apply the nominal force on the specimens

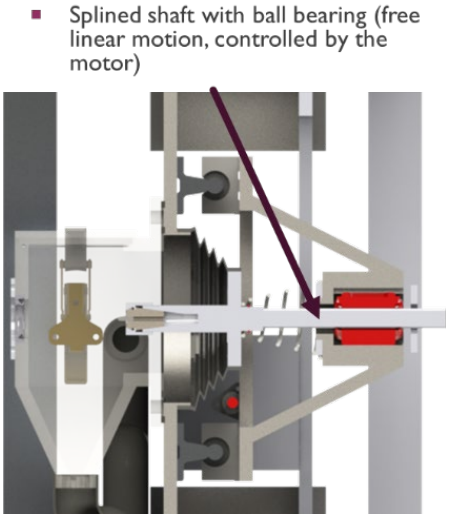

Figure 52 The location of the spline of the shaft and the splined ball bushing

The shaft on which the spring is applied holds the specimen. On the other end of it, it has a splined detail which allows its attachment on a splined linear ball bushing, since the rotation of the shaft must be fixed. The oil hub, where the tests take place, needs to be sealed. For this reason, a rotary seal is applied where the shaft of the rotary specimen enters the hub. Right behind this seal there is a ball bushing that will allow the axial linear motion of the oil hub, relative to the shaft. Also, on the side of the other specimen, a conical rubber bellow is applied. It connects the shaft to the back plate which is tangentially located on the side of the oil hub. This bellow allows the biaxial motion of the shaft which is needed for the force control with the springs and for the radial placement of the pin specimen for instance.

Inside the hub there is another heating element for a further increase of the oil temperature. This heating element acts additionally to the heating element inside the oil storage to protect the elements of the oil circulation system from extreme temperatures. This way the highest temperature is only achieved inside the closed oil hub, which can even be isolated from the circulation system by means of valves. This allows the further increase of the temperature of the lubricant oil to a total maximum of 150^{o}C.

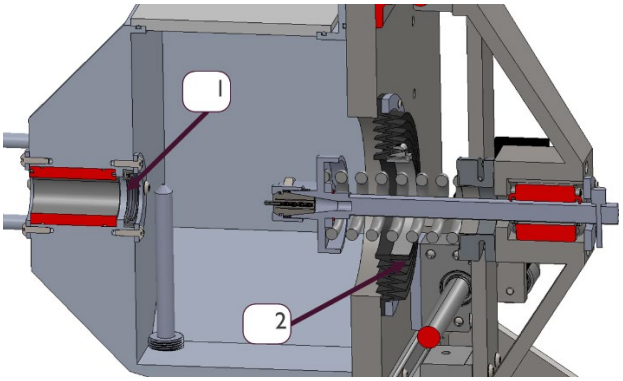

Figure 53 The rotary seal and the rubber bellow (in resting position)

The angular speed and the total revolutions of the rotary specimens are measured by the use of an encoder on the main servo motor of the assembly.

In order to verify that the wear tests follow the standards and they don't deviate in any of the values of the required test parameters, control sensors have been placed on the assembly, inside the oil hub. The sensors inside the hub are:

1. Compression Force sensors
2. Ambient temperature/humidity sensor
3. Temperature sensor for the specimen contact
4. Inductive eddy current distance measurement sensors

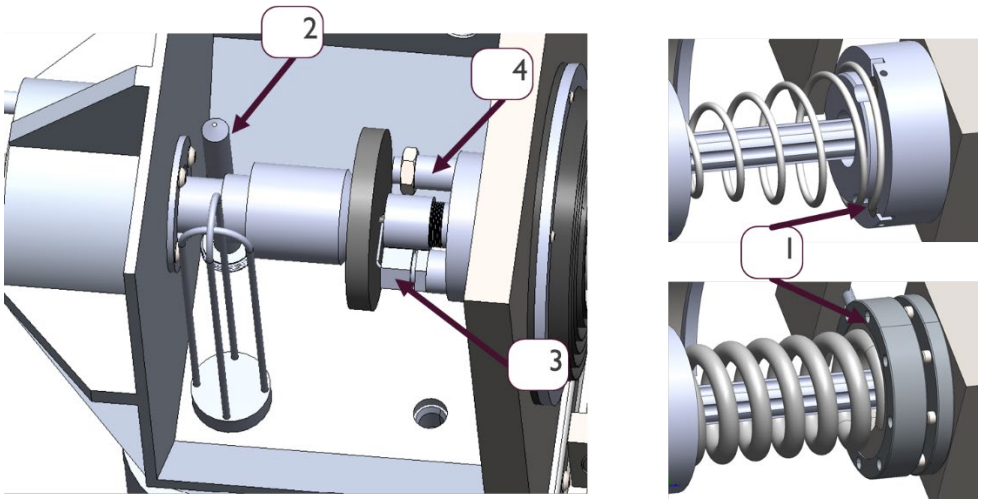

Figure 54 All the sensors of the wear multi-tester

The force sensors [1] have been placed directly behind the loading springs. There are two different force transducer configurations used, to accommodate for the different diameters of the springs. In the case of the spring for the disk-on-disk test, the force sensor is a single cylindrical cell with a capacity of 5kN to accommodate for the high testing loads and an accuracy of ± 12,5N. For the rest of the tests where the loads are smaller and the springs have different diameters, a different combination is used. A steel adaptor part is placed behind the spring, and three smaller button force transducers are placed inside three sockets, touching the surface of the springs. These button force transducers have a rated capacity of 220N to and an accuracy of ± 0.5N. The requirement for this sensor is to satisfy the needed accuracy of the dry testing of the Ball-on-Flat test, where the nominal force is 25N and the needed control accuracy is 2% of the load, or 0,5N.

A probe that measures the ambient environment [2] is placed behind the disk specimen. It measures temperatures from -70 to +180 °C and relative humidity in the entire range between 0 to 100 % RH.

On the other side of the small specimen, a temperature probe [3] is placed. This sensor is made of a semi-flexible material and it will be inserted on a hole cut out of the specimen itself, in order to accurately measure its temperature. Like the distance sensor it is water tightly applied on the shaft. It has a temperature range from -200 °C to 160 °C and a calibration accuracy of ± 0.05 °C.

There is a no-contact distance eddy current sensor [4] for the measurement of the distance between the specimens. It can potentially be used for the wear groove depth of the specimen opposite to it, but it is not the best practice, since the measurement from non-contact sensors can be affected by debris inside the groove. This sensor is placed right next to the small specimen (i.e., the pin) and it is water tightly applied on the shaft. It has a resolution of 0.04μm.

5.4 Design Steps of the Open Clutch Single Disc Lubrication Testing Assembly

The initial design for the Single clutch disk test rig included a precision worm gear screw mechanism powered by a stepper motor to control the clearance between the clutch disk and the stationary disk. As the worm gear rotated, a thread located on the back of the enclosure would move the stationary disk forwards or backwards. Only the drag torque of the clutch disk was measured by a torque transducer located on the rotary shaft.

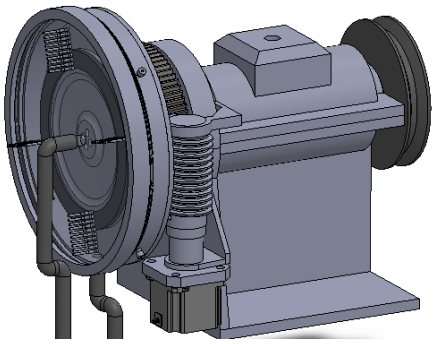

Figure 55 The initial design

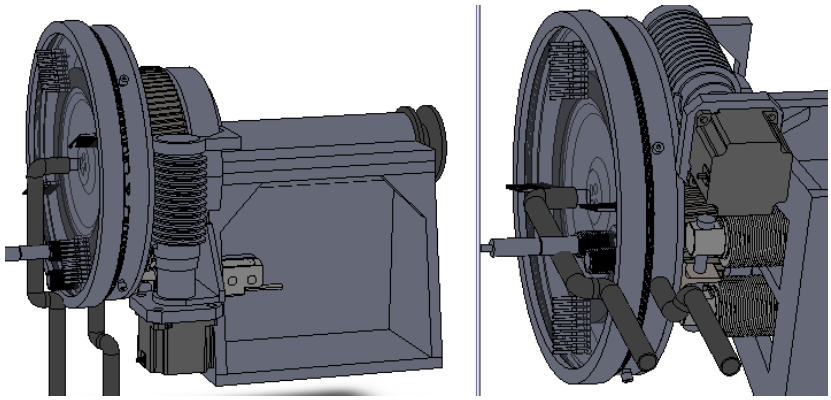

Figure 56 Reinforcements on the body of the assembly

Early eigenfrequency FEA showed that the assembly needed some extra rigidity, so the main body was further reinforced. A pair of loadcells were introduced for the drag torque measurement of the static plate, placed on the back of the enclosure.

This mechanism was found to suffer in the case of high frequency directional changes that were needed for the oscillation motion. Another drawback was that the drag torque measurement would not be accurate, since it was measured on the back of the oscillating enclosure, and most of it would be received by the worm mechanism instead of the loadcell. For this reason, the worm gear was replaced by a servo motor and lead screw assembly. The enclosure was supported by four round rail guides.

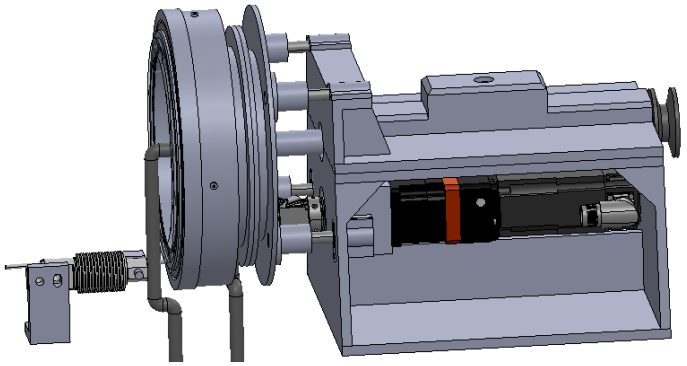

Figure 57 Change in the reciprocation motion mechanism

An alternative design was considered, on which the drag torque was still measured on the enclosure but a pivot point was introduced on the other side of the load cell, in order to further stabilize the assembly. This implementation would also interfere with the measurements though and it was abandoned.

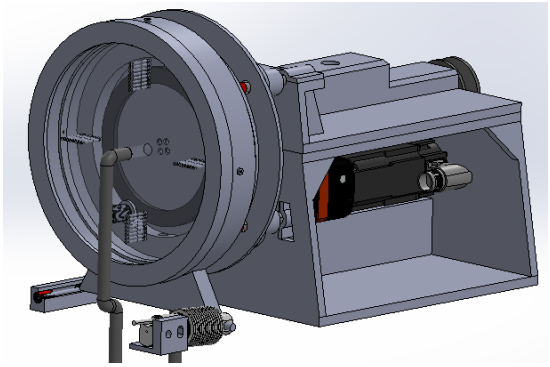

Figure 58 Alternative design attempting to further stabilize the machine

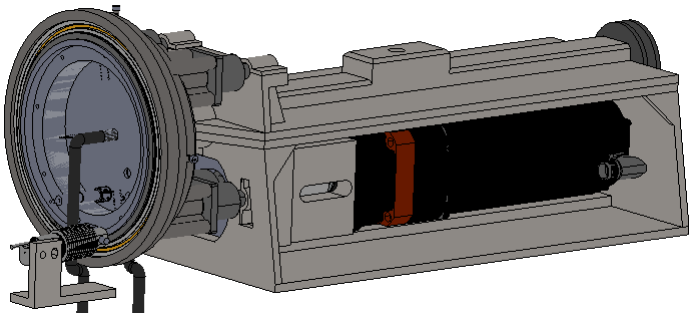

Figure 59 Final design

In the final design of the tester, the linear guides shortened with the bearings moving closer to the enclosure, the length of the tester was augmented to accommodate for a larger motor and a system of a bearing and a rotary seal were located around the static plate. This way the plate would be able to rotate due to the drag torque and this rotation can be blocked and measured by a load cell.

5.5 Final Design of the Open Clutch Single Disc Lubrication Testing Assembly

In order to be able to simulate both Cavitation (Multi-phase flow) and Wobble phenomena with this device, a modular design was needed. More specifically, the rig allows for:

1. Application of different clutch disc sizes
2. A disc can be solidly attached on the rotary shaft by means of a rigid connector, or by means of a spline connection that will allow the disc to flex, bend and move axially freely.
3. The static plate opposite of the clutch disk is interchangeable and it can be either a glass part (for flow visualization by a high-speed camera and studying of cavitation, aeration, bubble flow etc.) or a more durable metal part (for studying the fluid squeezing characteristics and vibrational behavior of discs, i.e., wobbling, non-uniform clearance, free-vibrations due to pressure differential effect test)

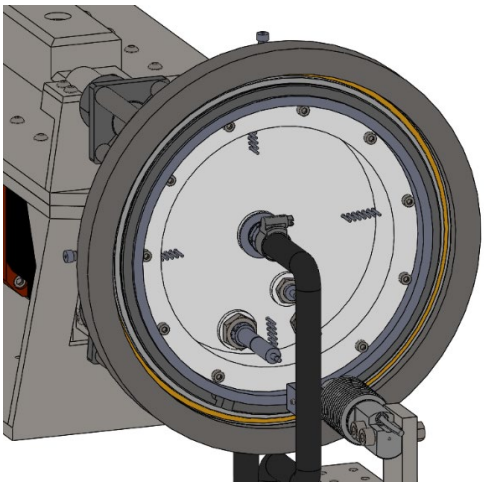

Figure 60 For the simulation of the wobble effect a metal plate (silver part) is applied opposite of the clutch disk

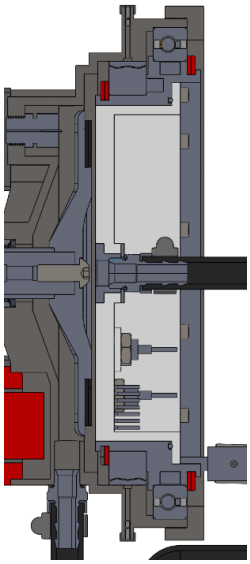

Figure 61 Section of the assembly with the metal plate

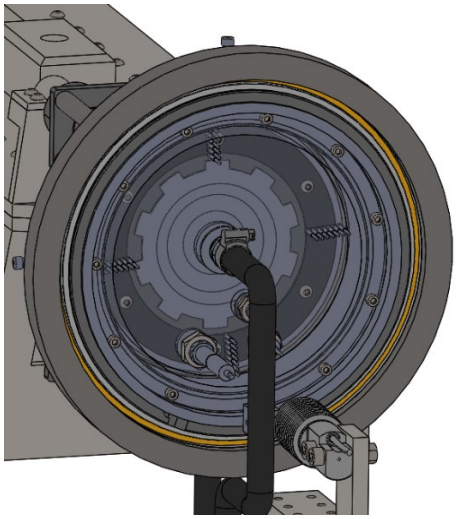

Figure 62 For the simulation of the two-phase flow, a transparent glass plate is applied opposite of the clutch disk

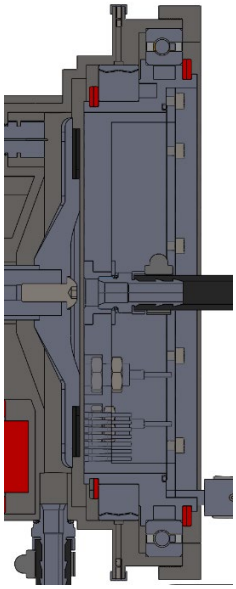

Figure 63 Section of the assembly with the transparent glass plate

The two-phase flow is made possible by the application of ball check valves. These valves allow the introduction of air inside the wet clutch hub, but prevent the oil to exit. Caps can be applied on top of the valves to block them, if the introduction of air is not wanted.

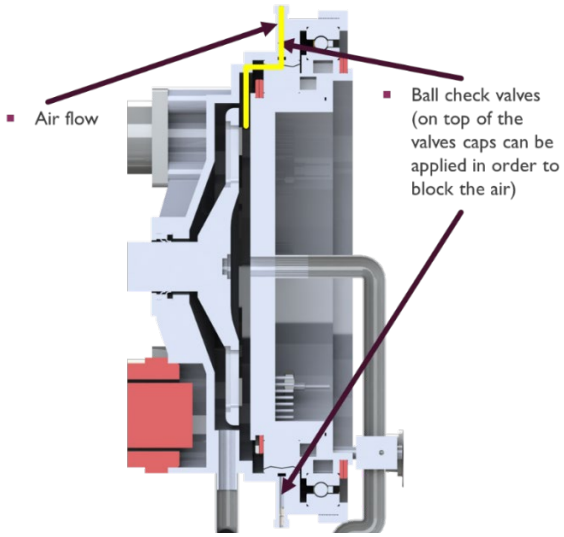

Figure 64 Section of the clutch disk tester. The flow of the air is sucked inside the enclosure from the ball check valves and it follows the path highlighted by the yellow line

In order to test the Multi-phase flow, the clutch disc is solidly attached on the shaft and the disc opposite of the clutch is made of a transparent material (i.e., a glass plate). In this case there is only Rotational motion, no Reciprocating motion.

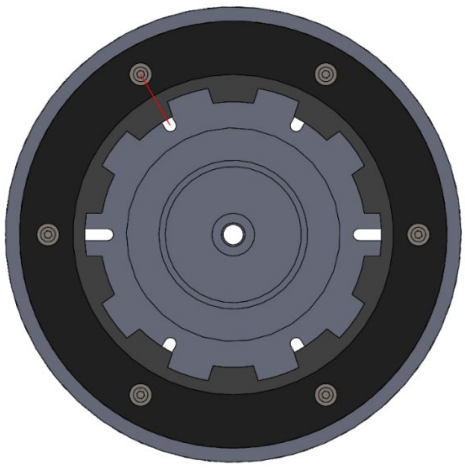

Figure 65 Rigid disk attachment method

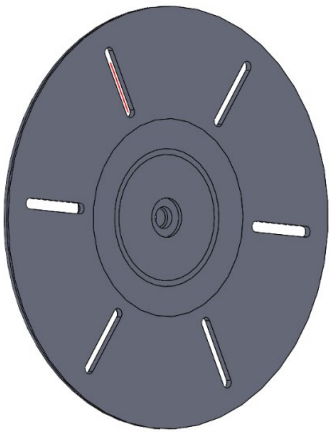

Figure 66 Adaptor plate of the rigid disk attachment method

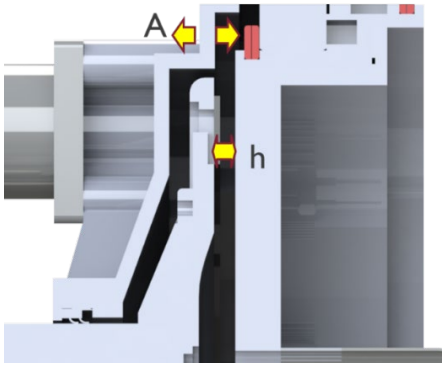

Figure 67 Clearance distance h between the clutch disk and the opposite disc and oscillation width A (the oscillation is applied on the enclosure, not on the disk itself

In order to simulate the Wobble effect, the clutch disc is not solidly attached on the shaft. Instead, it is free to move in the axial direction, but its rotational movement is fixed on the shaft by means of a spline. This way it is free to collide with the opposite disc, which, in this case is made out of metal.

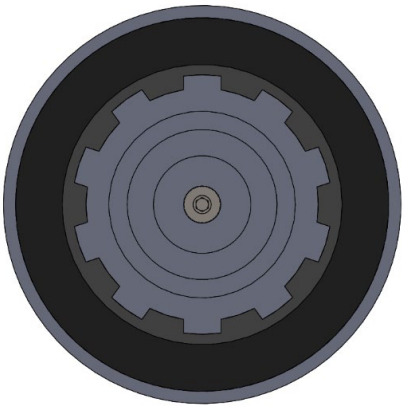

Figure 68Flexible disk attachment method. The disk is free to move in the axial direction

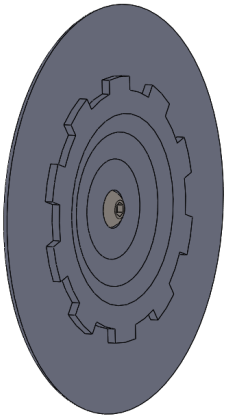

Figure 69 Adaptor disk of the flexible disk attachment method

There are two types of motion that can be applied on the assembly: linear reciprocating motion and rotational motion. Each motion is controlled by a servo motor. The rotational motion is applied on the clutch disk by means of a pulley/belt system, that connects the main motor of the assembly to the shaft of the disk.

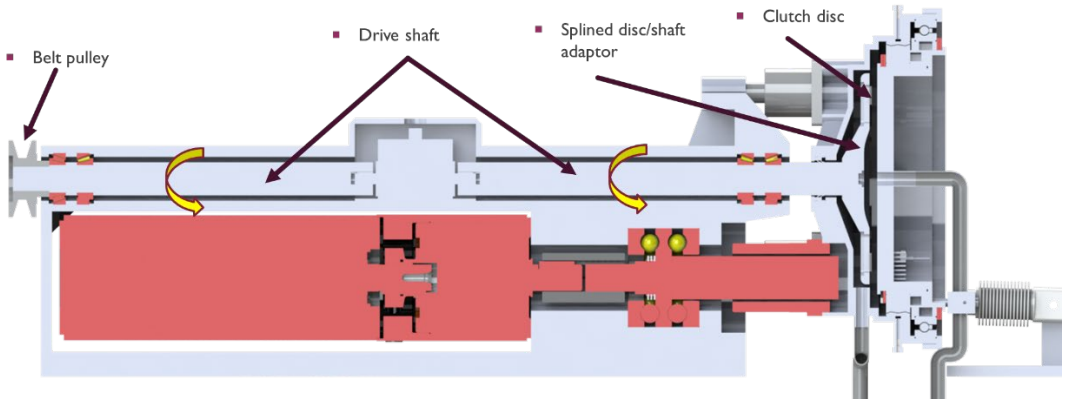

Figure 70 The rotating parts of the assembly from the belt pulley to the clutch disk

The reciprocating motion is not applied to the clutch disk but to the enclosure around it which is connected to the disk opposite to the clutch. Specifically, the servo motor is connected to a ball screw which is attached to the back of the enclosure.

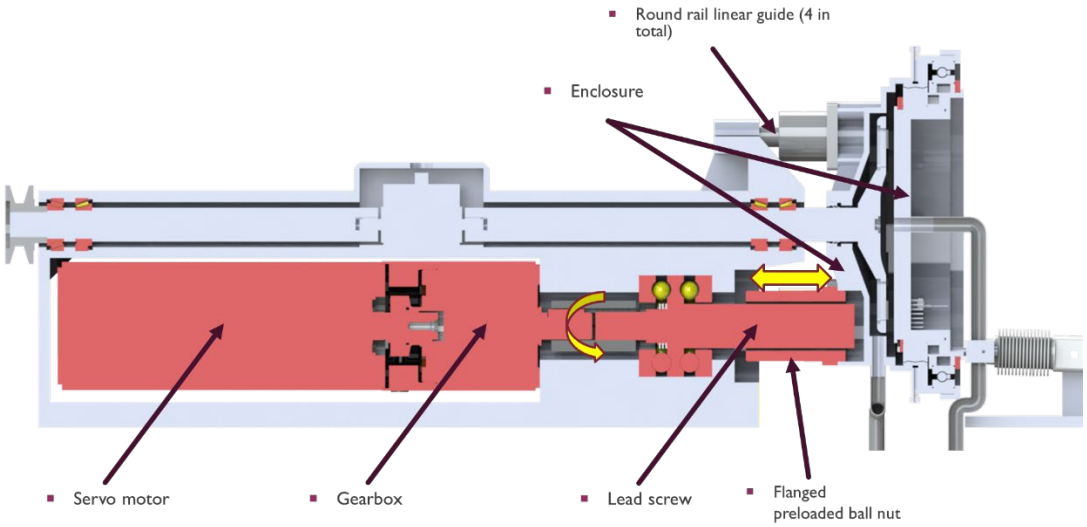

Figure 71 Parts that contribute to the reciprocating linear motion of the enclosure surrounding the clutch disk

The reciprocating enclosure can move along four round linear rail guides that connect it to the rest of the assembly.

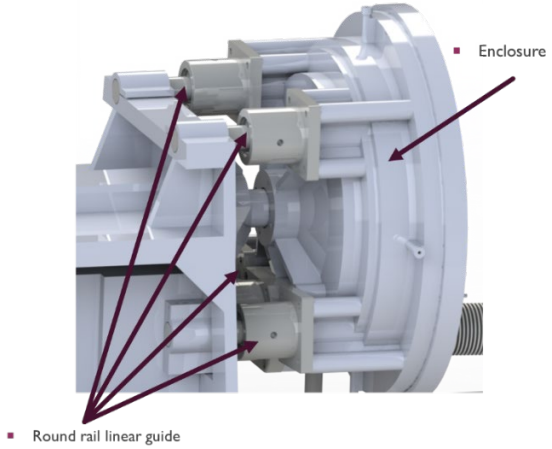

Figure 72 Linear round rail guides

In order to correctly measure the drag torque on the plate opposite to the clutch disk, the reciprocating enclosure's components are must be free to rotate. This rotation is confined by a small shaft attached on the adaptor disk metal ring, on a specific radius of 113mm. The drag torque can be measured there, knowing the value of the holding force on this rod and the radius. The rotational motion is made possible by a combination of a bearing and a labyrinth seal. Both the labyrinth and the bearing are attached to a metal ring, which acts as an adaptor for the glass or metal disk plate. This way, the glass and metal plate part are easily interchangeable, as they are screwed on the adaptor ring.

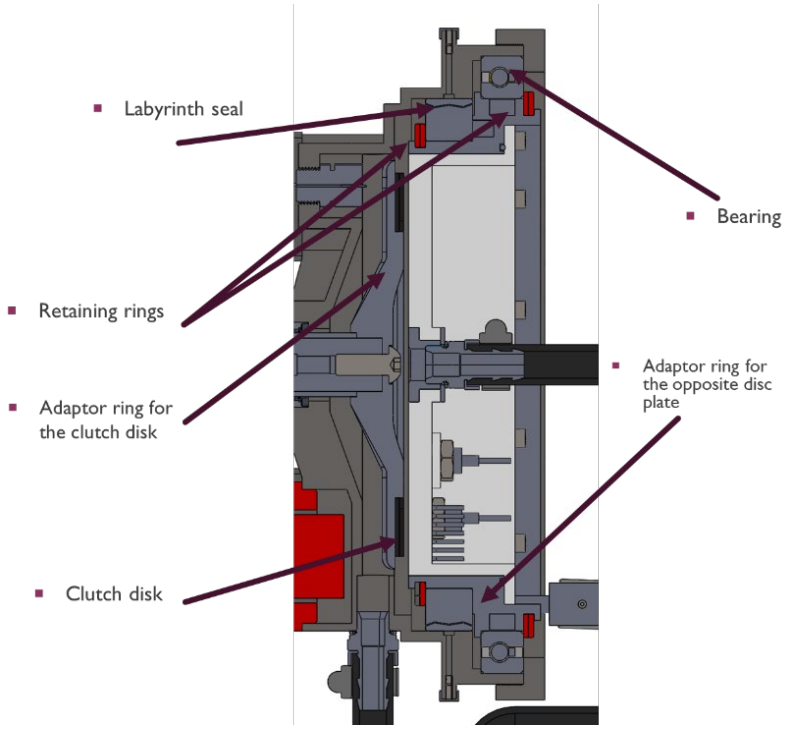

Figure 73 The assembly inside the enclosure.

There sensors that are included in this compartment are:

1. Torque transducer (drag torque measurement on the moving clutch disk)
2. Load cell (drag torque measurement on the opposite disk)
3. Pressure transducers
4. LVDT (distance measurement)
5. Inductive eddy current sensors (impact measurement)
6. Temperature sensor

The torque transducer [1] is applied on the rotary shaft in order to measure the drag torque on the clutch disk. The transducer is able to measure torque up to 10 Nm with a precision of 0.03 Nm.

The drag torque is also measured on the opposite disk plate. Instead of measuring directly the torque on this side, the tangential force is measured on a specific radius, as mentioned. Since the shaft where the force measurement of the force takes place is attached on the enclosure it also reciprocates along with the rest of the assembly. For this reason, a bushing is applied around it, which is connected to a load cell [2]. The load cell has a rated capacity of 200N and a accuracy of 0.04N which translates to roughly 0.005Nm for the radius of its position.

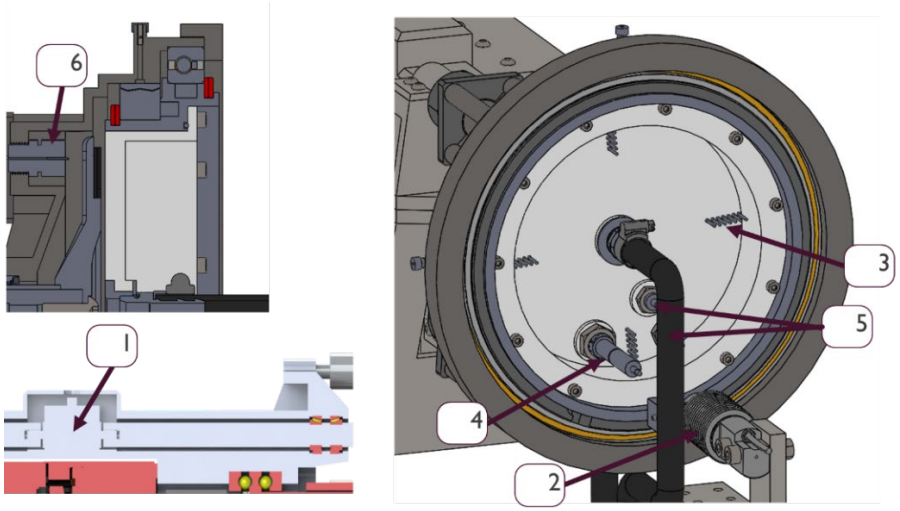

Figure 74 All the sensors of the single clutch disk assembly

Pressure transducers [3] are permanently glued at four regions along the perimeter of the disk, and at seven points along the radius on each of these regions. They have a rated capacity of 35kPa with an accuracy of 170Pa.

The LVDT distance sensor probe [4] is used to measure the distance between the disk surface and the opposite disk (it basically measures the clearance h), for the initial positioning. Afterwards it can be removed and a plug can be placed on the opening. The sensor can measure distances up to 5mm with a linearity of 0.025mm.

The Inductive eddy current sensors [5] are used for the impact detection. They also measure distance (they can be used supplementary to the LVDT sensor) with a resolution of 0.04μm, but they have a much higher measuring rate at 50 kSa/s

The temperature sensor [6] is applied right behind the clutch disk, inside a socket on the enclosure. It can measure up to 160ºC with an accuracy of ± 0.05 °C.

Finally, a high-speed camera can be placed in front of the disk faces, in order to record the multi-phase flow effect. This camera needs to be placed outside of the structure or on an extension support, since there is no available space for it on the table.

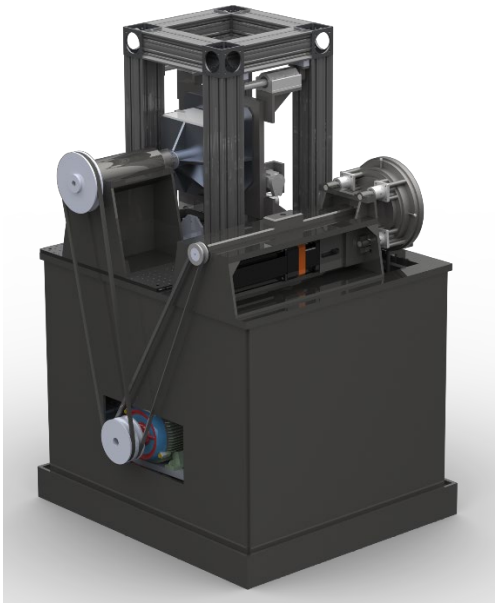

Figure 75 Render of the final assembly, including both of the testers

5.6 Oil Circulation/Heating System

The lubricant for the wear test rig as well as the oil for the wet clutch tester is provided by a circulation and heating system, located underneath the table bed of the assembly. The oil is gathered in a storage unit with a capacity of 15 liters and from there it can be supplied to each testing unit individually, via a different set of pipes. The testing units can even be isolated by the circulation system, by means of ball valves. A heating element is located on the side of the oil reservoir that is responsible for the oil temperature for the clutch tester. For the wear test rig, it acts along with another heating element inside the oil hub of the tester. More precisely, the heating element on the reservoir elevates the oil temperature up to 90ºC and for a further increase up to 150ºC, the secondary heating element is used. The temperature is measured by a temperature probe also on the side of the reservoir, but there are temperature sensors on each tester too. Following the reservoir, the oil is introduced to the oil filter to clean possible debris and after that it is sucked in the gear pump, in order to be propelled to the testers.

The main parts of the oil circulation assembly are the following:

1. Ball valve/inlet from wear test rig
2. Ball valve/inlet from clutch tester
3. Oil reservoir
4. Oil filter
5. Gear pump
6. Ball valve/outlet to wear test rig
7. Ball valve/outlet to clutch tester
8. Temperature probe
9. Heating element

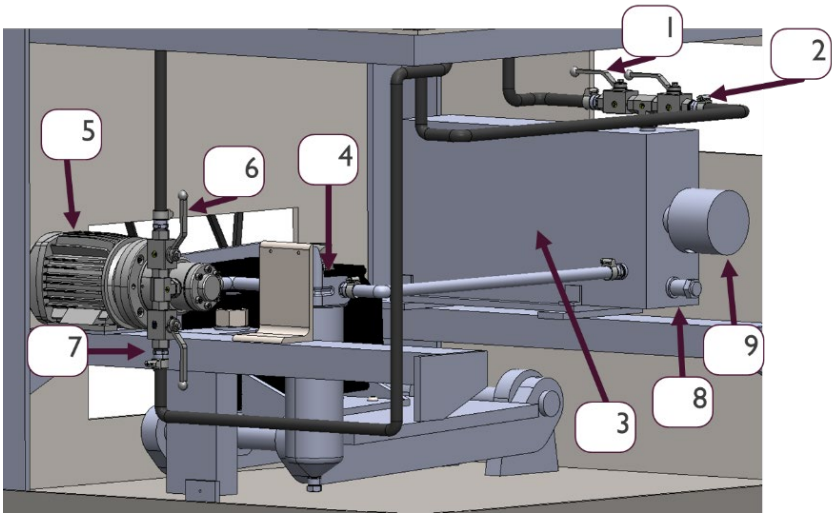

Figure 76 Parts of the oil circulation assembly

The ball valves [1,2,6,7] are used to control the oil flow and to include or exclude a tester from the oil circulation. For example, when a Pin-on-Disk wear test is performed, the valves [2] and [7] are closed, to exclude the clutch disk assembly. The oil from the testers is stored inside the 15lt reservoir [3] where it is also heated by the heating element [9]. The temperature is measured by the probe [8] next to the outlet flow of the reservoir. After the reservoir the oil is led to the filter, where the wear particles and debris from the tests are removed. The gear pump [5] can propel the oil from the filter to the testers with a maximum flow of 2,5l/min.

5.7 Cost Estimation

In conclusion, a rough cost estimation for the manufacturing and the purchase of the needed parts for the machine, at the time of the design process, suggest a total cost of 15000 euros. This cost is relatively low compared to the commercial multi-testers. The costliest parts of the assembly are the precision preloaded leadscrews, the motors and the sensor, since the rest of the parts are manufactured by common methods.

6 Analytical calculations and FEA studies

6.1 Frame Eigenfrequency calculation

The frame of the assembly consists of a combination of structural steel beams and panels with a typical yield strength value of 250 MPa.

The eigenfrequencies of the frame were calculated in a modal analysis in ANSYS. The high resulting frequencies prove that no further reinforcement was needed to the frame.

The first six eigenfrequencies of the frame assembly are the following:

Mode	Frequency
1	127,76 Hz
2	134,84 Hz
3	157,75 Hz
4	178,65 Hz
5	184,48 Hz
6	194,79 Hz

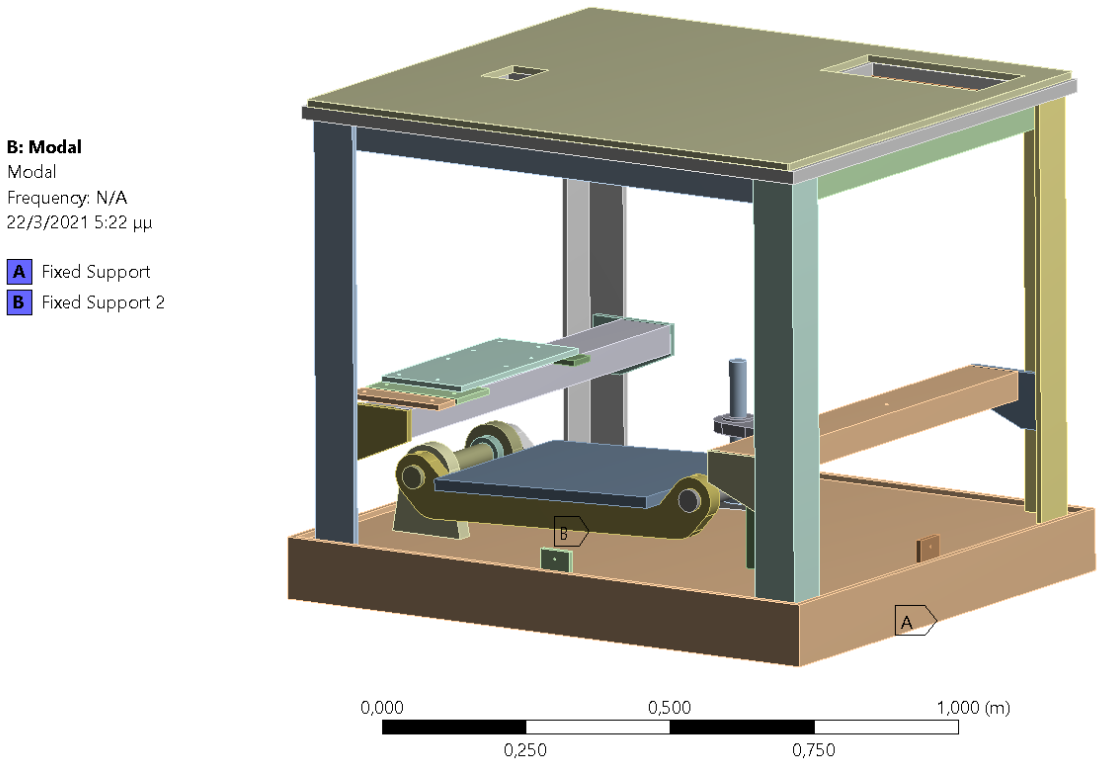

Figure 77 The supports of the frame

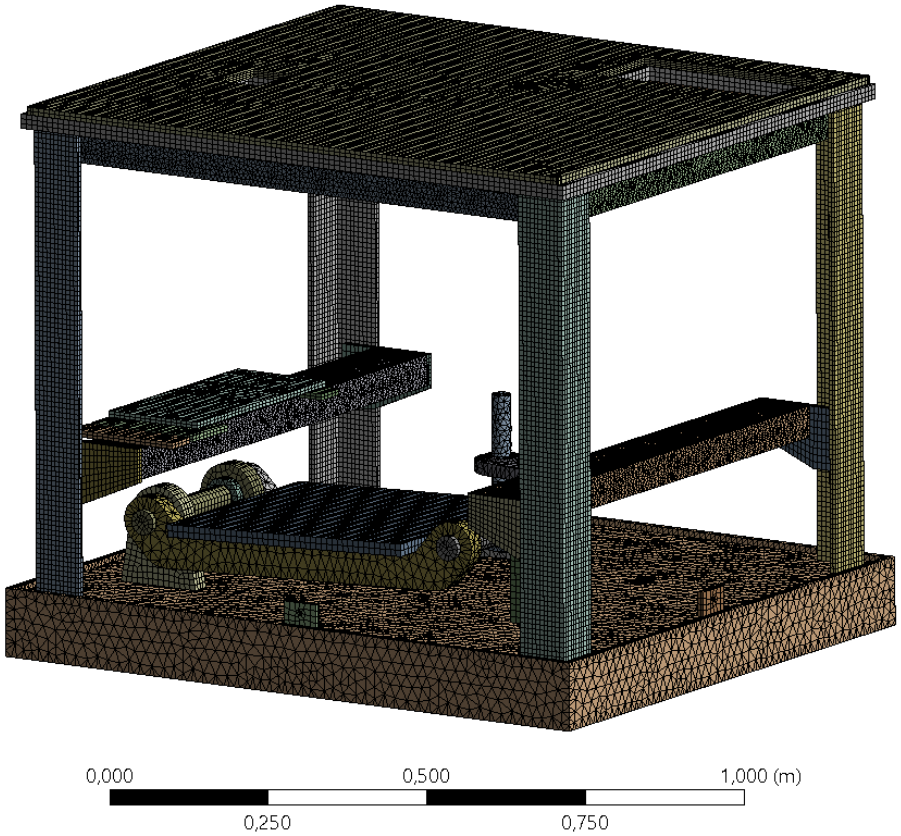

Figure 78 Mesh with 268351 elements and 930945 nodes

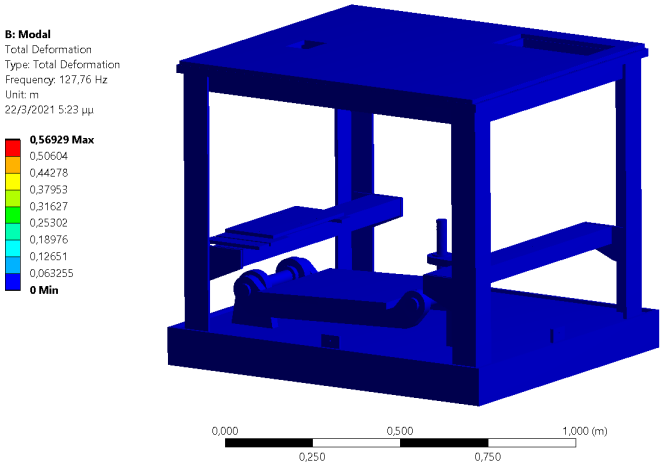

Figure 79 Frequency of 127,76 Hz

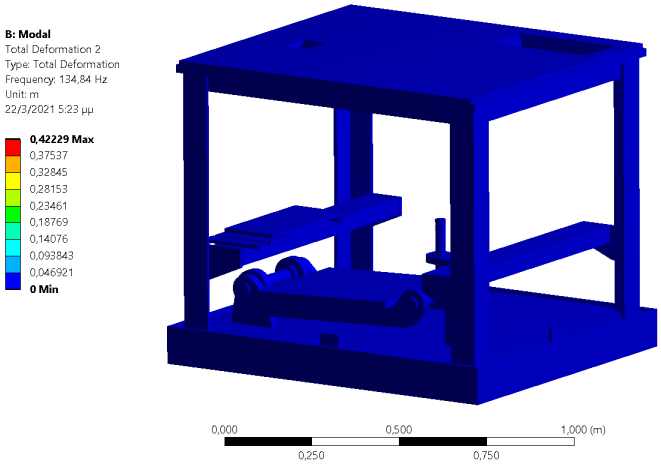

Figure 80 Frequency of 134,84 Hz

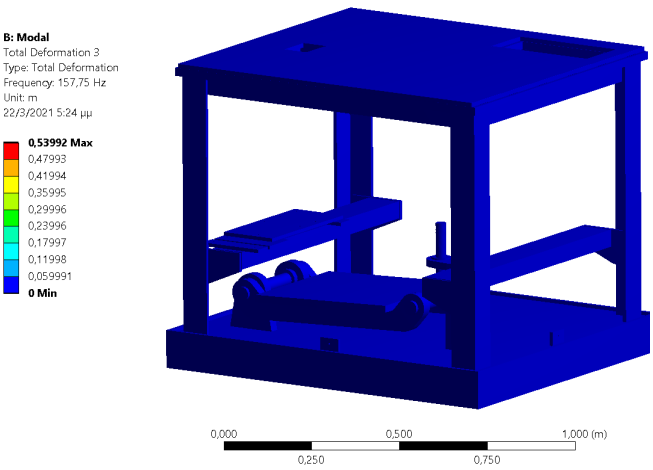

Figure 81 Frequency of 157,75 Hz

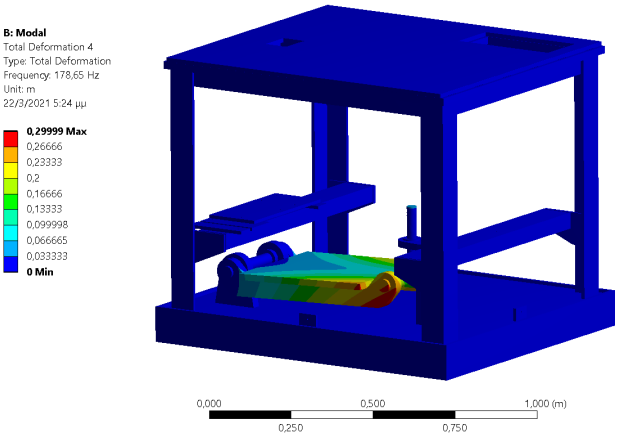

Figure 82 Frequency of 178,65 Hz

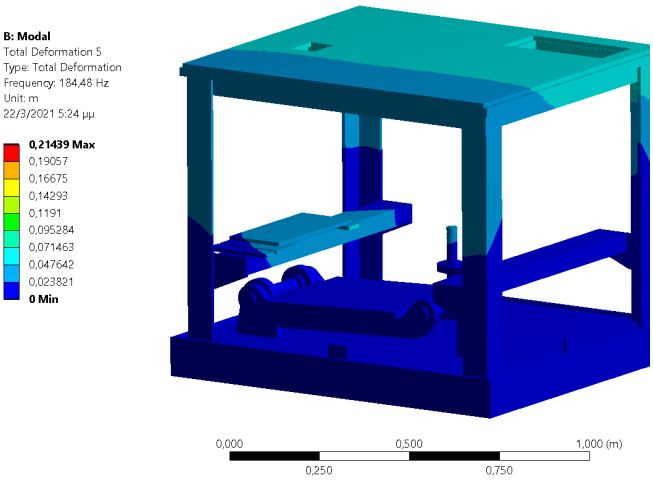

Figure 83 Frequency of 184,48 Hz

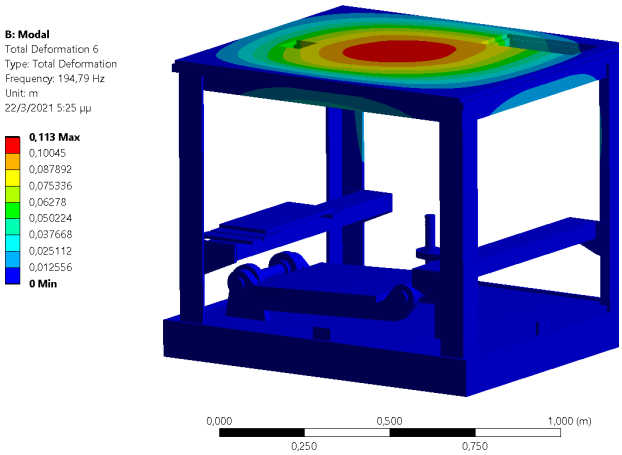

Figure 84 Frequency of 194,79 Hz

6.2 Wear test rig Static Structural Analysis

For the assembly of the rotary specimen, steel AISI 4130 was chosen as the building material, to provide the needed strength and stiffness. For most of the parts of the linear motion assembly, a lighter alloy material was used, to reduce the total moving mass with the properties shown below.

Property	Value	Units
Elastic Modulus	205000	N/mm^2
Poisson's Ratio	0.285	N/A
Shear Modulus	80000	N/mm^2
Mass Density	7850	kg/m^3
Tensile Strength	560	N/mm^2
Compressive Strength		N/mm^2
Yield Strength	460	N/mm^2

Figure 85 Steel AISI 4130

Property	Value	Units
Elastic Modulus	69000	N/mm^2
Poisson's Ratio	0.33	N/A
Shear Modulus	25800	N/mm^2
Mass Density	2700	kg/m^3
Tensile Strength	255	N/mm^2
Compressive Strength		N/mm^2
Yield Strength	240	N/mm^2

Figure 86 Aluminum 6063-T83

There are two kinds of linear guides that were used in the assembly. The four guides that support the full assembly structure are rated for 13,6 kN each and the set of two linear guides used for the high frequency reciprocating motion are rated for 1,5 kN dynamic loading each, since they lift less weight and the heaviest loading case on them is a static loading case.

Two sets of tapered roller bearings are used on the rotary shaft assembly. The basic dynamic load of each bearing is 33.2 kN, which is sufficiently more than the maximum axial load of the tests.

Since the loading on this assembly varies depending on the experiment, the cases of the heaviest loads were examined. Static structural analyses were carried out in ANSYS, first for the case of the Disk-on-Disk test, and then for the case of the Ball-on-Flat test.

For the Ball-on-Flat test, the force was applied on the specimen region, in two directions, since there is a nominal variant and a horizontal frictional variant. The highest nominal load is 200N and for a typical metal to metal lubricated contact with a friction coefficient of 0,3 (i.e., Aluminum to Aluminum), the friction force is 60N.

The highest stresses of 268 MPa are on the shaft/spline assembly which is strong enough to withstand it, since both components are made out of steel with a yield strength of 460MPa.

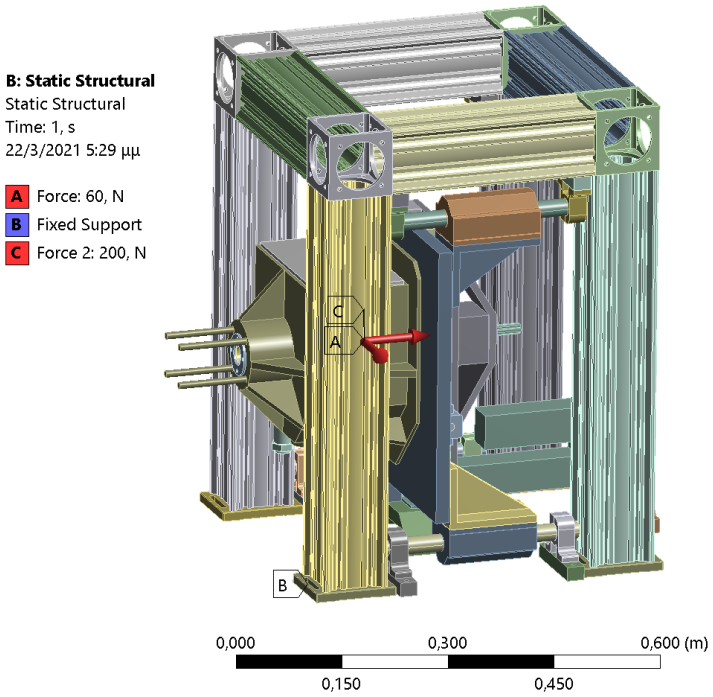

Figure 87 The input loads

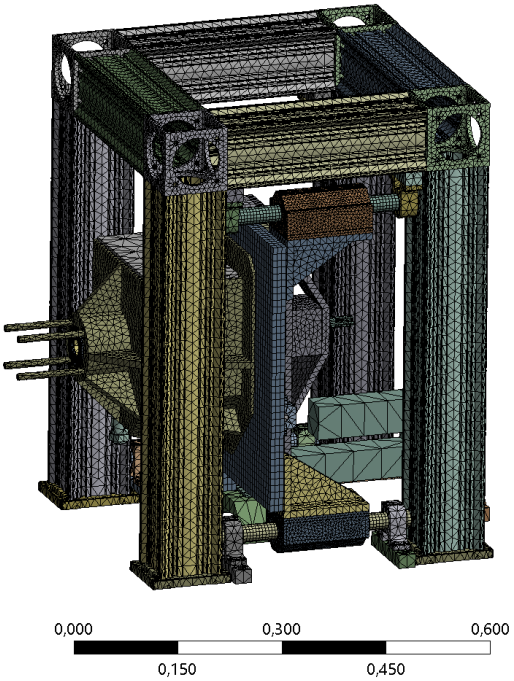

Figure 88 Generated mesh with 642069 elements and 1174067 nodes

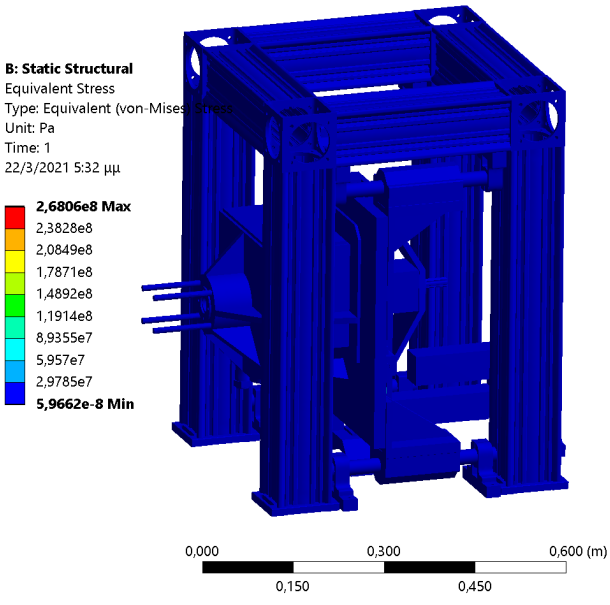

Figure 89 The equivalent Von-Misses stresses

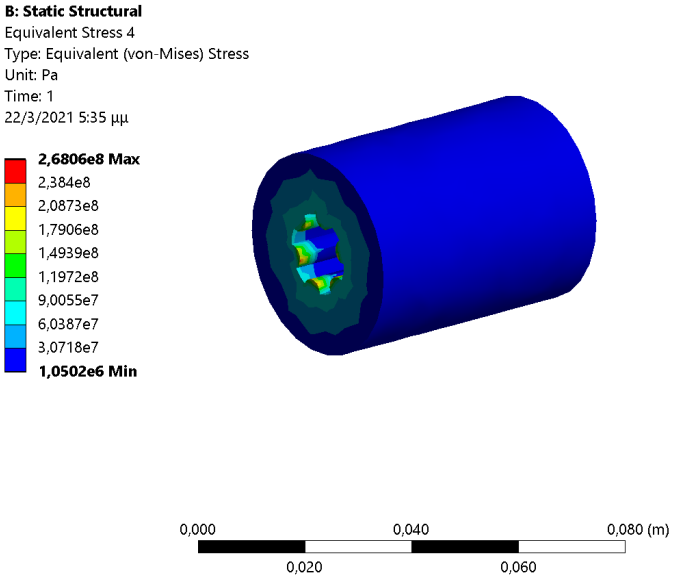

Figure 90The area of the spring and the spline where the stresses have the higher values

For the Disk-on-Disk test the highest loading nominal force is 2,6kN. In this case there is also a torque input which, for an Aluminum disk sample of a 100mm diameter under lubricated conditions when the friction coefficient is 0,3, is 1300x0,3x0,1=39Nm. The same meshed geometry as in the previous structural analysis was used.

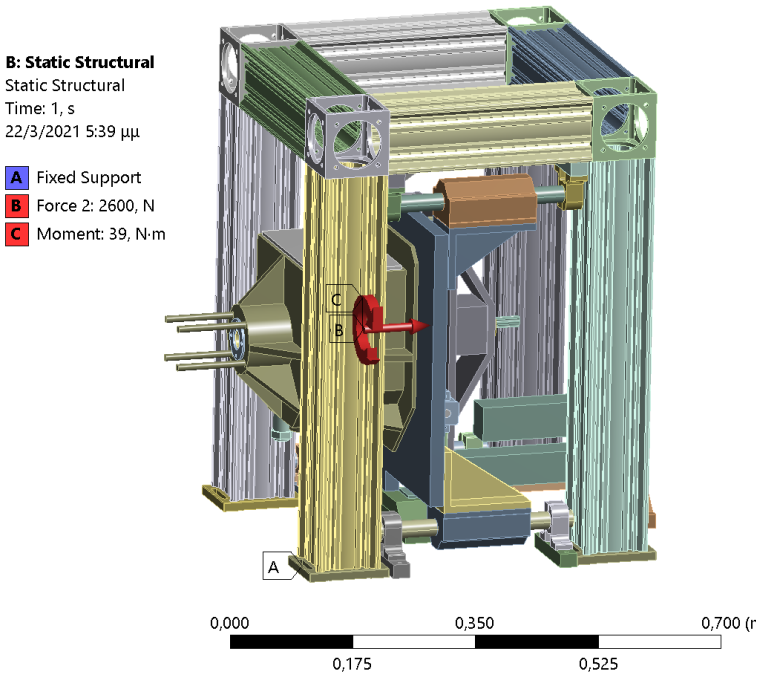

Figure 91 The input loads

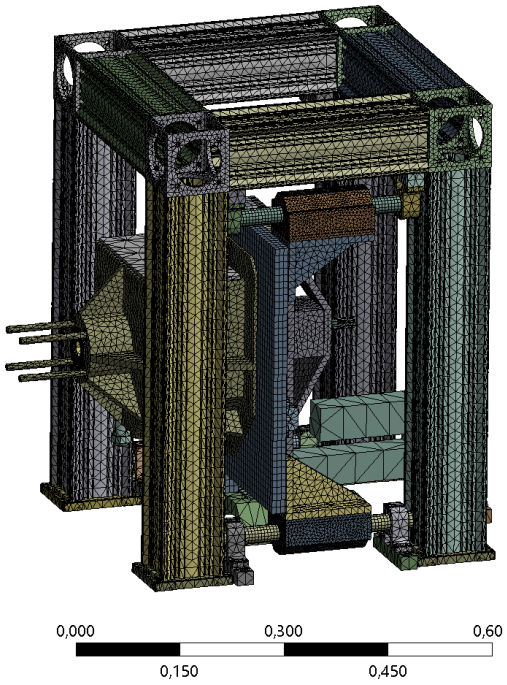

Figure 92 Generated mesh with 642069 elements and 1174067 nodes

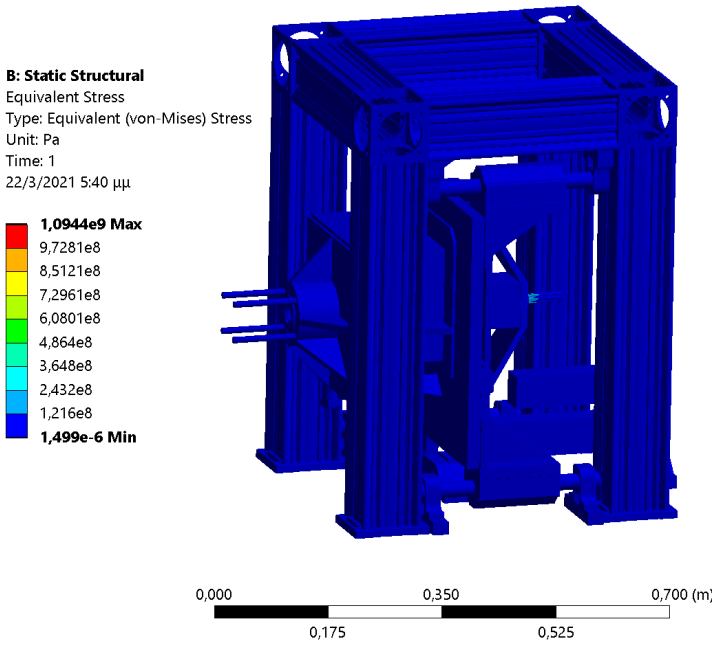

Figure 93 The equivalent Von-Misses stresses

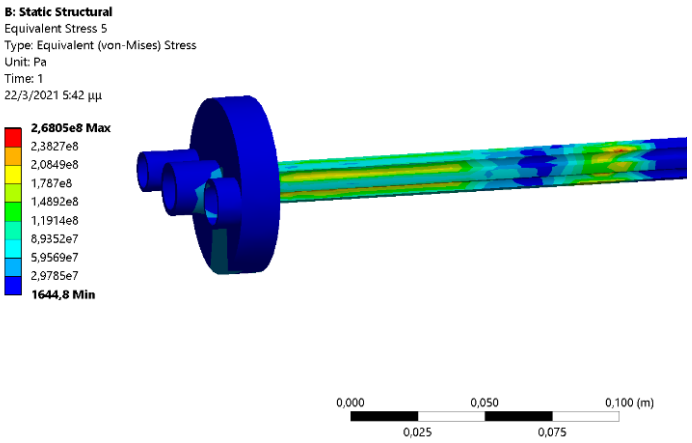

Figure 94 The areas of the shaft with the highest stresses

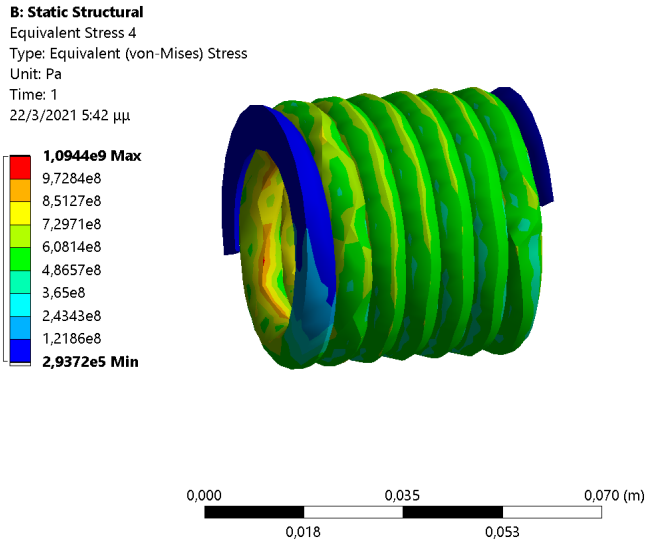

Figure 95 The equivalent Von-Misses stresses on the spring

As expected, the stresses are much higher in this simulation, due to the higher load. The highest stresses appear on the spring, the splined shaft assembly. The stresses on the spring reach 1094MPa, which are within the limits of the tensile strength of the selected spring material EN 10270-1 SH, which is 2940MPa. The stress on the splined shaft reach 268MPa which again is within the materials 460MPa Yield strength limit.

6.3 Wear test rig Rotordynamics / Eigenfrequency calculation

The high rotational speeds affect the eigenfrequencies of a device with rotating elements and need to be considered during the calculation of the former. For this reason, a modal analysis with rotordynamic controls was carried out in ANSYS. The range of rotational speeds for the study were up to 60 rad/sec.

Since the highest frequency during any test of the wear test rig is 10Hz (during the Ball-on-Flat experiment), there should be no implications.

Mode	Frequency
1	57.14 Hz
2	73,21 Hz
3	87.27 Hz
4	87.48 Hz
5	150.77 Hz
9	171.63 Hz

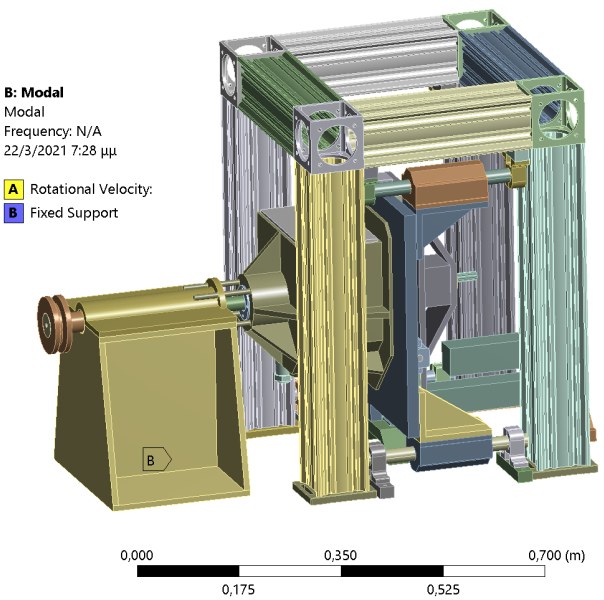

Figure 96 The rotational velocity and fixture supports

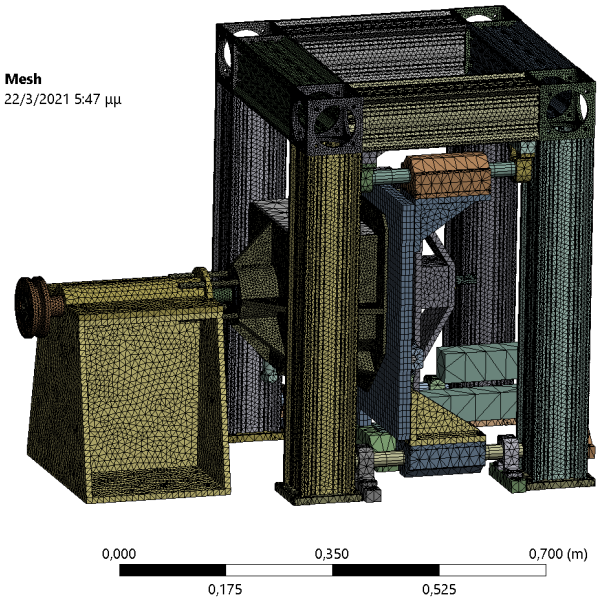

Figure 97 Mesh with 635061 elements and 1214149 nodes was used

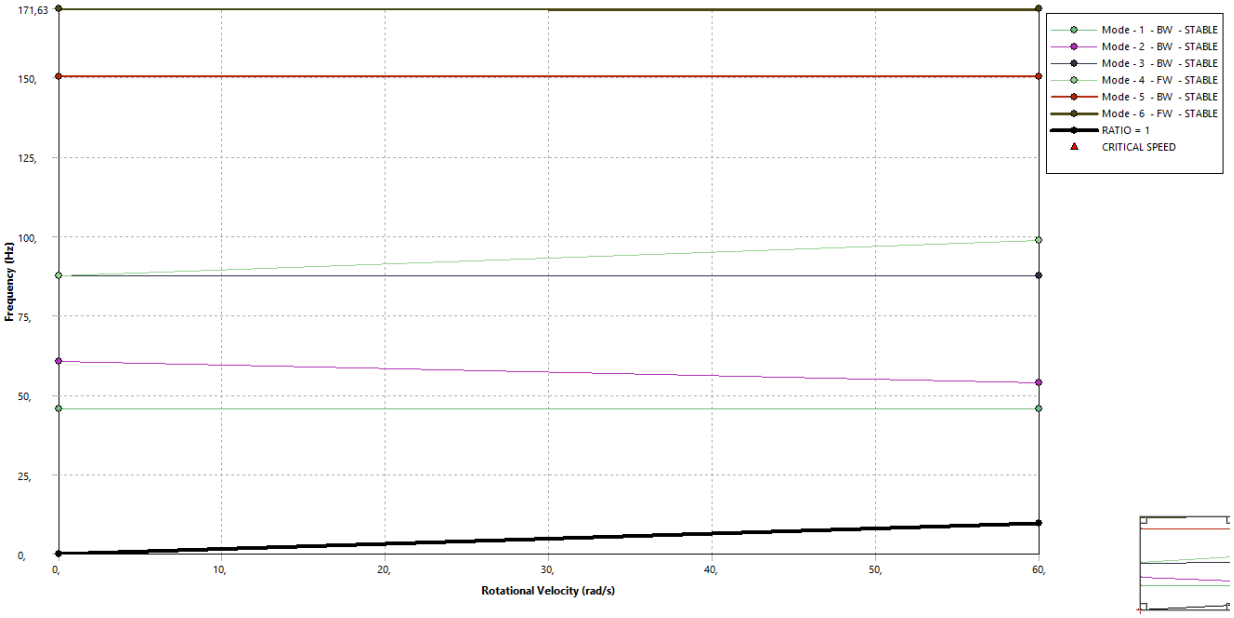

Figure 98 The variation of the frequencies with the rotational speed, according to the Campbell diagram

In the Campbell diagram the variation of the frequencies (modes) relatively to the increase of the rotational speed can be seen. No critical speeds are reached in the range from 0 to 60 rpm, which suggests that higher rotational speeds can be used if needed. The excitation of the first six frequencies can be seen in the results.

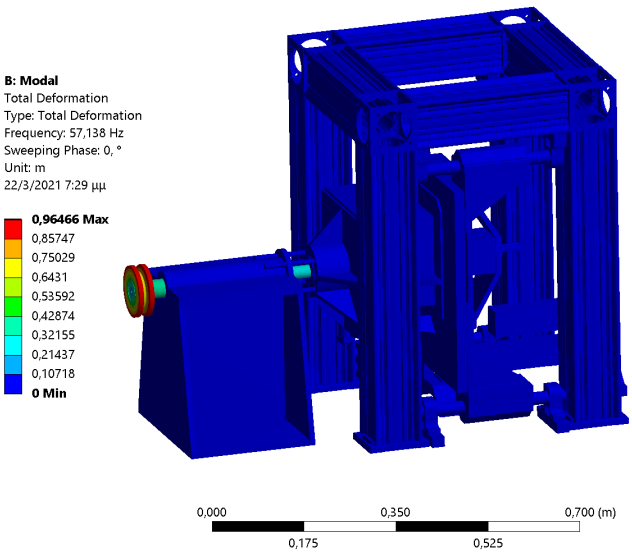

Figure 99 Frequency of 57,14 Hz

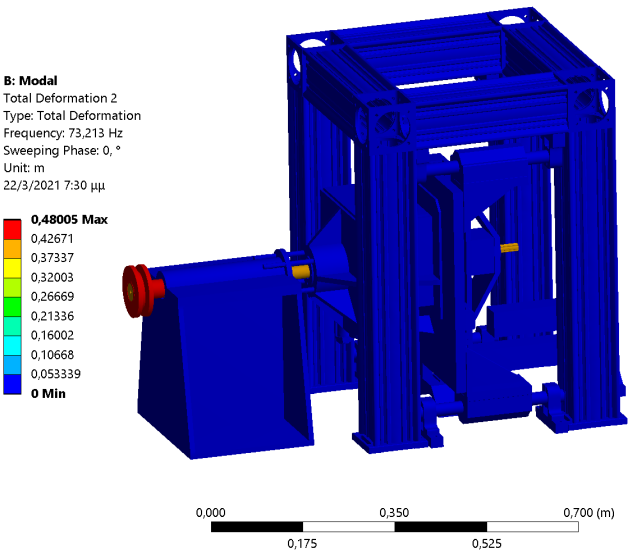

Figure 100 Frequency of 73,21 Hz

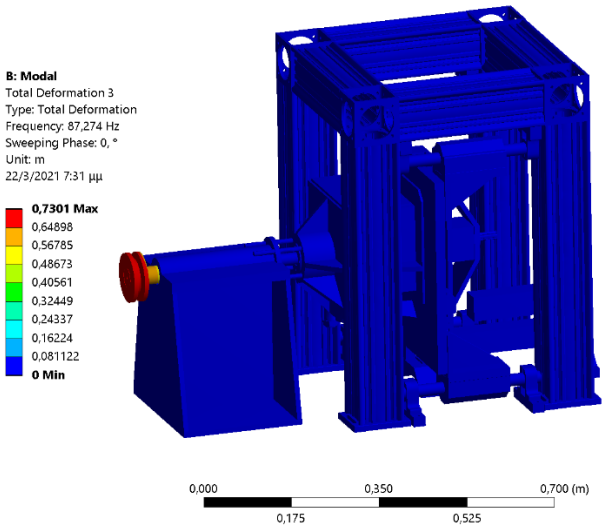

Figure 101 Frequency of 87,27 Hz

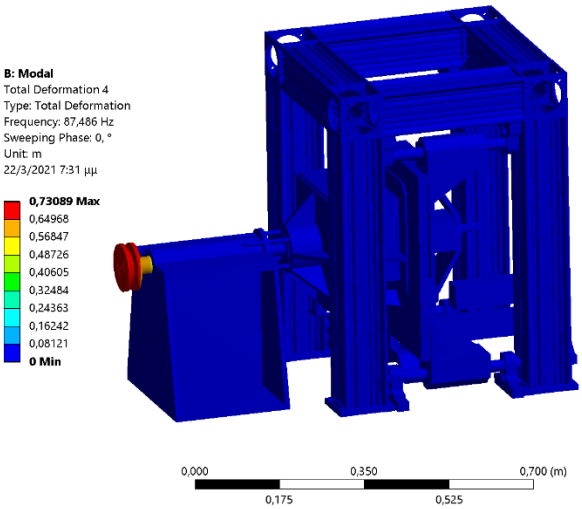

Figure 102 Frequency of 87,48 Hz

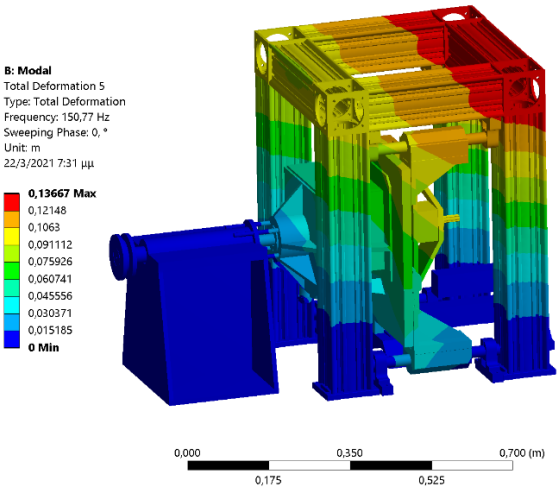

Figure 103 Frequency of 150,77 Hz

6.4 Clutch Tester Transient Structural Analysis

For the parts of the single disk tester, steel AISI 4130 has been chosen for the main body, to provide the necessary strength and rigidity and aluminum 6063-T83 for the parts that are included in the high frequency reciprocating motion.

The linear guides used to connect the reciprocating parts to the rest of the assembly were four sets of ball bushings capable of a dynamic load capacity of 5kN each, with 1566 Carbon Steel Shafts.

Two sets of tapered roller bearings were used on the rotary shaft. The basic dynamic load of each bearing is 33.2 kN. These bearings receive the full impact load during the reciprocating motion. Another single four-point contact bearing with a dynamic thrust load of 57,9kN was used inside the reciprocating enclosure to allow the rotary motion of the disk plate opposite to the clutch.

To verify the strength of this design a transient structural study was held in ANSYS 19.0, that provided the following results. The force applied on the surfaces of the clutch disk and the opposite disk is a function of time.

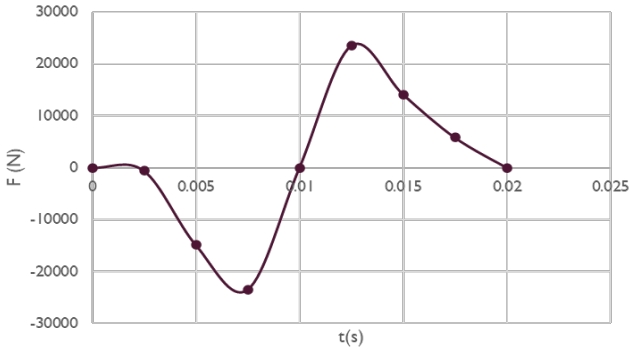

Figure 104 The transient force load graph

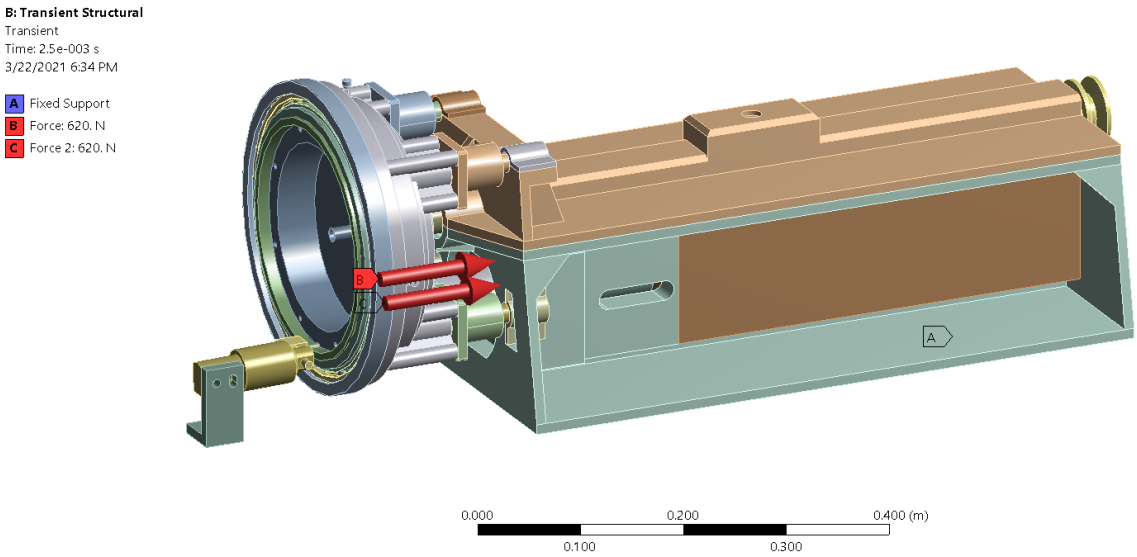

Figure 105 Supports and loads application

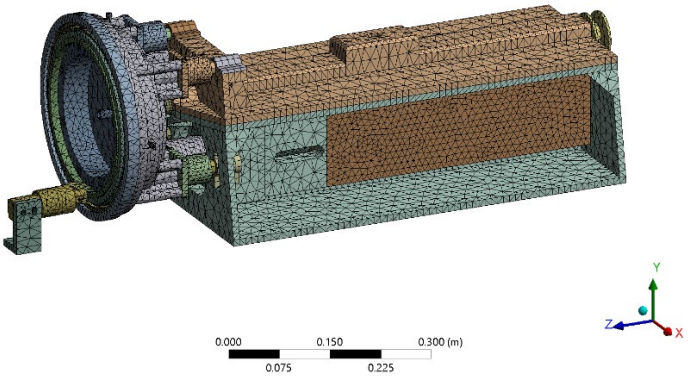

Figure 106 Meshing with 256980 elements and 612187 nodes

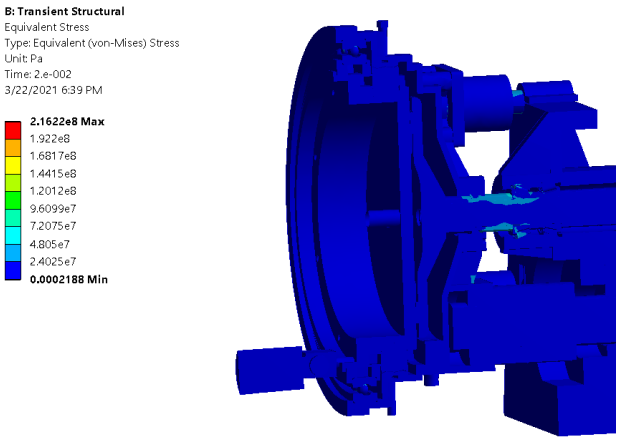

Figure 107 The stresses reach the higher values in the area of the shaft (section)

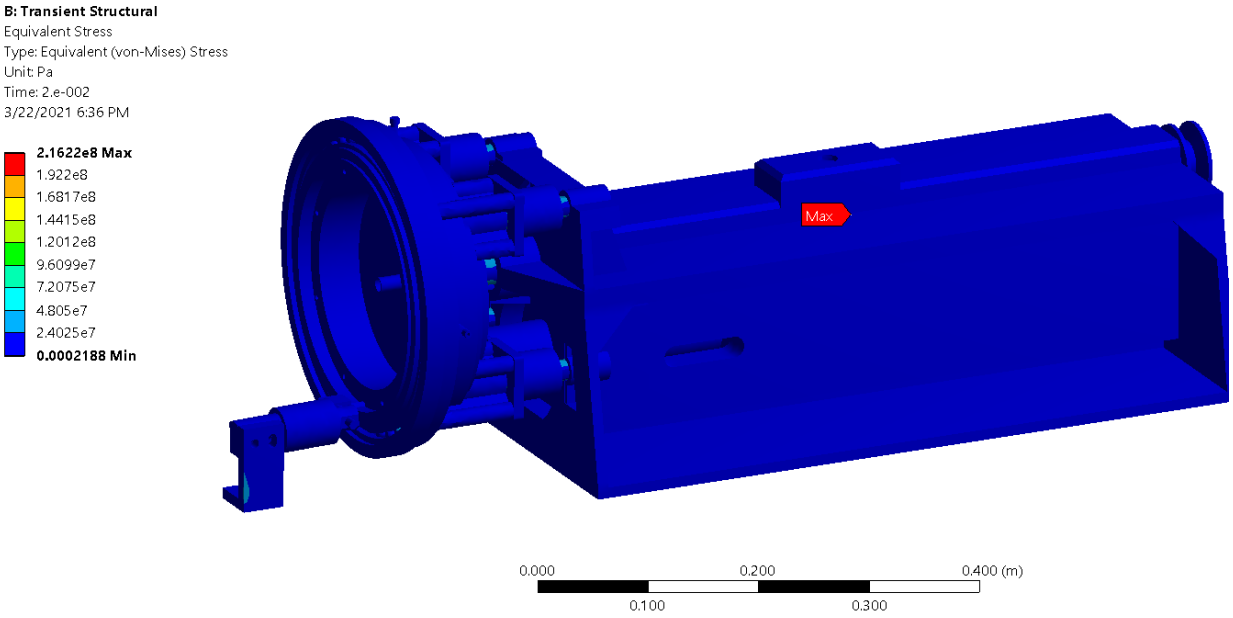

Figure 108 Equivalent resulting stresses (Von-Misses)

The results indicate that the highest stresses are on the rotary shaft, in the region where it enters the reciprocating enclosure and on the shafts of the ball bushings, with a highest stress value of 216 MPa, which is an acceptable value.

6.5 Clutch Tester Force Analytical calculation for transient stractural

The values of the force that were the input of the transient study were calculated both analytically and using FEA, with a 2D axisymmetric model on Ansys Fluent. The highest frequency reciprocating motion was considered, since it caused the highest loads.

For the analytical model, the equation of Axial and Rotational motion of two discs with central openings and combined conditions was used (53):

$$F = \frac{pi}{2}\left[r_{in}^2 r_{\text{out}}^2 + 2{r_{in}}^4(\ln r_{\text{out}} - \ln r_{\text{in}}) - r_{\text{out}}^4\right]\left[\rho(\omega_2^2 + \Delta\omega\omega_2 + 0.3\Delta\omega^2) + \frac{\mu}{h^3}\dot{h}\right]$$

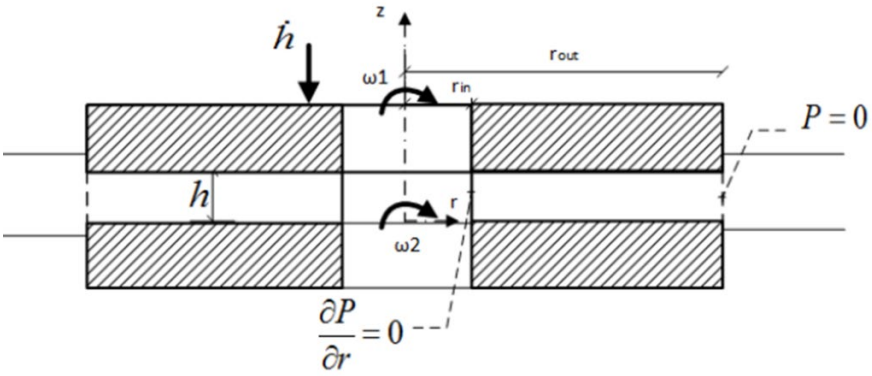

Figure 109 Axial and Rotational motion of two discs with central openings

The parameters that were chosen were:

f=50 Hz	ω_1=80 rad/sec
ω=314 rad/sec	ω_2=0 rad/sec
A=0,6 mm	μ=0,22 kg/ms
r_{in}=0.04 m	ρ=844 kg/m^3
r_{out}=0.085 m	h_{min}= 0,3mm

The resulting graph of the Force versus time is:

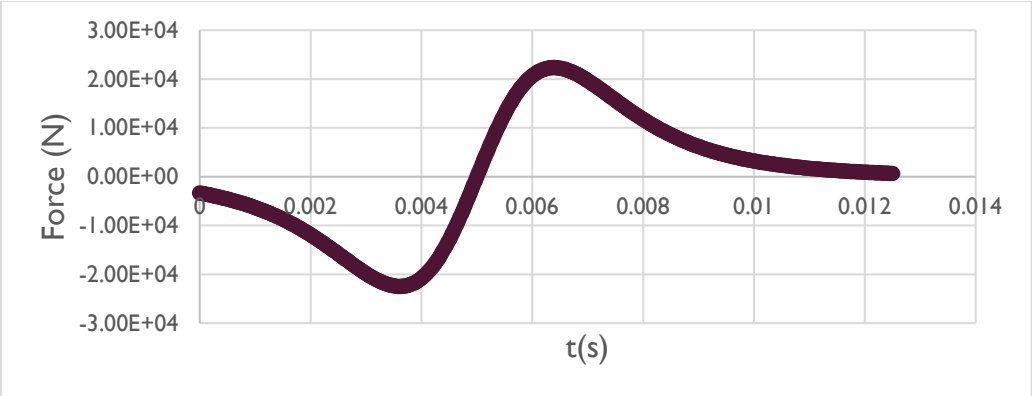

The maximum reached force value is 22,3 kN, which is slightly higher than the maximum value provided by the FEA simulation, thus, these worst-case scenario values were used on the transient analysis.

6.6 Clutch Tester Rotordynamics / Eigenfrequency calculation

The high rotational speeds affect the eigenfrequencies of a device with rotating elements and need to be considered during the calculation of the former. For this reason, a modal analysis with rotordynamic controls was carried out in ANSYS. The range of rotational speeds for the study were up to 1000 rad/sec. This study was paired to the transient study, so the same geometry, materials and mesh were used.

The resulting frequencies of the simulation are:

Mode	Frequency
1	87.42 Hz
2	160.20 Hz
3	236.49 Hz
4	261.89 Hz
5	283.86 Hz
9	295.58 Hz

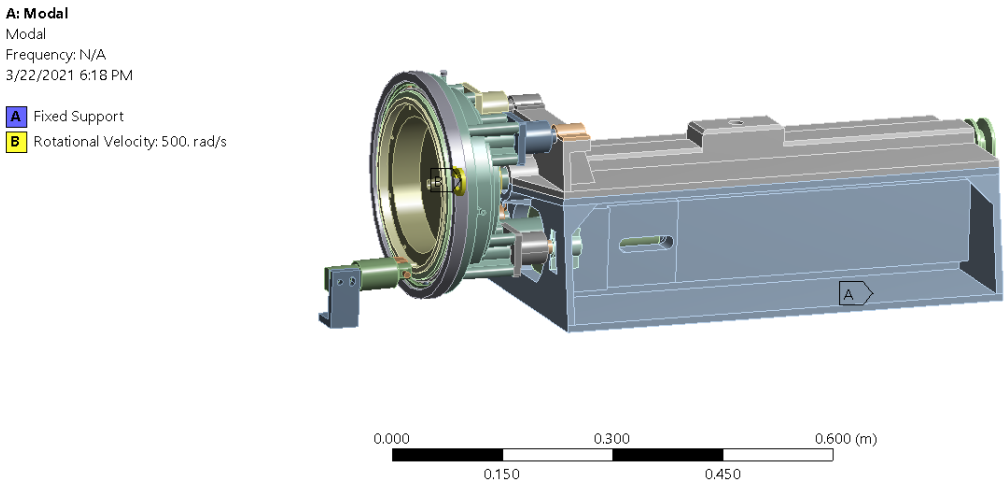

Figure 110 The supports and the rotational velocity input

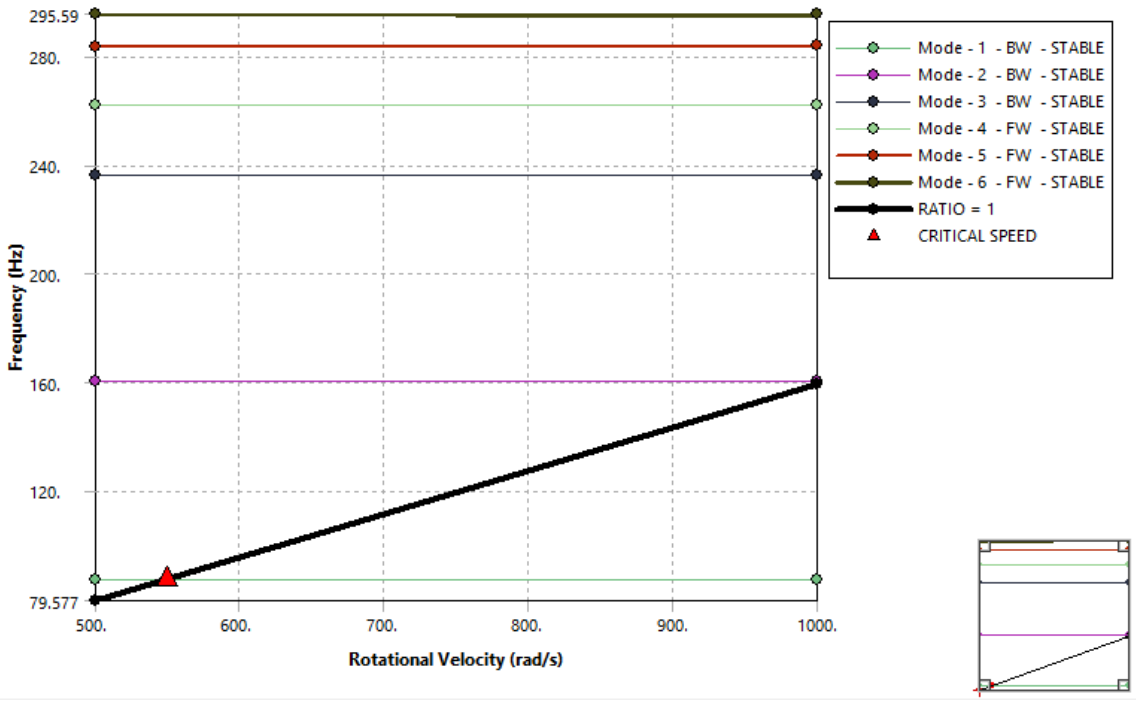

Figure 111 The Campbell diagram

According to the Campbell diagram a critical speed is reached at 549 rad/sec at the first eigenfrequency of 87 Hz. For this reason, the operation of the tester is limited to a rotational speed of 500 rad/sec and a reciprocation frequency of 50Hz. The excitation of the first six frequencies can be seen in the results.

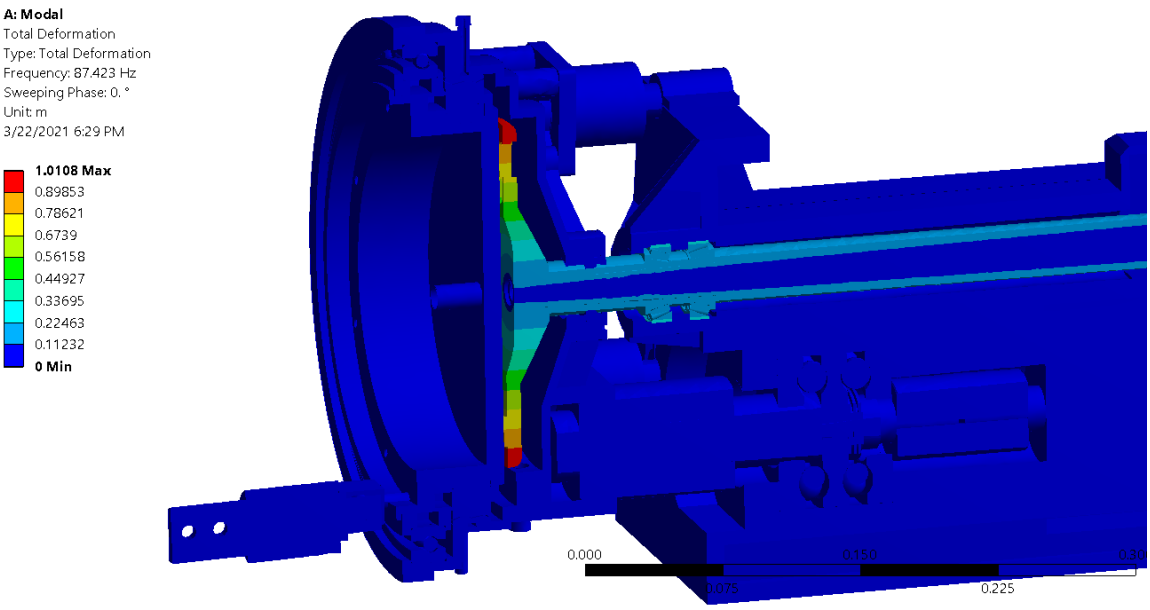

Figure 112 Frequency of 87 Hz (model section)

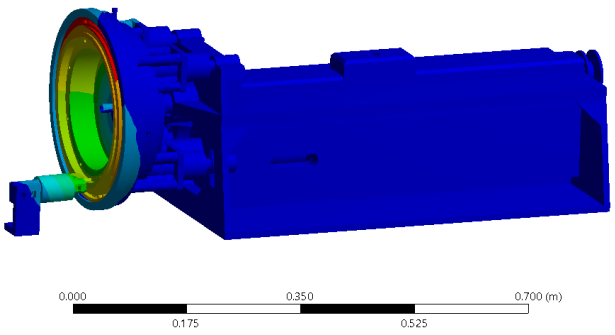

Figure 113 Frequency of 160 Hz

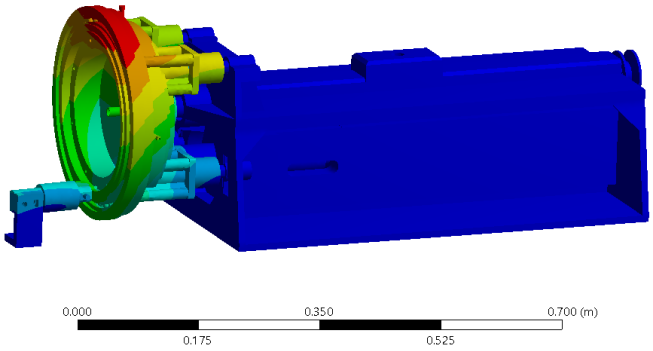

Figure 114 Frequency of 236 Hz

6.7 Motion Related Calculations

6.7.1 Motor selection

For the selection of the motors used in this multi-tester, the constant required torque as well ass the acceleration and deceleration torque were calculated. Depending on the needed rotational speed profiles, the needed power was then calculated for each motor. The constant torque is defined as:

$$T_c = T_d + T_p + T_f$$

Where T_p is the torque due to preload, Tf is the torque due to friction of support bearings and T_d is the torque to drive the load:

$$T_d = \frac{F_a \cdot P}{2000 \cdot \pi \cdot \eta}$$

Where P is the lead screw pitch, η is the efficiency of the ball screw and F_a the total axial force:

$$F_a = F + m \cdot g \cdot \mu$$

The total torque during acceleration T_a is:

$$T_a = T_c + T_{acc}$$

Where T_{aa} is the torque due to acceleration:

$$T_{acc} = J \cdot \omega'$$

With ω΄ the angular acceleration:

$$\omega' = \frac{2\pi \cdot N}{60 \cdot t}$$

N is the angular velocity in rpm and J is the inertia of the system (kgm^2) :

$$J = J_m + J_s + J_l$$

J_m is the inertia of the motor, Js is the inertia of the screw shaft and J_l is the inertia of the load:

$$J_l = m \cdot \left(\frac{P}{2\pi}\right)^2 \times 10^{-6}$$

Finally, the deceleration torque is:

$$T_g = T_c - T_{acc}$$

In most cases a servo motor was chosen in order to maintain high torque values at high rotational speeds and to be able to control the motor and the number of the revolutions via an encoder. On the motions that no such requirements existed, stepper motors were chosen to reduce the cost. According to these calculations the following motors were chosen:

Motor	Description	Type	Power
Main motor of the multi-tester	Provides rotational motion to the shafts of the two subassemblies	Servo motor with brake	11.8 kW
Clutch tester motor	Provides the reciprocating motion of the tester	Servo motor with brake	10.1kW
Wear test rig main motor	Provides the axial linear motion of the tester and compresses the springs	Stepper motor with precision actuator and brake	0.18kW
Wear test rig secondary motor	Provides the linear reciprocating motion for the tester	Servo motor with brake	0.94kW

6.7.2 Spring selection

Three different springs of the same length are used for the nominal force application on the wear test rig, in order to maintain an unchanged force value by controlling the compression of the spring. With controlled motions of the stepper motor actuator, the springs move one specimen closer to the other, as the material wears off. The selected springs are able to maintain constant force values of 25, 200 and 2800N each, but more force values within this range can be achieved, with the application of a different spring of the same length. The minimum linear steps of the actuator to achieve the force control indicated by the test standards are the following:

	Ball on Flat, procedure A (light load)	Ball on Flat, procedure B (heavy load)	Disc on Disc
Spring No	6722	6732	6305
Fmax (N)	25	200	2800
Fcontrol (N)	0.5	4	56
Ftarget (N)	25.5	204	2856
Spring specs			
Spring force at full compression Fst (N)	120	290	2850
Unloaded length Lo (mm)	90	90	90
Solid length Lst (mm)	6	7.5	66
Spring constant (N/mm)	1.42	3.51	118.75
Elongation at max (mm)	17.5	56.89	23.57
Elongation at control (mm)	17.85	58.03	24.05
Actuator Control Displacement (mm)	0.35	1.13	0.47
Resulting total length at max elongation	72.5	33.1	66.42

7 Conclusion

From the requirements of this machine and the mechanical drawings, it appears that there are several strict design characteristics for this unit. Even though stock parts and common materials have been used when possible, the annotations requirements in certain areas render the manufacturing of some of the parts quite complex, with more than one manufacturing method and surface treatment needed. Still, such a thing is to be expected when designing a precision test rig that follows several international standards. Moreover, the fact that the multi-tester combines different wear testing rigs means that, compared to the standalone tribometers, the offered value in manufacturing effort and cost is much greater.

Based on the process of this thesis, from the parts of an old machine, a new prototype is created, which combines many functionalities and provides many configuration possibilities. Such a thing underlines the effectiveness of recycling and reusing old laboratory parts with no sacrifices to the operation parameters.

8 Areas for further improvement / investigation

An idea that was initially considered but later abandoned due to lack of space, is to mirror the assembly of the single clutch disk tester and create a rig that tests not only the oil flow phenomena, but also the wear of clutches of more than one disk, like the mentioned SAE No2 test rigs. This modification could be made possible, if the assembly of this tester is transferred on a different structure, with more available space.

Another suggestion is to create even more custom modular wear rigs inside the tribometer. The force control application in the form of springs means that a wide range of loading cases can be applied on the selected specimens, and the available space inside the oil hub can fit possible extension fixtures.

9 Mechanical drawings: Files are attached in separate file

10 Bibliography

1. **Holmberg Kenneth, Erdemir Ali.** *Influence of tribology on global energy consumption, costs and emissions.* 2017.

2. **R. Biczó, G. Kalácska, Z. Szakál, G. Fledrich.** *Composite Friction Materials for Brakes and Clutches.* 2016.

3. **Nagesh S.N, Siddaraju C, S V Prakash, M R Ramesh.** *Characterization of brake pads by variation in composition of friction materials.* 2014.

4. **K. Naresh Kumar, Dr. K. N. S. Suman.** *Review of brake friction materials for future development.* 2017.

5. **Glenn Kwabena Gyimah, Ping Huang , Dong Chen.** *Dry Sliding Wear Studies of Copper-Based Powder Metallurgy Brake Materials.* 2014.

6. **Vlastimil Matějka, Yafei Lu, Yanli Fan, Gabriela Kratošová, Jana Lešková.** *Effects of silicon carbide in semi-metallic brake materials on friction performance and friction layer formation.* 2008.

7. **Hentati Nesrine, Anne-Lise Cristol, D. Najjar, Riadh Elleuch, Yannick Desplanques.** *Influence of Hot Molding Parameters on Tribological and Wear Properties of a Friction Material.* 2014.

8. **D Chan, G W Stachowiak.** *Review of automotive brake friction materials.* 2004.

9. **Menard, D., Boutard, J., Guerin, R. and Jacq, G.** *Friction material designed for fitting to a device employing friction in a liquid medium, and a method of producing such a friction material and the device to which it is fitted.* 1998.

10. **Liang Yu, Biao Ma, Man Chen, Heyan Li, Chengnan Ma, Jikai Liu.** *Comparison of the Friction and Wear Characteristics between Copper and Paper Based Friction Materials.* 2019.

11. **Konstantine Fetfatsidis, David Jauffres, James Sherwood, Julie Chen.** *Characterization of the tool/fabric and fabric/fabric friction for woven-fabric composites during the thermostamping process.* 2011.

12. **J. Wahlström, D. Gventsadze, L. Olander, E. Kutelia, L. Gventsadze, O. Tsurtsumia, U. Olofsson.** *A pin-on-disc investigation of novel nanoporous composite-based and conventional brake pad materials focussing on airborne wear particles.* 2011.

13. **A. Alavudeen, Mani Thiruchitrambalam, A. Athijayamani.** *Clutch plate using woven hybrid composite materials.* 2011.

14. **Tej Singh, Mukesh Kumar Rathi, Amar Patnaik, Ranchan Chauhan, Sharafat Ali, Gusztáv Fekete.** *Application of waste tire rubber particles in non-asbestos organic brake friction composite materials.* 2018.

15. **R.S. Fono-Tamo, O.A. Koya.** *Influence of Palm Kernel Shell Particle Size on Fade and Recovery Behaviour of Non-asbestos Organic Friction Material.* 2017.

16. **Kussuma, Fendy.** *Testing of mechanical characteristics of coconut fiber reinforced for composite brake pads for two-wheeled vehicles.* 2019.

17. **Talib Ria Jaafar, Ramlan Kasiran, Noor Iswadi Ismail, Mohd Fauzi Ismail, A. O. Eliasidi.** *Bamboo Fibre-reinforced Semi-Metallic Brake Friction Materials for Automotive Applications.* 2016.

18. **Arunachalam, K., Dr, G. Sundara Pandian.** *Modeling and Analysis of Clutch Facing Made up of Biodegradable Coir Fibre Based Composite Material.* 2016.

19. **Craciun A. L., Pinca-Bretotean C., Utu D., Josan A.** *Tribological properties of nonasbestos brake pad material by using coconut fiber.* 2017.

20. **W. Krenkel, B. Heidenreich, R. Renz.** *C/C-SiC Composites for Advanced Friction Systems.* 2002.

21. **Nico Langhof, Michael Rabenstein, Jens Rosenlöcher, Reinhard Hackenschmidt, Walter Krenkel, Frank Rieg.** *Full-ceramic brake systems for high performance friction applications.* 2016.

22. **Xu Ma, Shangwu Fan, Haodong Sun, Chenghua Luan, Juanli Deng, Litong Zhang, Laifei Cheng.** *Investigation on braking performance and wear mechanism of full-carbon/ceramic braking pairs.* 2020.

23. **Omkar Aranke, Wael Algenaid,Samuel Awe, Shrikant Joshi.** *Coatings for Automotive Gray Cast Iron Brake Discs: A Review.* 2019.

24. **Shangwu Fan, Yang Chuan, Liuyang He, Juanli Deng, Litong Zhang, Laifei Cheng.** *The effects of phosphate coating on friction performance of C/C and C/SiC brake materials.* 2017.

25. **A. P. Krelling, Matheus Machado de Souza, C. Costa, J. Milan.** *HVOF-sprayed Coating Over AISI 4140 Steel for Hard Chromium Replacement.* 2018.

26. **C. S. Dunleavy, I. O. Golosnoy, J. A. Currana, T. W. Clynea.** *Characterisation of discharge events during plasma electrolytic oxidation.* 2009.

27. **X Nie, E. I Meletis, J. C Jiang, A Leyland, A. L Yerokhin, A Matthews.** *Abrasive wear/corrosion properties and TEM analysis of Al2O3 coatings fabricated using plasma electrolysis.* 2002.

28. **Aleksey Yerokhin, Xw Nie, A. Leyland, A. Matthews.** *Characterisation of oxide films produced by plasma electrolytic oxidation of a Ti–6Al–4V alloy.* 2000.

29. **J. A. Curran, T. W. Clyne.** *The thermal conductivity of plasma electrolytic oxide coatings on aluminium and magnesium.* 2005.

30. **J.A. Curran, T.W. Clyne.** *Porosity in plasma electrolytic oxide coatings.* 2006.

31. **T.S. Sidhu, Satya Prakash, R.D. Agrawal.** *State of the Art of HVOF Coating Investigations-A Review.* 2005.

32. **Andrei Verstak, Viatcheslav Baranovski.** *Deposition of carbides by activated combustion HVAF spraying.* 2004.

33. **Giovanni Bolelli, Valeria Cannillo, Luca Lusvarghi, Tiziano Manfredini.** *Wear behaviour of thermally sprayed ceramic oxide coatings.* 2006.

34. **Mari, D.** *Cermets and hardmetals BT—Reference module in materials science and materials engineering.* 2016.

35. **J. A. Picas, A. Forn, A. Igartua, G. Mendoza.** *Mechanical and tribological properties of high velocity oxy-fuel thermal sprayed nanocrystalline CrC NiCr coatings.* 2003.

36. **Bolt AM, Mann KK.** *Final report on carcinogens background document for cobalt-tungsten carbide: powders and hard metals.* 2009.

37. **Marc Ingram, J. Noles, R. Watts, S. Harris.** *Frictional Properties of Automatic Transmission Fluids: Part II-Origins of Friction-Sliding Speed Behavior.* 2011.

38. **Olga Terleeva, Aleksandra I Slonova, Aleksey Rogov, Allan Matthews, Aleksey Yerokhin.** *Wear Resistant Coatings with a High Friction Coefficient Produced by Plasma Electrolytic Oxidation of Al Alloys in Electrolytes with Basalt Mineral Powder Additions.* 2019.

39. **Okamura, Toshikazu.** *Experimental Study of Effect of Brake-Disc Surface Texture on Friction and Wear through Small-Scale Tests on Tribotester.* 2013.

40. —. *Study of Difference in Friction Behavior of Brake Disc Rotor with Various Surface Textures during Running-In by Using Simple Model.* 2017.

41. **D. W. Wang, J. L. Mo, M. Q. Liu, J. X. Li, H. Ouyang, M. H. Zhu, Z. R. Zhou.** *Improving tribological behaviours and noise performance of railway disc brake by grooved surface texturing.* 2017.

42. **Meng Li, M. M. Khonsari, D.M.C. McCarthy, Joakim Lundin.** *Parametric analysis for a paper-based wet clutch with groove consideration.* 2014.

43. **Meng Li, M. M. Khonsari, DMC McCarthy, Joakim Lundin.** *Parametric analysis of wear factors of a wet clutch friction material with different groove patterns.* 2017.

44. **Ian Hutchings, Philip Shipway.** *Tribology. Friction and Wear of Engineering Materials.* 2017.

45. **Bhushan, Bharat.** *Introduction to Tribology, Second Edition .* 2013.

46. —. *Modern Tribology Handbook.* 2000.

47. **G99-17, ASTM.** *Standard Test Method for Wear Testing with a Pin-on-Disk Apparatus.*

48. **05(2016), ASTM G133 -.** *Standard Test Method for Linearly Reciprocating Ball-on-Flat Sliding Wear.*

49. **G77-17, ASTM.** *Standard Test Method for Ranking Resistance of Materials to Sliding Wear Using Block-on-Ring Wear Test.*

50. **T. Neupert, D. Bartel.** *High-resolution 3D CFD multiphase simulation of the flow and the drag torque of wet clutch discs considering free surfaces.* 2019.

51. **Hu Jibin, Peng Zengxiong, Wei Chao.** *Experimental Research on Drag Torque for Single-plate Wet Clutch.* 2012.

52. **Jibin Hu, Shiyang Hou, Chao Wei.** *Drag torque modeling at high circumferential speed in open wet clutches considering plate wobble and mechanical contact.* 2018.

53. **Ρόγκας, Νικόλαος.** *Μοντελοποίηση και παραμετρική διερεύνηση της δυναμικής συμπεριφοράς πολύδισκου συμπλέκτη υγράς τριβής με αναλυτικές και αριθμητικές μεθόδους.* 2017.

54. **St. Nowotny, A. Techel, A. Luft, and W. Reitzenstein.** *Microstructure and wear properties of laser clad carbide coatings.* 2018.

55. **Shengfeng Zhou, Xiaoyan Zeng, Qianwu Hu, Yongjun Huang.** *Analysis of crack behavior for Ni-based WC composite coatings by laser cladding and crack-free realization.* 2008.

56. **Andrea Gatto, Elena Bassoli, M. Fornari.** *Plasma Transferred Arc deposition of powdered high performances alloys: Process parameters optimisation as a function of alloy and geometrical configuration.* 2004.

57. **F. Fernandes, B. Lopes, A. Cavaleiro, A. Ramalho, A. Loureiro.** *Effect of arc current on microstructure and wear characteristics of a Ni-based coating deposited by PTA on gray cast iron.* 2011.

58. **Champagne, V.K.** *The Cold Spray Materials Deposition Process.* 2007.

59. **P. Richer, M. Yandouzi, L. Beauvais, B. Jodoina.** *Oxidation behaviour of CoNiCrAlY bond coats produced by plasma, HVOF and cold gas dynamic spraying.* 2010.

60. **Filofteia-Laura Toma, Annegret Potthoff, Lutz-Michael Berger, Christoph Leyens.** *Demands, Potentials, and Economic Aspects of Thermal Spraying with Suspensions: A Critical Review.* 2015.